

# **SANDIA REPORT**

SAND2001-0312

Unlimited Distribution

Printed May 2001

## **Statistical Validation of Engineering and Scientific Models with Application to CTH**

Richard G. Hills and Timothy G. Trucano

Prepared by

Sandia National Laboratories

Albuquerque, New Mexico 87185 and Livermore, California 94550

Sandia is a multiprogram laboratory operated by Sandia Corporation,  
a Lockheed Martin Company, for the United States Department of  
Energy under Contract DE-AC04-94AL85000

Approved for public release; further dissemination unlimited.



**Sandia National Laboratories**

Issued by Sandia National Laboratories, operated for the United States Department of Energy by Sandia Corporation.

**NOTICE:** This report was prepared as an account of work sponsored by an agency of the United States Government. Neither the United States Government nor any agency thereof, nor any of their employees, nor any of their contractors, subcontractors, or their employees, makes any warranty, express or implied, or assumes any legal liability or responsibility for the accuracy, completeness, or usefulness of any information, apparatus, product, or process disclosed, or represents that its use would not infringe privately owned rights. Reference herein to any specific commercial product, process, or service by trade name, trademark, manufacturer, or otherwise, does not necessarily constitute or imply its endorsement, recommendation, or favoring by the United States Government, any agency thereof or any of their contractors or subcontractors. The views and opinions expressed herein do not necessarily state or reflect those of the United States Government, any agency thereof or any of their contractors.

Printed in the United States of America. This report has been reproduced directly from the best available copy.

Available to DOE and DOE contractors from

U.S. Department of Energy  
Office of Scientific and Technical Information  
P.O. Box 62  
Oak Ridge, TN 37831

Telephone: (865)576-8401  
Facsimile: (865)576-5782  
E-Mail: [reports@adonis.osti.gov](mailto:reports@adonis.osti.gov)  
Online ordering: <http://www.doe.gov/bridge>

Available to the public from

U.S. Department of Commerce  
National Technical Information Service  
5285 Port Royal Rd  
Springfield, VA 22161

Telephone: (800)553-6847  
Facsimile: (703)605-6900  
E-Mail: [orders@ntis.fedworld.gov](mailto:orders@ntis.fedworld.gov)  
Online order: <http://www.ntis.gov/ordering.htm>



SAND2001-0312  
Unlimited Release  
Printed May 2001

## **Statistical Validation of Engineering and Scientific Models with Application to CTH**

Richard G. Hills  
Department of Mechanical Engineering  
New Mexico State University  
Las Cruces, New Mexico 88003

Timothy G. Trucano  
Optimization and Uncertainty Estimation  
Sandia National Laboratories  
P. O. Box 5800  
Albuquerque, New Mexico 87185-0819

### **Abstract**

Our increased dependence on computer models leads to the natural question – how do we know whether a computer model is valid? Models have traditionally been tested against experimental measurements through simple comparisons such as x-y plots, scatter plots, or two-dimensional contour plots. We are then faced with two questions: When is the agreement between experimental measurement and model prediction good enough, and how should we quantify this agreement?

Here we present the use of statistical methods to develop metrics for this agreement. We start with the simplest case in shock wave physics for which one can use the validation results directly to develop probability-based metrics. As an example, common statistical methods are used to test the validity of CTH hydrocode predictions of shock wave speed using experimental data for aluminum on aluminum impact. We then move to more complex multivariate validation scenarios for which the model predictive uncertainty is characterized using propagation of uncertainty analysis. Methodology for the multivariate case is developed and examples are presented using CTH predictions of shock wave speed.

## **Acknowledgements**

This report is an account of contract research (Doc. # AX-0620) performed by the first author in cooperation with the second author during the 1999 Fiscal Year. The authors would like to thank Marlin Kipp and Daniel Carroll for reviewing the manuscript prior to publication. Lalit Chhabildas reviewed parts of the manuscript prior to publication. We would also like to thank William Oberkamp, Robert Easterling, Martin Pilch, Brian Rutherford, and Tom Paez for commenting on drafts of this report. Many other people at Sandia have provided the authors with thoughtful comments about this work over the past two years. We are grateful to all for their support.

## Table of Contents

Abstract .....	3
Acknowledgements .....	4
Table of Contents .....	5
List of Figures .....	7
List of Tables .....	9
1.0 Introduction .....	11
2.0 Statistical Model Validation: Background .....	15
2.1 Introduction .....	15
2.2 Scientific Validation .....	15
2.3 Engineering Validation .....	16
2.4 Probabilistic Methods .....	16
2.4.1 Direct Use of Prediction Differences .....	16
2.4.2 Propagation of Uncertainty Analysis .....	17
3.0 High Speed Impact of Aluminum on Aluminum .....	19
3.1 The Shock Hugoniot: An Introduction .....	19
3.1.1 The Shock Hugoniot .....	19
3.1.2 Measurement of the Shock Hugoniot .....	23
3.2 One Dimensional Impact of Aluminum on Aluminum: Experimental Data .....	27
3.3 One Dimensional Impact of Aluminum on Aluminum: The Model .....	31
3.4 Two-Dimensional Impact of Aluminum on Aluminum: The Application .....	36
3.5 Summary .....	38
4.0 Model Validation using Standard Statistical Methods .....	43
4.1 Introduction .....	43
4.2 Nonparametric Methods .....	44
4.3 Functional Dependence of Us on Up .....	46
4.4 Summary .....	51
5.0 Model Validation using Propagation of Uncertainty .....	53
5.1 Introduction .....	53
5.2 Observations/Prediction Space .....	54
5.3 Integrated Measures .....	58
5.4 Application Specific Measures .....	60
5.5 Overview of Validation Examples .....	61
5.6 Calibration and Measurement Data .....	61
5.7 Model for Uncertainty in the Validation Measurement Data .....	62
5.8 Model for Uncertainty in the Model Parameters .....	64
5.9 Model for Prediction Uncertainty .....	65
5.10 Model of Uncertainty of Validation Exercise .....	69
5.11 The Point Validation Test .....	71
5.12 Application-Based Metric .....	73
5.12.1 The Application .....	73
5.12.2 Reduced Data Set .....	73

5.12.3 Application Defined Metric.....	74
5.13 Summary.....	80
6.0 Discussion and Recommendations.....	83
6.1 Overview of Work Accomplished .....	83
6.2 Application to Nonlinear Problems .....	84
6.3 Recommendations.....	85
6.4 Comment on the Discrepancy.....	86
References .....	89
Appendix A: Multiple Runs of CTH and Post Processing.....	93
Appendix B: CTH Input File Listing for the Validation Measurement Predictions .....	95
Appendix C: CTH Input File Listing for a Two Dimensional Application .....	99
Appendix D: Data.....	104

## List of Figures

Figure 3.1:	The symmetric impact of two aluminum plates.....	20
Figure 3.2:	The Idealized Shock Wave Pressure Profile: $P_0$ , $P_1$ – pressure in front and behind shock, $U_S$ – shock velocity, $U_{P1}$ – particle velocity behind shock. ....	21
Figure 3.3:	Schematic of a two-stage light-gas gun, the modern instrument of choice for shock wave studies. ....	24
Figure 3.4:	Schematic of a realistic projectile used for shock wave studies on smooth bore guns. ....	25
Figure 3.5:	Explosive-metal geometry feasible for performing shock Hugoniot measurements.....	28
Figure 3.6:	Hugoniot Data for Aluminum 2024: $U_P$ – particle velocity, $U_S$ – shock velocity (from Marsh, 1980).....	31
Figure 3.7:	One Dimensional CTH Model: Impact occurs at time = 0. ....	32
Figure 3.8:	Prediction vs. Experiment - Low Resolution Results: 100 cells across each aluminum plate, SESAME AL2024 EOS model. (The computational data is presented in Table D1.) .....	35
Figure 3.9:	Prediction vs. Experiment - High Resolution Results: 200 cells across each aluminum plate, SESAME AL2024 EOS model. ....	36
Figure 3.10:	Impact of Small Aluminum Slug on a Thick Aluminum Plate .....	37
Figure 3.11:	CTH Predictions at Time=0: Left half of plot illustrates material locations; Right half of plot represents the magnitude of the particle velocities. ....	38
Figure 3.12:	CTH Predictions at Time=1.0 $\mu$ sec: Left half of plot illustrates material locations; Right half of plot represents the magnitude of the particle velocities.....	39
Figure 3.13:	CTH Predictions at Time=4.0 $\mu$ sec: Left half of plot illustrates material locations; Right half of plot represents the magnitude of the particle velocities.....	40
Figure 3.14:	CTH Predictions at Time=7.0 $\mu$ sec: Left half of plot illustrates material locations; Right half of plot represents the magnitude of the particle velocities.....	41
Figure 4.1:	Prediction vs. Experiment for the Shock Wave Experiments, SESAME AL2024 EOS model.....	43
Figure 4.2:	Scatter Plot of Experimental vs. Predicted Shock Wave Speed: Dashed line is $U_{S\_exper} = U_{S\_pred}$ .....	46
Figure 4.3:	Scatter Plot of Experimental vs. Predictions Shock Wave Speed: Dashed line is given by $U_{S\_exper} = U_{S\_pred}$ ; Solid line is the regression ( $U_{S\_exper} = 0.950 U_{S\_pred} + 360.2$ ). ....	47
Figure 4.4:	Regression Residuals vs. Predictions Shock Wave Speed.....	48
Figure 4.5:	Histogram of the Residuals.....	48

Figure 4.6:	Prediction Bounds on the Regression of $U_s\_exper$ vs. $U_s\_pred$ . Solid thin lines are the 95% prediction bounds, solid thick line is the regression, dashed line is $U_s\_exper = U_s\_pred$ .....	50
Figure 5.1:	$n$ -Dimensional Validation Space .....	54
Figure 5.2:	Prediction and Measurement Uncertainty in the $n$ -Dimensional Validation Space .....	55
Figure 5.3:	Combined Prediction and Measurement Uncertainty. ....	56
Figure 5.4:	95% Confidence Acceptance Region: Dashed line – outer boundary of the acceptance region. ....	58
Figure 5.5:	Integrated Measure as Mapped onto a Subspace of the Validation Space. ....	59
Figure 5.6:	Integrated Measure # 2 as Mapped onto a Subspace of the Validation Space. ....	60
Figure 5.7:	Validation Measurements: 120 measurements randomly sampled from the 232 experimental shock wave speed vs. particle speed measurements. Solid line – linear regression ( $U_s = 5377 + 1.294 U_p$ ). (The computational data is presented in Table D2.).....	63
Figure 5.8:	Calibration Measurements: 112 measurements randomly sampled from the 232 experimental shock wave speed vs. particle speed measurements. Solid line – linear regression ( $U_s = 5344 + 1.305 U_p$ ). (The computational data is presented in Table D3.).....	65
Figure 5.9:	Validation Predictions and Experimental Observations: 120 measurements	67
Figure 5.10:	Standard Deviation of Predicted Shock Wave Speeds .....	70
Figure 5.11:	Predicted Standard Deviation for the Prediction Differences.....	71
Figure 5.12:	Model Validation Sub-Space as Defined by an Application Decision Variable .....	76
Figure 6.1	Comparison of 2024 aluminum shock data with predicted Hugoniot data from the 3700 SESAME table. ....	87

## List of Tables

Table 3.1:	Hugoniot Data for Aluminum 2024: All speeds are in m/s .....	30
Table 4.1:	Statistics for the Sign Test .....	45
Table 4.2:	Statistics for the Kolmogorov-Smirnov Test for a Normally Distributed Residuals. ....	49
Table 4.3:	Regression of the Experimental Shock Wave Velocity as a Function of the Predicted Shock Wave Velocity.....	49
Table 5.1:	Statistics for the Kolmogorov-Smirnov Test for Normally Distributed Residuals: Validation Data.....	64
Table 5.2:	Calibration Constants.....	66
Table 5.3:	Statistics for the Kolmogorov-Smirnov Test for Normally Distributed Residuals: Calibration Data .....	66
Table D1:	Predicted Shock Speed vs. Experimental Measurements (m/s): 232 data sets, see Figure 3.8. ....	104
Table D2:	Predicted Shock Speed vs. Experiment (m/s) - Validation Data: 120 data sets, see Figure 5.7. ....	106
Table D3:	Experimental Shock vs. Particle Speed (m/s) – Calibration Data: 112 data pairs, see Figure 5.8. ....	107

(Page Left Blank)

## 1.0 Introduction

The use of numerical models for the simulation of physical systems has greatly influenced our approach to engineering and science. These models are used to design commercial and military equipment, to design scientific experiments and to analyze the results, and to perform conceptual studies. The increased ease of use, the greater ability to model complex phenomena with higher fidelity, and the decreasing cost of modern computers have accelerated the use of numerical models. Such models are reducing the engineering design cycle time and cost, and are increasing the reliability of the resulting products.

The increased dependence on computer models leads to the natural question – are these models valid (for example, in the sense that Roache, 1998 uses the word)? Traditionally, modelers have tested their models against experimental data whenever possible. This testing often takes the form of comparisons of predictions to measurements through simple x-y plots, scatter plots, or two-dimensional contour plots. Such testing is, on the face of it, insufficient for our need. After plotting the results, we are still faced with two questions: When is the agreement between experimental measurements and model predictions good enough? How does one *accurately* and *meaningfully* measure this agreement?

In this report we use concepts from statistics to develop metrics for the agreement between prediction and experimental results relative to the intrinsic uncertainty in the validation exercise. (In this report, the word “metric” is used in the informal sense of “measure,” not in the mathematical sense. The development of a model for uncertainty can be one of the more difficult aspects of the definition of such measures, and much of the present report is devoted to this topic.

Several approaches to the development of these metrics are presented. In this report we will call these metrics **validation metrics**. In the first approach, the model for the uncertainty is estimated from the prediction differences directly (differences between the model predictions and the experimental observations). This approach is commonly used in statistical inference and relies on basic assumptions about the statistical characteristics of the prediction differences.

In the second approach, we utilize a propagation of uncertainty analysis to develop the statistical model for the uncertainty. This approach is appropriate when it is easier to statistically characterize the uncertainty in the model input parameters and perform a propagation of uncertainty analysis, than it is to estimate the statistical characteristics of the differences between prediction and observation directly. This second approach is used when one cannot perform a sufficient number of validation experiments to characterize the statistics of the prediction differences from the results directly, or when the prediction differences have a complex correlation structure due to the characteristics of the predictive model.

Finally, we present a variation of the second approach where the validation metric is modified to reflect the desired application of the model. This approach recognizes that the model validation experiments are not necessarily exact or even near replicates of the desired application of the model. As such, a model of the application is used to modify the validation metric so that the validation data is weighted in a fashion appropriate for the application.

We demonstrate these three approaches using data and a numerical model from shock wave physics. The Eulerian shock wave physics code CTH (McGlaun, et al. 1990, Bell et al., 1998, Hertel and Kerley, 1998) is used to model the impact of an aluminum plate with an equal sized, but initially stationary, aluminum plate in the km/s range. As a result of the high impact speeds, a shock wave forms and propagates through the aluminum at supersonic speeds. Model predictions for the shock wave speed are tested against experimental measurements using the three statistically based approaches introduced above.

This report is a continuation of a previous report by Hills and Trucano (1999) which provided a tutorial on the propagation of uncertainty analysis and model validation, and presented a literature review of model validation methodology. The role of uncertainty analysis is currently viewed as important to high quality validation by the DOE Accelerated Strategic Computing Initiative (ASCI) verification and validation (V&V) program (Lee, 1998; Ang, et al., 1999). However, this report is one of the first pieces of work to go beyond programmatic generalities and perform specific technical work that is aligned with the program objectives in this focus area.

We will discuss the experimental data that underlie this paper in greater detail below. However, it is worth stressing at this point that these data are quite unusual in terms of quantity, quality, and simplicity of their experimental functional relationship. In particular, the form of the data subjected to analysis here are substantially linear. We do not expect the experimental data underlying any future work that targets code validation in the context of uncertainty analysis to be better than what we analyze here. We encourage the attentive reader of this report to maintain a perspective that focuses on our methodology, rather than on the particular niceties of our data. We believe that our methodology is quite general. It certainly does not require either the quantity or linearity of the validation data discussed in this report.

In Section 2 we make brief comments on statistical model validation. Section 3 is a discussion of the shock wave physics background necessary to understand the validation data used in this report. We aim this discussion at readers who may be unfamiliar with the peculiarities of shock wave data. Based on our intended goal of illustrating methodology and discussions we have had during drafting the final form of this report, we believe that it is critical for our purpose to clearly define the nature and context of our data. Sections 4 and 5 present the two primary approaches to model validation with uncertainty mentioned above (model uncertainty estimated from data – Section 4; model uncertainty estimated

from uncertainty propagation – Section 5). We conclude the paper with a discussion of the key points in this report and recommendations for future work in Section 6.

Unless otherwise clear from the context, the word “model” in this report *always* means the code CTH and *all* of the input associated with its use, including material model specification, grid generation and material geometric fills, and specific choices for computational control parameters associated with given calculations. Examples of such input specifications are given in the Appendices.

(Page Left Blank)

## **2.0 Statistical Model Validation: Background**

### **2.1 Introduction**

When performing model validation, it is critical that we determine whether differences between model predictions and experimental observations from a model validation exercise are significant. To address this problem, we must first ask, “what metrics should we use to measure these differences?” and “how large should the values of these metrics be in order to declare a model invalid for this particular set of data?” Here we use statistical methods to define these metrics – called validation metrics – and their critical threshold values. Background on this statistical approach to model validation is presented in the previous report by Hills and Trucano (1999).

### **2.2 Scientific Validation**

The statistical approach to model validation is based on refining the above issue. The question we must really ask is – are the differences between the predictions and the experimental observations significant relative to the uncertainty in the validation exercise? Possible sources of uncertainty in this exercise are 1) uncertainty in the values of the parameters used in the predictive model, 2) uncertainty in the initial and/or boundary conditions for the model of the validation experiment, 3) uncertainty in the model predictions due to truncation error in the numerical model, 4) uncertainty in the times and/or spatial locations of the measurements, and 5) uncertainty in the values of the measurements themselves. In principle, all of these sources must be accounted for when we attempt to determine whether experimental – computational differences are significant.

Our logic is thus one of falsification. If the differences between prediction and experimental observation are significant relative to the total uncertainty, we conclude that the model is not valid in a fundamental scientific sense. We reject the scientific validity of the model. In contrast, if the differences are not significant relative to the uncertainty, then we have no reason to reject the model. Note that if the validation exercise has significant uncertainty, we are less likely to reject an invalid model. In contrast, if the validation exercise is very precisely defined and controlled such that there is very little uncertainty, then we will have a greater chance of rejecting an invalid model. We will also have a greater chance of rejecting a model in some sense as scientifically valid, even though it may provide useful but approximate predictions. In such cases, we should relax our definition of a “valid” model and introduce an engineering definition and approach to validation, which we now discuss.

## **2.3 Engineering Validation**

The engineering approach is based on asking the question - are the differences between the predictions and the experimental observations significant relative to the uncertainty in the validation exercise plus some acceptable error? In contrast to scientific validation, this form of validation requires that the user of the model define what level of error is acceptable. Alternatively, we can use statistical methods to evaluate error bounds on the predictions which may be more useful since this approach does not require the user to define what level of error is acceptable a-priori. Of course, the decision that the error bars are “small enough” still requires a decision about acceptable levels of error.

## **2.4 Probabilistic Methods**

A common feature of both scientific and engineering validation, as defined above, is they both require a probabilistic model for the uncertainty in order to evaluate whether the differences between model prediction and experimental observation are significant relative to this uncertainty. There are two basic approaches that can be used to determine the probabilistic models. One is to use prediction differences (differences between the predictions and the experimental measurements) directly to develop the model for the uncertainty. The second is to use knowledge of the uncertainty of the predictive model's input parameters, and perform a propagation of uncertainty analysis to estimate the corresponding uncertainty in the model predictions, and add this uncertainty to that of the measurements. A tutorial on this second approach is presented in Hills and Trucano (1999). We will demonstrate both of these approaches in Chapters 4 and 5 using the validation test problem introduced in Chapter 3.

### **2.4.1 Direct Use of Prediction Differences**

The usual approach in statistics is to develop a model for the uncertainty using the observed scatter of the data. This approach is exploratory in the sense that one must hypothesize a probability model for the uncertainty, use the data to estimate the relevant statistical parameters that characterize the probability model, then test this parameterized probability model against the data. If the resulting statistical model shows behavior consistent with the data, then it can be used as a basis to statistically compare model predictions to experimental observations.

This approach works well if the scatter in the prediction differences (model predictions minus the experimental observations) have a structure well modeled by common probability distributions, if the errors are independent, and if we have sufficient experimental data to resolve the statistical parameters for the probability models. If the errors are not independent, then we may still be able to use this approach if one of the

standard correlation models can be shown to apply or if we can remove this correlation by other means.

In general, we do not expect errors to be uncorrelated for the kind of validation data that we will be dealing with in the ASCI V&V program. This approach is difficult to apply when the prediction differences have a complex correlation structure. As an example, consider the comparison of temperature predictions in a heat-conducting solid against measurement of temperature taken at various times and locations throughout the solid. Typically, if a prediction difference is positive at some measurement location and time, it will likely be positive at an adjacent measurement location and time. The prediction differences are thus correlated with the correlation structure closely associated with the physics of heat conduction. For cases such as this, standard correlation models are not appropriate and we must consider a different approach.

#### 2.4.2 Propagation of Uncertainty Analysis

The second approach is to model the uncertainty in the prediction errors using the predictive model, knowledge about the uncertainty structure of the model input parameters, and knowledge about the uncertainty structure of the measurements. This approach works well for cases for which it is easier to characterize the uncertainty in the model input parameters and in the measurements than it is to characterize the uncertainty directly from the population of prediction differences. For example, it may be easier to generate sufficient data to evaluate the uncertainty structure of the thermal conductivity using multiple samples in a simple, divided-bar apparatus, than it is to run multiple validation experiments for which measurements of temperature are taken in multiple samples of a complex three-dimensional object. It is also generally easier to determine or control the correlation structure of the experimental measurements themselves since the measurement system can often be designed to provide independent measurements or measurements with an easy-to-estimate correlation structure.

Given the model for the uncertainty in the model input parameters, we can use propagation of uncertainty analysis to evaluate the corresponding uncertainty in the model's predictions of the measurements. Given this model for the prediction uncertainty, and the uncertainty for the experimental measurements, we can then evaluate the corresponding uncertainty for the prediction differences.

Examples of the propagation of uncertainty approach are provided in Hills and Trucano (1999) for simple physical models. Here we will demonstrate both the direct approach and the propagation of uncertainty approach for a shock physics model for the high-speed impact of aluminum on aluminum. This model has been selected to be one of the simplest illustrations of the comparison between experiment and calculation for shock wave physics that we can think of. The philosophy behind this choice is further discussed in Section 3.0.

(Page Left Blank)

## 3.0 High Speed Impact of Aluminum on Aluminum

### 3.1 *The Shock Hugoniot: An Introduction*

The canonical problem that we are concerned with in this report is the symmetric impact of an aluminum plate upon an aluminum plate under conditions that guarantee that the resulting material response is in uniaxial strain. This is a specific example of a more general case in which two different materials undergo the same type of impact. The resultant state of uniaxial strain is the most important part of the experiment, not the assumption that the materials are identical (which creates a significant simplification of the overall event as we will see). Uniaxial strain states induced by such an impact mean that the shock wave generated in the impact is a square-wave (at least in the ideal) and also guarantees that the resulting shock wave propagation can be analyzed as a one-dimensional Cartesian geometry wave propagation problem. It is the purpose of this section to demonstrate the implications of these facts for understanding the key data that might be accumulated from experiments of this type.

Figure 3.1 illustrates schematically the specific example of this type of impact that we care about in this paper. To fully understand this particular experiment we intend to provide a summary of the experimental techniques and the data that result. Without this understanding, our focus on the specific data discussed later in this paper will likely be misunderstood by the reader. The meaning of the symbols in this figure will also be explained below.

#### 3.1.1 The Shock Hugoniot

The plate impact problem that we are concerned with has been extensively modeled and studied experimentally for many years. The main reason is that this problem and variations of it are an important experimental method for determining data characterizing the ***shock Hugoniot*** (Zel'Dovich and Raizer, 1967) for various materials.

The Hugoniot can be characterized in a variety of ways, as discussed below. But the experimental measurements that simultaneously determine shock velocity and particle (material) velocity on the Hugoniot have special significance in the characterization of the response of materials to high pressure shock waves. The experimental determination of the relationship of shock velocity and particle velocity is also very repeatable and is consistent from experiment to experiment and from experimental technique to experimental technique. The response of aluminum (and other materials) to such an impact can be simulated by computational shock wave physics codes. These codes rely upon appropriate equation of state models for their accurate performance. These models are almost always developed using empirical knowledge about the shock Hugoniot of the material. The functional relationship between shock velocity and particle velocity is

particularly useful for this application. Therefore, it is of importance to understand what is being measured and why it is important, both experimentally and theoretically.

The Hugoniot of a material is the locus of thermodynamic final states that is generated by steady state shock waves of varying strength (Zel'Dovich and Raizer, 1967; Davison and Graham, 1979; Graham, 1993). The key state variables of interest in the present discussion, as well as fundamental to the Hugoniot, are material density ( $\rho$ ), material pressure ( $P$ ), material internal energy ( $e$ ), and material (or “particle”) velocity ( $U_p$ ). The ideal steady state shock wave is a step wave. It is common to parameterize the strength of this shock wave by its speed ( $U_s$ ) in the frame of reference of a stationary observer. Such a wave, and the associated state variables are shown in Figure 3.2. We designate the initial state of the material state variables by the index “0,” the final state in the wake of the shock wave with the index “1,” as shown in Figure 3.2.

Given the initial state and the shock velocity, the final state is uniquely determined by algebraic relationships called the **Rankine-Hugoniot conditions**. It is in this sense that the speed of the shock wave “parameterizes” the locus of Hugoniot states. The most general form of these equations is:

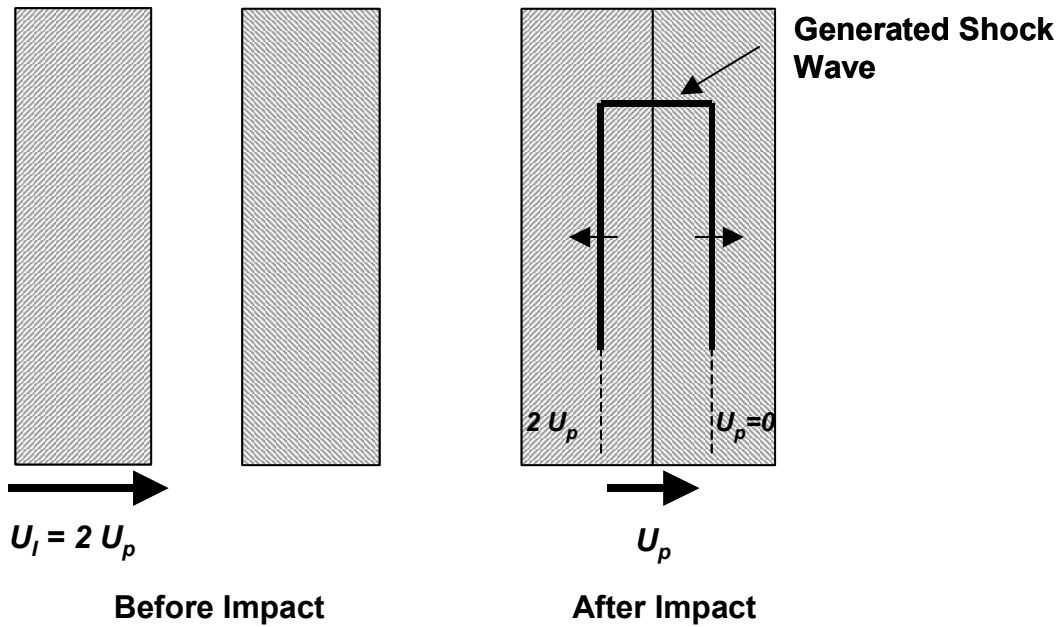


**Figure 3.1:** The symmetric impact of two aluminum plates.

$$\rho^1 = \rho^0 \frac{U_s - U_p^0}{U_s - U_p^1}$$

$$P^1 = P^0 + \rho^0 (U_s - U_p^0)(U_p^1 - U_p^0) \quad (3.1)$$

$$e^1 = e^0 + \frac{1}{2}(P^0 + P^1) \left( \frac{1}{\rho^0} - \frac{1}{\rho^1} \right)$$

The Rankine-Hugoniot (R-H) relations, which are derived from the basic conservation laws of mass, momentum, and energy, represent three equations relating nine different quantities, of which four define the reference conditions. It is possible to reduce the number of free quantities in (3.1). For example, if the equation of state of the material is given as  $P = P(\rho, e)$ , then the pressures can be eliminated from the equations in terms of the densities and internal energies. In a particularly simple case, suppose that  $P^0 = 0$  and  $e^0 = 0$ , a good approximation to the standard reference conditions for many solids undergoing shock loading. Further, suppose that the material is initially motionless, so that  $U_p^0 = 0$ . Then the R-H relations (3.1) reduce to:

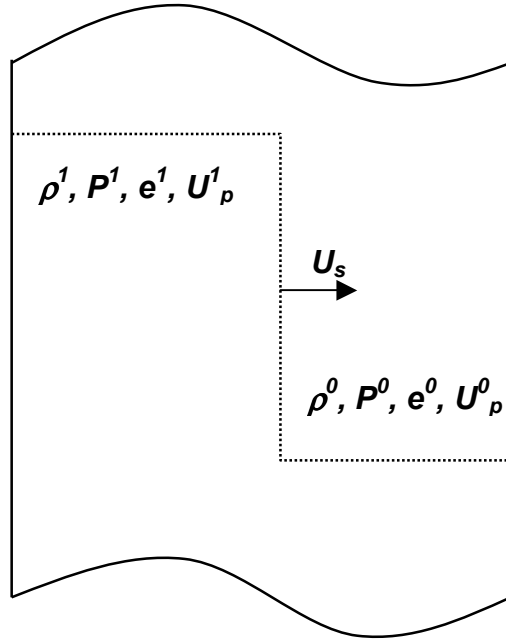


**Figure 3.2:** The Idealized Shock Wave Pressure Profile:  $P^0, P^1$  – pressure in front and behind shock,  $U_s$  – shock velocity,  $U_p^1$  – particle velocity behind shock.

$$\begin{aligned}
\rho^1 &= \rho^0 \frac{U_s}{U_s - U_p^1} \\
P^1 &= \rho^0 U_s U_p^1 \\
e^1 &= \frac{P^1}{2} \left( \frac{1}{\rho^0} - \frac{1}{\rho^1} \right)
\end{aligned} \tag{3.2}$$

We now have three equations relating five quantities. Then, for example, if we can provide a relationship between particle velocity and shock velocity, for example in the form  $U_p^1 = f(U_s)$ , then (3.2) defines the final state of the material behind the shock wave in terms of the initial density and the shock speed. For a fixed material, only shock speed can vary. It is in this sense that we mentioned above that the Hugoniot states (the final states) can be parameterized by a single parameter, the shock speed in this case. The parameterization could also have been in terms of the final particle velocity, density, pressure, or internal energy.

We can also simplify the R-H conditions directly in terms of the conceptual experiment of Figure 3.1. There, the impact of a material upon an identical material is depicted, which generates a shock wave in both materials. The Hugoniot state of this material is governed by the R-H relations as described above. Now, however, because of the very special form of this so-called symmetric impact, we know the final particle velocity. If the impact velocity is  $U_I$ , then conservation of momentum can be applied to show that  $U_p^1 = U_I/2$ . Since the target plate in this case is assumed to be at reference conditions and stationary, equations (3.2) still apply with this specialization of the final state particle velocity:

$$\begin{aligned}
\rho^1 &= \rho^0 \frac{U_s}{U_s - U_I/2} \\
P^1 &= \rho^0 U_s U_I/2 \\
e^1 &= \frac{P^1}{2} \left( \frac{1}{\rho^0} - \frac{1}{\rho^1} \right)
\end{aligned} \tag{3.3}$$

What is particularly attractive about (3.3) is that it implies that experimentally, all that needs to be measured is the impact velocity and the shock velocity. But, of course, (3.3) is only true for symmetric impacts, which have certain limitations.

A relationship between final particle velocity and shock velocity is thus of particular interest from the theoretical view. The R-H relations demonstrate that it is not necessary to perform thermodynamic measurements in shock wave experiments to characterize density, pressure and internal energy on the Hugoniot of a material. Only the quantities specifically associated with shock wave motion – particle velocity and shock velocity – need to be measured. These are the quantities that are most directly accessible in classic shock wave experiments. Many of these experiments directly realize the ideal of Figure 3.1. We briefly describe these experiments below.

Temperature on the Hugoniot has not been included in our list of thermodynamic quantities and this is a particularly troublesome quantity to determine experimentally. Discussion of this issue is well beyond the scope of this report. The interested reader can find a useful introduction to the problems in Zel'Dovich and Raizer (1967). Why our picture of the response of matter to high pressure shock waves is not complete without considerations of temperature is part of the subject matter of high pressure equations of state. A modern introduction to this topic from the point of view of shock wave physics is Avrorin, et al., (1993).

### 3.1.2 Measurement of the Shock Hugoniot

Experimental techniques for measuring states on the shock Hugoniot are necessarily demand precise time resolution capabilities (Nicholas and Rajendran, 1990). There are a variety of methods for measuring shock velocity and particle velocity, only one of which will be of direct interest to us in this report. The simplest, and in principle the most accurate, means of measuring such data uses smooth bore gun technology. In this particular technology, the experiment is almost exactly replicated in its major principles by the idealized experiment suggested in Figure 3.1. In other words, some type of high velocity gun is used to accelerate an *impactor* under conditions that control the state of the impactor and the geometry of the impact. The impactor is then allowed to strike a static material, called the *sample*, in a normal impact, just as depicted in Figure 3.1.

Brief descriptions of gun technology for performing shock wave experiments are given in Cable (1970) and Asay (1981). Multi-stage light-gas guns achieve the highest impact velocities to measure the Hugoniot for materials. Using high impedance impactors (see below) shock wave pressures of up to approximately a few megabars in aluminum are achievable by means of the controlled impacts these guns provide. Far greater shock wave pressures are achievable by other means, such as specially designed explosive systems (Al'tschuler, et al., 1996), high-power laser systems (Trainor, et al., 1979) and the use of underground nuclear explosions (Mitchell, et al., 1991; Trunin, et al., 1994).

The two-stage light-gas gun, invented in 1948, is the most common approach for achieving the highest controlled shock wave pressures in the laboratory. The operation of this instrument is briefly described in Cable (1970). As shown in Figure 3.3, the first “stage” of the gun is typically an explosively driven piston which compresses a volume of light gas, typically hydrogen for its very high sound speed. Upon compression the large pressures developed by the light gas burst a carefully manufactured diaphragm in the second “stage” of the gun, releasing the gas. At this point the gas becomes a working fluid, and serves to accelerate the impactor assembly (projectile) to velocities that can be greater than nine km/s depending upon the details of the design of the gun. Such projectiles are necessarily mass-limited, but are fully adequate in size to allow the acquisition of high accuracy quantitative shock wave data.

In real gas gun experiments, the projectile and sample assemblies are considerably more complex than we have suggested in the simple schematic of Figure 3.1. For one thing, it may be obvious to the reader that some craft is required simply to design projectiles that will withstand the enormous accelerations provided by the second stage of a two-stage gun and remain viable for generating accurate (uniaxial strain) shock wave data. Because the shock wave research community is also interested in understanding the response of materials to compressive loading waves which are more complex than the simple square wave that we have used to motivate the above analysis, projectiles (and sample configurations) are also designed to achieve these more complex goals. A discussion of these issues can be found in Asay, et al., (1985).

The simplest type of projectile that can be used to generate the Hugoniot data that we discuss in this paper is sketched in Figure 3.4. A plastic body, typically plexiglass or lexan, designed specifically to launch properly under the acceleration of the compressed hydrogen gas, is fronted with the working impact material, typically a metal. For the symmetric aluminum impacts of this paper, for example, the working impact material would be aluminum. Typically the diameter of this projectile is roughly 10 to 25 mm. The overall length of the simple projectile in Figure 3.4 in this case would be roughly four times that amount, and the thickness of the facing material would be on the order of one millimeter.

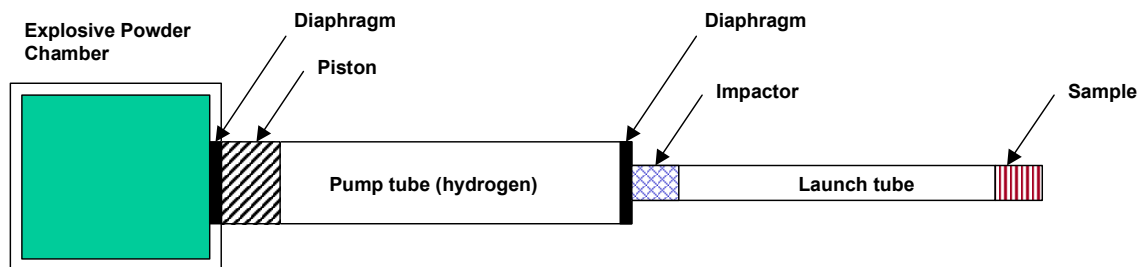


**Figure 3.3: Schematic of a two-stage light-gas gun, the modern instrument of choice for shock wave studies.**

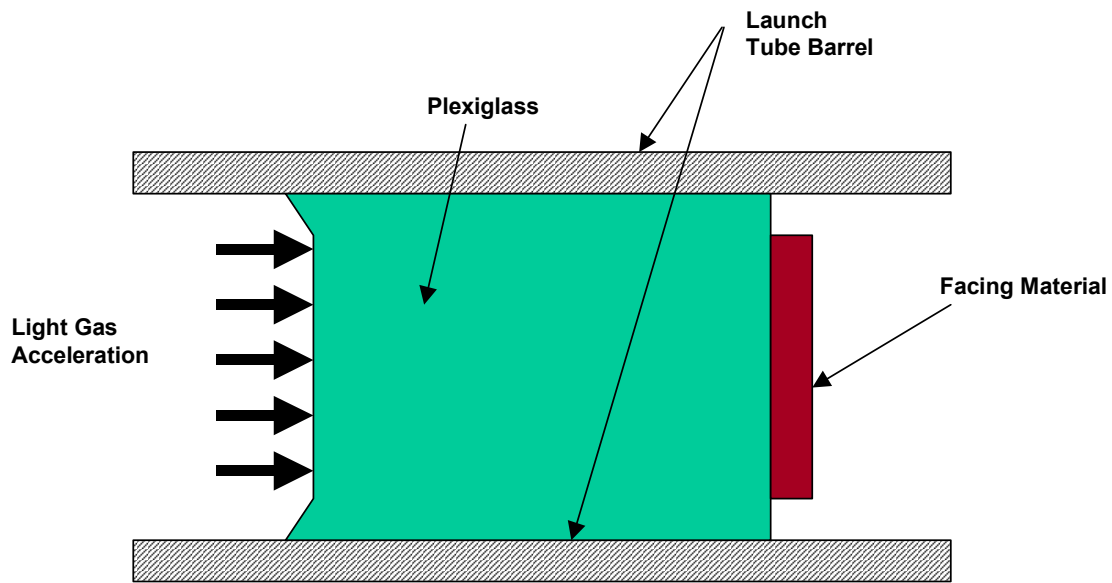


**Figure 3.4: Schematic of a realistic projectile used for shock wave studies on smooth bore guns.**

The impactor and sample specifics may deviate significantly from the simple schematic depicted in Figure 3.4, however. For example, it is typically the case to allow an impactor to be a different material than the sample. The reason for this is the strength of the shock is controlled by the shock impedance (product of sound speed and density) of the impactor as well as the sample. For example, aluminum-on-aluminum impacts for a given impact velocity will generate lower pressure (hence lower speed) shock waves than an iron impactor on an aluminum sample.

For the experimental data we discuss in this report, symmetric aluminum impacts could have been used to generate the data without being limited by maximum achievable velocities on two-stage gas guns. However, the data were in actuality gathered in explosive experiments in which the impactor need not have been aluminum, but a higher impedance material instead (Rice, et al., 1957; McQueen, et al., 1970; and Marsh, 1980). A conceptual view of the type of explosive system that could be used to generate these data is shown in Figure 3.5. Clearly such experiments need to be designed carefully to maintain integrity of the impactor and control of the impact conditions.

The schematic in Figure 3.4 suggests some of the constraints in performing even a simple shock wave experiment. For example, data acquisition should not take place over a time scale that is longer than the time for waves to propagate from the outer boundary of the projectile to the radial location of a measurement gauge. Also, upon impact the shock wave that is generated, which moves backwards into the projectile body, will eventually

pass through the boundary between the metal impactor and the plastic projectile body. This will generate a rarefaction wave, which propagates toward the impact region. The acquisition time should not be greater than the time it takes for this rarefaction to propagate into the measurement region.

Therefore, potential sources of uncertainty – hence deviation of actual experimental data from computational results predicated on a one-dimensional analysis – in the plate impact experiment include:

- Edge effects, which would cause the experiment to deviate from uniaxial strain. For example, if the geometry of the impactor/sample configuration had too small a radius, then rarefactions propagating from the outer radius would enter the region where shock velocity was measured, corrupting the data.
- Impact tilt, although this is a very small problem in modern gun operations. Steps are usually taken to measure impact tilt in situ. Data for which tilt is too great (a few milliradians) would be rejected. The presence of any tilt, of course, is in principle a fully three-dimensional impact problem. The argument that slight amounts of tilt do not corrupt the data is based mainly on empirical experience acquired over many years.
- Impact surface smoothness, which is essential for producing a steady state planar shock. If the surfaces are sufficiently rough, the generated shock wave will be temporarily unsteady and vary as a function of position across the surface area of the impact region, thus corrupting data acquisition.
- Structured (non-steady) shock waves resulting from more complex projectile designs (as discussed in Asay, et al., 1985). As we have stressed, the “perfect” wave for the present discussion is a step wave. Depending on the sample, and on the specific construction of the impactor, as well as the impact velocity, many deviations from a step wave may result. For example, if the impact velocity is sufficiently small, the loading shock wave will exhibit the two-wave structure characteristic of elastic-plastic materials.

We do not directly incorporate an analysis of these effects in this report, but the reader is advised to be aware of the fact that even gun driven plate impact experiments can be considerably more complex than discussed here.

We make one final comment on the matter of instrumentation for shock wave physics experiments. McQueen, et al., (1970) is particularly relevant to the type of experimental diagnostics that were utilized on the original explosive experiments that determined the shock wave data discussed in this report. That instrumentation was characteristic of the 1950's. The modern era is characterized by the evolution of highly accurate fast time-resolved instrumentation. Insight into the nature of these diagnostics can be found in Duvall and Graham (1977), Davison and Graham (1979), Asay (1981), Chhabildas (1987), and Graham (1993).

### 3.2 One Dimensional Impact of Aluminum on Aluminum: Experimental Data

The aluminum of specific interest in this report is 2024 aluminum (un-sintered), which is an alloy of aluminum with the following elemental composition (by atomic weight); aluminum (93.4%), copper (4.5%), magnesium (1.5%), manganese (0.6%). Our purpose is to compare a computational construction of the Hugoniot for this material with that reported experimentally in Marsh (1980). Our approach to the calculation is fully defined in Figure 3.1, capturing the substance of the actual experiment as we described above. Our computations will treat each experimental  $U_S - U_P$  point as having been generated by an appropriate symmetric impact of 2024 aluminum on 2024 aluminum. As discussed in Section 3.1.1, this simplified “experiment” (and such an experiment could actually be performed with a gun) is defined by an impact velocity  $U_I$  that is twice the reported particle velocity for the specific data point given in Marsh’s compendium.

The experimental data we are concerned with for 2024 aluminum are reported in Table 3.1. A particle velocity of 278 m/s is the smallest reported in Table 3.1. The corresponding impact velocity of 556 m/s is required for the symmetric impact that should reproduce this data point. Similarly, 4.041 km/s is the highest reported value of particle velocity, and an impact velocity of 8.082 km/s is required to reproduce this point. (This value is at the upper limit of performance for a two-stage light-gas gun, illustrating why higher impedance impact materials are desirable for generating such data.)

The R-H relations (3.2) can be used to determine that the lowest impact velocity in the data we analyze produces a shock wave having a pressure of approximately 44 kbars, which is a factor of more than fourteen times the yield stress of 2024 aluminum. In this case, therefore, we accept without further discussion that the aluminum can be accurately modeled as a fluid rather than as an elastic solid. The equation of state of the aluminum thus becomes the only important constitutive description in the problem. At all other data points in Table 3.1 the pressure is higher, so this modeling assumption is made for the entire range of data that we discuss. (A future study, of course, should be performed to also demonstrate the truth of this assumption.)

As suggested by equations (3.2), if both final particle velocity and shock velocity are measured in an impact experiment then the Hugoniot state of the sample is defined. A significant amount of work has been performed where the impactor is a so-called **shock standard** (McQueen, et al, 1970). For such a material, independent experimental studies have carefully defined that material’s Hugoniot. When such a standard material is used as an impactor, only the shock velocity needs to be measured in an experiment with a differing sample material. This is because the pressure can be inferred from the known Hugoniot of the impactor, and the continuity of Hugoniot pressure across the impact interface. This has historically been an experimental approach of great significance, especially for ultrahigh pressure shock wave measurements. For instance, this technique is dominant in the ultra-high pressure explosive experiments reported in Al’tshuler (1996).

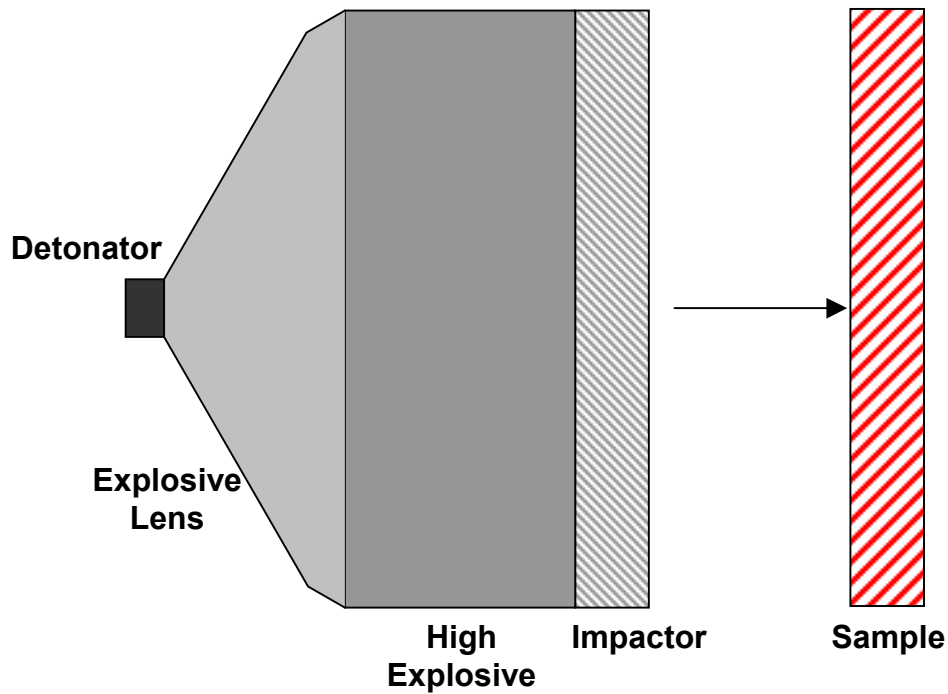


**Figure 3.5: Explosive-metal geometry feasible for performing shock Hugoniot measurements.**

For symmetric impacts, careful measurement of the impact velocity and shock velocity through embedded diagnostics or rear-surface shock breakout timing diagnostics provide a  $U_S - U_P$  pair for that experiment. For explosive systems, such as that presented in Figure 3.5, even if the impact were symmetric it is not as simple to measure impact velocity as for gun experiments. In general, though, standards are used in explosive experiments, further complicating the measurement process. Then, either the pressure must be directly measured or the particle velocity behind the shock wave must be directly measured. Embedded gauges can measure pressure up to specified limits (Graham, 1993). But for very high pressures particle velocities turn out to be easier to measure directly using a technique that we describe below.

High accuracy time-resolved diagnostics, such as laser velocity interferometry, were not available during the period of time when most of the classic shock wave data summarized in Marsh (1980) were collected. The following approach for gathering data requires no assumptions about the nature of the impactor. The time of arrival of the shock wave at various points within or on the back of the sample in the explosive configuration depicted in Figure 3.5 was monitored through pin-contactors or optical techniques (Rice, et al, 1958; McQueen, et al, 1970), thus providing a measurement of  $U_S$ . These data also confirm the planarity of the shock wave, a necessary condition for validating the uniaxial strain condition. To measure  $U_P$  the location of the rear surface of the sample is monitored (also through pin-contactors or optical techniques) to measure its free surface

velocity upon breakout of the shock wave. The free surface velocity is the sum of the particle velocity due to the shock wave,  $U_P$ , and the particle velocity due to the resulting reflected rarefaction wave created by the intersection of the shock wave with the free boundary of the sample. Since each of these waves has approximately the same particle velocity (see Rice, et. al., 1958; McQueen, 1970), the free surface velocity is approximately twice the particle velocity  $U_P$ , thus providing an estimate of the particle velocity. Marsh (1980) describes the approach that is used to correct for small inaccuracies in this method of particle velocity determination.

By repeating the experiments using explosives designed to deliver different impact velocities, hence different amplitude shock waves, the  $(U_P, U_S)$  points (hence density, pressure and internal energy via the R-H conditions) on the Hugoniot curve are measured. While these data are not valid off the Hugoniot curve, they can be and are used to calibrate equation of state models for states near this curve (Rice, et al., 1958). We will say more about this below.

Table 3.1 presents  $(U_P, U_S)$  data for 2024 aluminum taken from several references in the research literature as tabulated in Marsh (1980). As mentioned above, the lowest pressure data point corresponds to an approximate pressure of 44 kbars on the Hugoniot, while the highest pressure point corresponds to an approximate pressure of 427 kbars. This pressure is well below the Hugoniot melt transition for aluminum (approximately a Hugoniot pressure of 1.3 Mbars). Thus, the melting transition does not enter any of our considerations of the comparison of computational and experimental data in this report. A plot of these data is given in Figure 3.6. Note that there is a strong linear relation between the shock speed and the particle speed. We will stress at this point, and again below, that this linearity is an empirically measured relationship. Also note that there appears to be little scatter in the data, illustrating the repeatability of the experiments from different sources. It is important to note that the error bars for individual experiments for these data are likely to be smaller than the symbols used in Figure 3.6, while differences between individual experiments are larger. The experimental variability appears to increase at higher impact velocities, suggesting either instrumentation response issues or experimental control issues are becoming more important in data acquisition.

Because of their quality and quantity, these data will be used to demonstrate model validation methodology for a one-dimensional shock wave model. These data are natural candidates for testing statistical validation methodologies that are aimed at shock wave physics codes. But the reader should realize that the quantity and quality of shock Hugoniot data rapidly decrease in the ultrahigh pressure regime. For example, in very carefully designed experiments utilizing an underground nuclear explosion, Mitchell et al (1991) achieved  $(U_P, U_S)$  data for aluminum with error bars of approximately 1% for  $(U_P, U_S) \sim (17.5 \text{ km/s}, 28 \text{ km/s})$ . These data correspond to a Hugoniot pressure of 13.3 Mbars, a Hugoniot density of about 2.7 times normal density. The reported error is larger than would be reported for experiments with current gun technology and diagnostics. And the experiment is virtually unique – no repeat of the data point is likely for the

**Table 3.1: Hugoniot Data for Aluminum 2024: All speeds are in m/s**

<i>Up</i>	<i>Us</i>	<i>Up</i>	<i>Us</i>	<i>Up</i>	<i>Us</i>	<i>Up</i>	<i>Us</i>	<i>Up</i>	<i>Us</i>
278	5811	859	6445	1318	7062	2206	8231	3287	9642
279	5782	859	6470	1352	7092	2306	8396	3293	9758
440	6021	860	6446	1362	7143	2327	8358	3297	9721
472	6054	862	6472	1362	7139	2335	8421	3347	9775
497	6025	863	6486	1383	7225	2371	8436	3361	9751
502	6098	864	6418	1426	7268	2446	8570	3376	9803
503	5996	865	6518	1432	7228	2449	8529	3376	9746
507	6055	871	6561	1437	7156	2467	8699	3381	9670
509	5947	873	6522	1445	7268	2477	8618	3387	9609
509	5953	888	6541	1446	7211	2595	8829	3395	9821
608	6125	891	6589	1461	7269	2604	8762	3400	9916
609	6103	892	6442	1465	7295	2604	8748	3406	9872
626	6262	896	6589	1467	7305	2605	8744	3419	9866
627	6228	897	6579	1479	7266	2608	8664	3463	9654
650	6226	901	6402	1481	7268	2641	8848	3472	9697
671	6164	910	6530	1498	7342	2645	8797	3481	9727
677	6277	910	6534	1539	7366	2650	8803	3487	9732
722	6367	953	6616	1557	7462	2664	8724	3500	9870
727	6323	953	6617	1558	7444	2671	8764	3508	9861
728	6310	966	6659	1568	7413	2687	8853	3508	9880
768	6348	975	6607	1574	7479	2709	8792	3538	9880
778	6388	979	6560	1574	7426	2710	8816	3563	10117
786	6312	988	6507	1578	7326	2735	8909	3618	10040
790	6304	990	6490	1588	7416	2738	8916	3629	10238
792	6314	1081	6824	1605	7407	2817	9144	3658	9876
792	6365	1107	6779	1617	7508	2878	8971	3680	10113
793	6308	1110	6844	1722	7678	2911	9070	3717	10190
798	6418	1116	6843	1728	7596	2935	9231	3718	10388
798	6342	1119	6846	1728	7612	2974	9236	3736	10138
799	6353	1121	6840	1728	7615	2987	9401	3745	10162
800	6393	1124	6818	1742	7690	3030	9177	3748	10370
800	6459	1128	6756	1744	7616	3031	9180	3772	10458
802	6397	1130	6823	1770	7659	3035	9198	3777	10409
802	6355	1134	6826	1779	7758	3081	9317	3778	10431
802	6393	1136	6831	1812	7775	3086	9317	3786	10341
803	6432	1141	6795	1851	7690	3108	9228	3930	10552
803	6432	1144	6783	1858	7850	3148	9446	3966	10513
805	6394	1146	6861	1939	7773	3148	9369	3967	10384
809	6422	1157	6893	1948	7973	3181	9596	3983	10611
809	6422	1157	6752	1957	8054	3187	9549	3988	10572
818	6366	1159	6915	1959	8015	3217	9365	3991	10542
831	6436	1206	6857	2095	8114	3225	9666	4001	10572
833	6483	1220	6981	2096	8076	3238	9762	4026	10631
839	6419	1220	7014	2130	8127	3251	9409	4041	10572
850	6415	1260	6955	2154	8149	3260	9477		
854	6443	1263	6938	2154	8150	3269	9426		
858	6488	1277	6943	2156	8332	3274	9617		

foreseeable future. Vladimirov, et al., (1984) report aluminum Hugoniot data that correspond to Hugoniot pressures of approximately 4000 Mbars and densities five times greater than normal. These data were again gathered utilizing an underground nuclear explosion and are unique. Also, the error bars are significantly larger than in the work of Mitchell and his colleagues. Finally, we point out that the techniques described by Al'tshuler (1996) achieve reported Hugoniot pressures of tens of Mbars, yet the accuracy of these data has been a source of controversy in the United States shock wave community for decades.

### 3.3 One Dimensional Impact of Aluminum on Aluminum: The Model

We use the Sandia Eulerian shock wave physics code CTH, which is described in McGlaun, et al. (1989) and Bell et al. (1998), to simulate the one-dimensional impact of 2024 aluminum on 2024 aluminum illustrated in Figure 3.7. Two equation-of-state models (EOS) are applied in this report (Hertel and Kerley, 1998). The first is a SESAME model for pure aluminum, SESAME 3700, which is a tabular EOS data. The second is the Mie-Grüneisen analytic model.

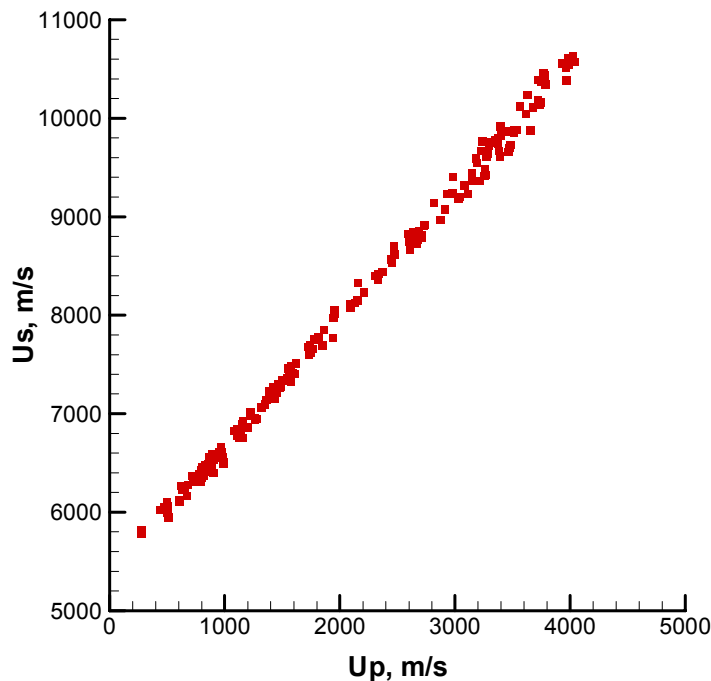


**Figure 3.6:** Hugoniot Data for Aluminum 2024:  $U_P$  – particle velocity,  $U_S$  – shock velocity (from Marsh, 1980)

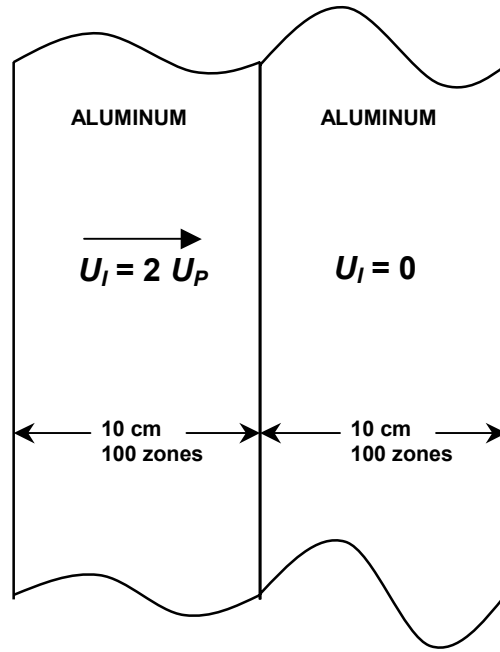


**Figure 3.7: One Dimensional CTH Model: Impact occurs at time = 0.**

The linearity of the locus of  $U_P - U_S$  states on the Hugoniot is widely observed in most materials, including the aluminum alloy of concern to us here (Marsh, 1980), but it is *not* universal. For example, cesium has a slight quadratic trend in this locus that is apparent at moderate pressures (less than several megabars). Other materials that show deviation from linearity at moderate pressures are compounds such as nylon and silastic, as well as water. “Linearity” of the  $U_P - U_S$  relationship in the Hugoniot state is not a fundamental consequence of simple material behavior. Rather, it is one particularly simple manifestation of complex, non-linear material behavior. It is important to keep this in mind during our discussion of the implications of comparing computational predictions of the linearity of this locus with experimental observations.

It is also important for the reader to understand how the linearity of the relationship between  $U_P$  and  $U_S$  may be used in the modeling we discuss. CTH calculations utilize a general equation of state (EOS) to describe the response of aluminum to the impact and subsequent propagation of a shock wave. It is hopefully clear at this point that the linearity of the particle velocity and shock velocity on the Hugoniot has its origin in more than simply the equation of state of a material. The dynamics has entered into this relationship because the Hugoniot implicitly is an artifact of the conservation laws. Thus, under any circumstances, CTH calculations that “predict” linearity of the particle velocity – shock velocity on the Hugoniot are expressing more than the simple encoding of this behavior in the constitutive model used by the calculations.

In addition, the equations of state which are commonly used in shock wave physics codes – and certainly in CTH – are called *semi-empirical*. This means that experimental data are used to calibrate the theoretical model for higher accuracy. In particular, below we will illustrate the use of the observed linearity of the Hugoniot  $U_P - U_S$  data in calibrating the two models we use in our studies: the Mie-Grüneisen EOS and the SESAME table. Because the EOS's are calibrated using the observed  $U_P - U_S$  data does not mean that we have therefore built that linearity into our calculations. If that were true there would be no point in performing this study. In fact, linearity of the computational  $U_P - U_S$  data is, if it is observed, fully a consequence of the material description *and* the numerical solution of the conservation laws. This is why asking the question of how a calculation may compare with these data is relevant to begin with. It is indeed true that if we expect to accurately calculate more general shock wave problems we must certainly reproduce the Hugoniot data with relatively good accuracy, or we will have little hope of performing reasonably accurate calculations in more difficult circumstances. This, of course, is why we refer to the present effort as being a *validation* study.

The SESAME EOS that we utilize is 3700, which is a tabular form of an equation of state for pure aluminum developed by Kerley (1987). (An alternative SESAME EOS for aluminum has been described by Holian, 1986.) One important component in an equation of state is an expression for the cold curve (0 Kelvin isotherm) of the material. Kerley's tool for developing an EOS, PANDA (Kerley, 1988), allows a theoretical approximation to the cold curve to be developed from knowledge of the empirical particle velocity – shock velocity Hugoniot relationship (including quadratic dependencies). As documented (Kerley, 1987), however, an analytic approximation for the cold curve was employed instead that was in agreement with zero temperature band theory calculations for aluminum. Thus, for the SESAME model we apply in the calculation in this paper, no direct use of the empirical linear Hugoniot data was made at all in its construction.

The other model we use is the Mie-Grüneisen EOS (see McQueen, et al (1970) for a brief introduction to this model). The Mie-Grüneisen EOS is by no stretch of the imagination as general as the SESAME EOS tables described above. In its most general form, the EOS expresses pressure as a function of density and internal energy in the following form:

$$P - P_{\text{ref}}(\rho) = \Gamma(\rho) \rho (e - e_{\text{ref}}) \quad (3.4)$$

$\Gamma(\rho)$  is called the *Grüneisen parameter*. Equation (3.4) is basically a Taylor approximation to the equation of state of a material when the anticipated thermodynamic state is “not too far” from a reference condition (expressed by the subscript “ref” in (3.4)). For compressive shock problems, it has been observed for many years that (3.4) produces computationally useful, somewhat accurate (depending on circumstances) EOS results by allowing the reference state to be the Hugoniot of a material. Since Hugoniots are typically known empirically, such a model necessarily rests on that empirical foundation. The question of whether the model can successfully reproduce that empirical foundation in computational studies is a focus of the current report.

Assuming linearity of the Hugoniot  $U_P - U_S$  we write

$$U_S = C_0 + sU_P \quad (3.5)$$

Then the appropriate reference states for use in (3.4) are written as  $P_H$  and  $E_H$  and are given by (from the R-H conditions)

$$P_H = \frac{\rho^0 C_0^2 \left(1 - \frac{\rho^0}{\rho}\right)}{\left(1 - s \left(1 - \frac{\rho^0}{\rho}\right)\right)^2} \quad (3.6)$$

$$E_H = \frac{P_H \left(1 - \frac{\rho^0}{\rho}\right)}{2\rho^0}$$

We intend to perform one assessment of the accuracy of this model in the present circumstances by comparing its predictions with the Hugoniot data in Table 3.1. We certainly expect the results to be reasonably accurate, since the data do not represent extreme deviations from the reference state we use in the construction of the model. But it is apparent that this model will not accurately reproduce a “linear” Hugoniot for all densities. This is because there is a singularity in the prediction of the Hugoniot pressure in (3.6) when  $\rho = s\rho^0/(s-1)$ . For aluminum, this represents a compression of approximately four. (Recall from Section 3 that Vladimirov and his colleagues claim to have achieved states on the Hugoniot where compression by a factor of five was achieved!) The Mie-Grüneisen EOS would fail in attempts to reproduce observed linearity of the Hugoniot in this region for aluminum, even though it might appear that we have somehow “built in” that linearity.

CTH does not provide shock wave speed directly because it is not a primary code variable. It must be constructed from calculation data. Thus, we monitor the predicted velocity of a particle initially located 4 cm from the impact face in the stationary aluminum plate to evaluate the time of arrival of the shock. We define this time as the time at which the particle velocity jumps to half the anticipated particle speed  $U_P$ . The corresponding shock speed is the distance traveled (4 cm) divided by the time of arrival. The algorithm used to do this is discussed in Appendix A.

A copy of a CTH input file is listed in Appendix B for a typical impact velocity. This file includes all of the necessary information for independent setup and execution of the calculations reported in this report. A script was written to modify this input file  $n$  times (once for each impact velocity modeled), run the appropriate modules of CTH, and

append the results to a results file. After the  $n$  runs are complete, a post processor is used to evaluate the shock speed,  $U_S$ , for each of the  $n$  runs to provide  $U_S$  as a function of  $U_P$ . Details of this process are discussed in Appendix A. The results of these shock wave speed predictions, using the SESAME EOS model for the 232 values of  $U_P$  listed in Table 3.1, are plotted in Figures 3.8 and 3.9 for two different grid resolutions. The experimental data are also shown. Note that there are very slight differences in the predictions using these two grid resolutions (0.1 and 0.05 cm) and these differences are very small compared to the scatter in the experimental data. Because of this, we will use the lower-resolution predictions for the analysis presented in the remainder of this report. We are not claiming that this observation represents a grid convergence study. Under other circumstances such a study would be performed independently of the work we report here.

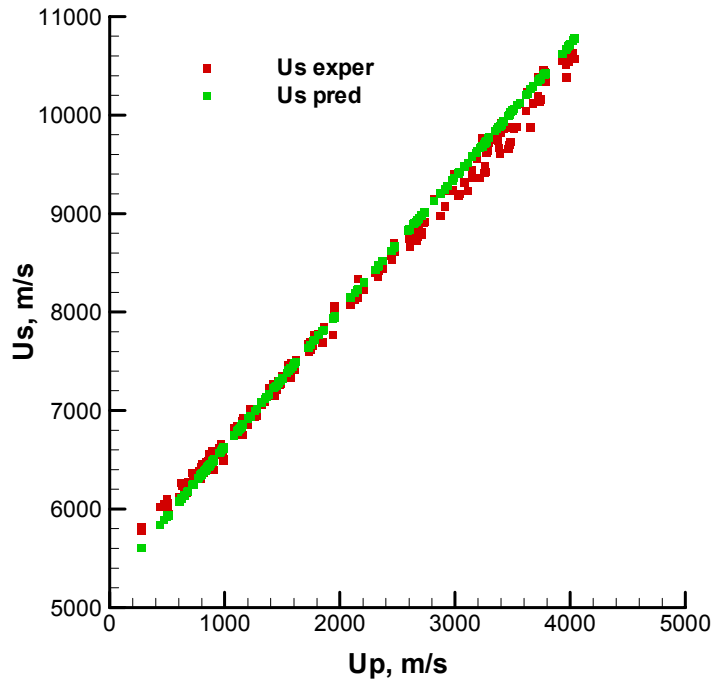


**Figure 3.8: Prediction vs. Experiment - Low Resolution Results: 100 cells across each aluminum plate, SESAME AL2024 EOS model. (The computational data is presented in Table D1.)**

We conclude this section by stressing one more point. The issue of full theoretical understanding of the basis for the apparent linearity in  $U_P - U_S$  on the Hugoniot has been somewhat thorny. We will not attempt to summarize work on this problem here. The  $U_P - U_S$  relationship on the Hugoniot is well known to deviate from linearity in the presence of phase transitions (Duvall and Graham, 1977). However, we have already suggested

that for the range of aluminum data we are considering phase transitions are not important. But even in the absence of phase transitions, a fundamental explanation for the observed linear  $U_P - U_S$  Hugoniot relationship is incomplete. Most recently, in fact, Johnson (1996, 1997) has suggested that the theoretical  $U_P - U_S$  Hugoniot relationship is in fact *bilinear*. We will stress one more time – linearity in the  $U_P - U_S$  Hugoniot data is not trivial, either experimentally or theoretically. Neither is such linearity directly built into shock wave physics codes as some kind of constraint. Therefore, the work that follows is not mainly about simply fitting a linear code model to a linear data collection.

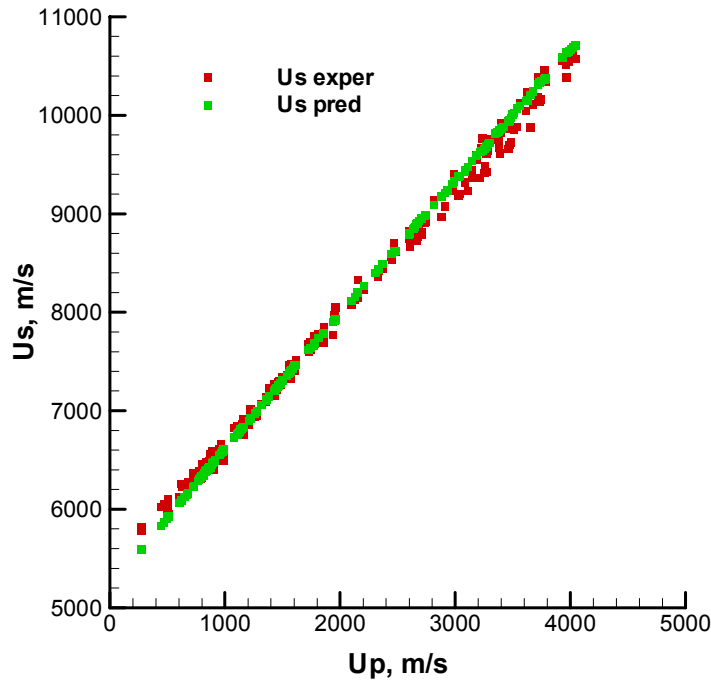


**Figure 3.9: Prediction vs. Experiment - High Resolution Results: 200 cells across each aluminum plate, SESAME AL2024 EOS model.**

### **3.4 Two-Dimensional Impact of Aluminum on Aluminum: The Application**

A common feature of model validation is that the desired application of the model may not be exactly represented by the validation experiments. For example, we may intend to use a predictive model to compute the arrival time of a shock wave in a two-dimensional geometry. However, our model validation experiments may only measure shock wave speed as a function of particle velocity for a one-dimensional geometry. Alternatively, we may have data to test our model over a large range of model parameters. But our application may only require that the model be valid over a small range of model parameters. In Chapter 5, we develop methodology to define validation metrics based on specific applications. To demonstrate this methodology, we must first choose a particular

application illustration. Here we consider our application to be the impact of a small 2024 aluminum cylindrical slug on a larger diameter 2024 aluminum plate at 6 km/s as shown in Figure 3.10. This application is two-dimensional since we can assume radial symmetry. The impact will result in a shock moving into the larger diameter plate with particle velocities that decrease with distance into this plate. Edge effects and decay of the propagating shock wave cause this reduction. Our validation experimental data clearly excluded these effects. Hence, this is indeed an interesting contrast and extension with respect to the validation experiments we use. Figures 3.11 through 3.14 show the progression of the material deformation and the progression of the shock wave through the large target plate as predicted by CTH. (Note that these figures have horizontal and vertical axes with differing lengths.) The CTH input file for this calculation is listed in Appendix C. Note that a shock wave propagates through the large plate at speeds considerably greater than the penetration speed of the smaller slug. Also note that the particle speeds calculated near the back of the target plate are considerably less than the projectile impact speed due to the geometric effect of the diverging shock, which is non-steady in this application. We will take the time at which the back surface particle speed reaches 0.25 km/s as our decision variable to focus validation for this application.

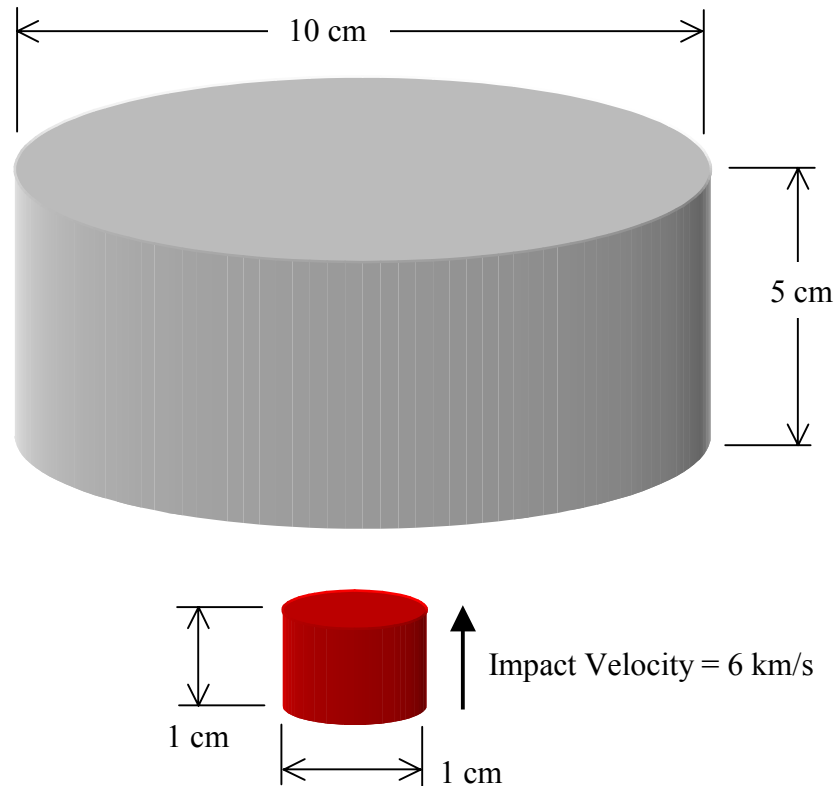


**Figure 3.10: Impact of Small Aluminum Slug on a Thick Aluminum Plate**

### 3.5 Summary

In the following chapters, we take several approaches to develop measures of model validity based on the model predictions and the experiment observations shown in Figure 3.8. One approach utilizes the data in Figure 3.8 directly to develop a statistical model for uncertainty. The other two approaches use propagation of uncertainty analysis to develop this statistical model. In addition, the third approach uses the application defined in Section 3.4 to further refine our definition of the validation metric. This last approach has the advantage that the validation metric is specifically designed for an anticipated application. We believe that application dependence will be a paradigm for the construction of quantitative validation metrics. The disadvantage is that each new application requires a redefinition of the validation metric.

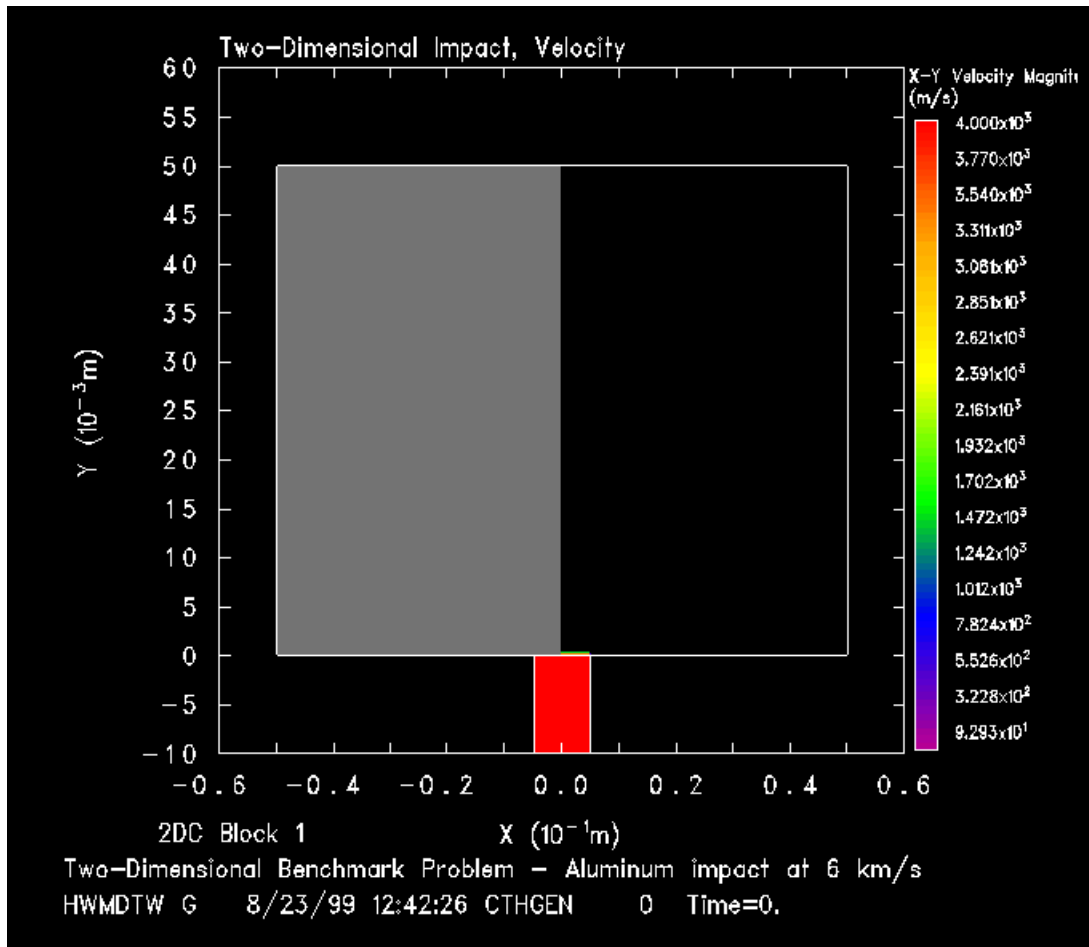


**Figure 3.11: CTH Predictions at Time=0: Left half of plot illustrates material locations; Right half of plot represents the magnitude of the particle velocities.**

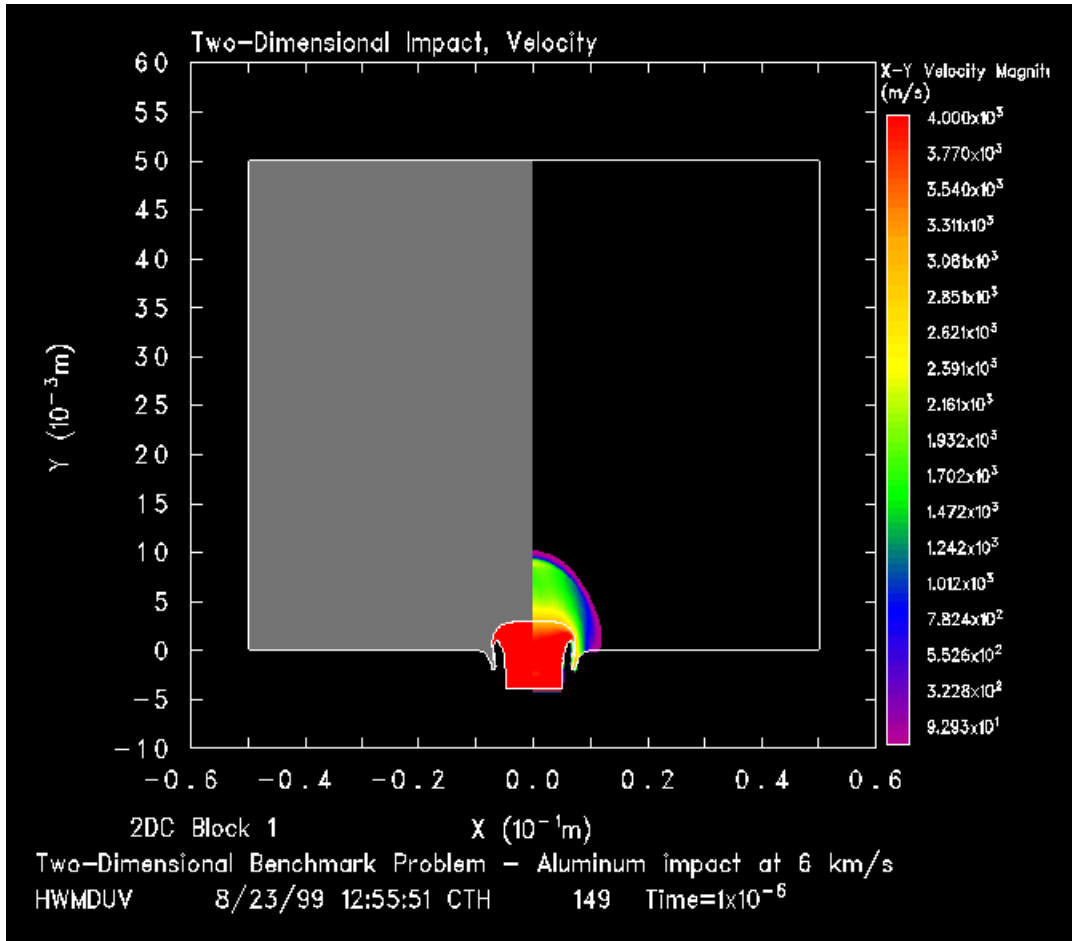


**Figure 3.12:** CTH Predictions at Time= $1.0 \mu$  sec: Left half of plot illustrates material locations; Right half of plot represents the magnitude of the particle velocities.

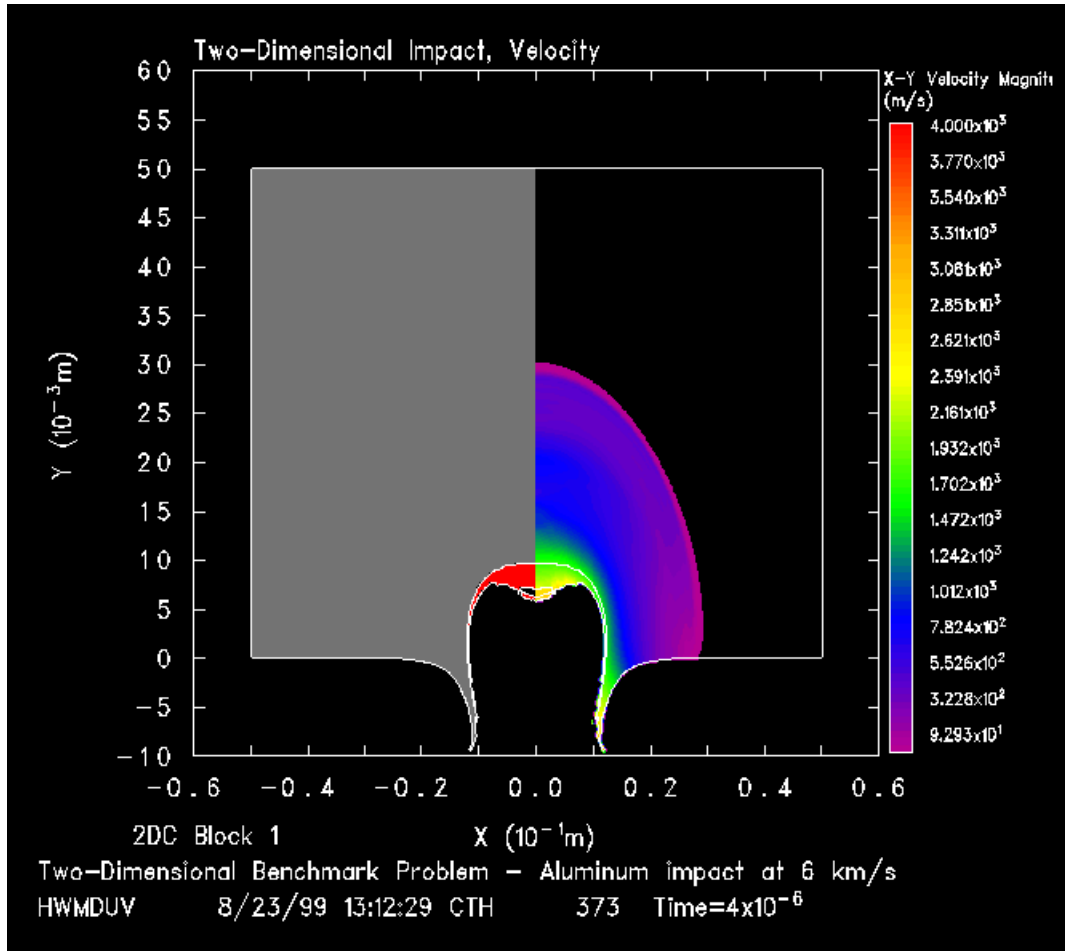


**Figure 3.13:** CTH Predictions at Time= $4.0 \mu$  sec: Left half of plot illustrates material locations; Right half of plot represents the magnitude of the particle velocities.

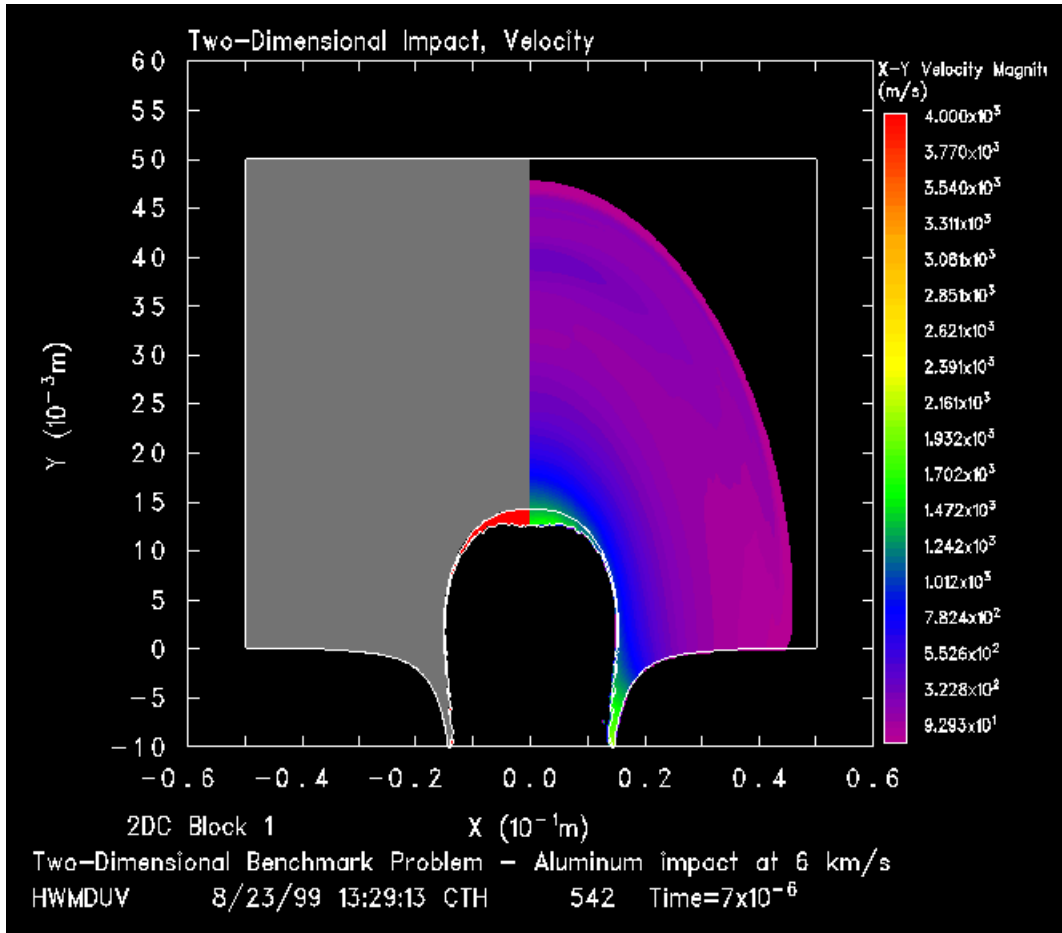


**Figure 3.14:** CTH Predictions at Time= $7.0 \mu$  sec: Left half of plot illustrates material locations; Right half of plot represents the magnitude of the particle velocities.

(Page Left Blank)

## 4.0 Model Validation using Standard Statistical Methods

### 4.1 Introduction

Figure 4.1 shows the CTH model predictions for shock wave velocity as a function of particle speed (i.e., half the impact velocity) for the SESAME EOS model, and the corresponding experimental measurements (this figure is a repeat of Figure 3.6). Clearly, the model over-predicts the experimental observations for larger values of  $U_p$ . Are the differences between model predictions and experimental observations statistically significant relative to the uncertainty in the validation exercise? To answer this question, we must first develop a model for the uncertainty in the prediction differences (i.e., predicted measurements minus experimental measurements for a given particle velocity).

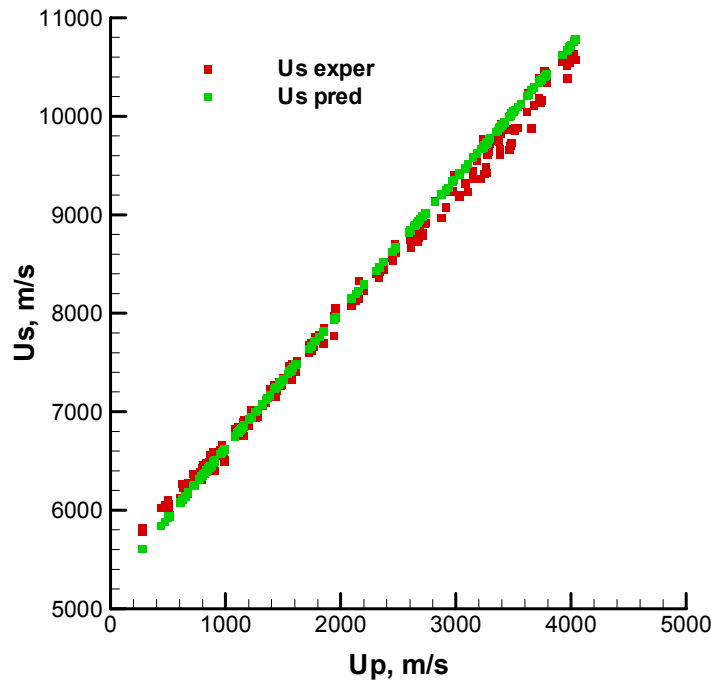


**Figure 4.1:** Prediction vs. Experiment for the Shock Wave Experiments, SESAME AL2024 EOS model.

We begin the process by noting from Table 3.1 of the previous chapter that we have very few repeated measurements of  $U_S$  for each  $U_P$ . Because of this, we do not have enough data to develop a statistical model for the prediction differences for each  $U_P$ . However, we may be able to develop such a model using the data for all  $U_P$  if certain statistical assumptions are valid. The usual procedure is to assume that the differences are independent and that the structure of the differences for each  $U_P$  is the same across all  $U_P$ . For example, if the differences are well modeled by a normal distribution, then we assume the distribution to have a uniform mean and standard deviation for all values of  $U_P$  and we assume independence of the prediction differences for different values of  $U_P$ . If these assumptions are valid, then we can use the prediction differences at all the  $U_P$  to estimate the corresponding mean and standard deviation for the normal distribution of differences for each  $U_P$ .

Unfortunately, inspection of Figure 4.1 suggests that the assumption of a uniform mean and standard deviation across all  $U_P$  does not appear to be valid since there is a very clear drift in the model predictions from the experimental results. We must either use nonparametric methods, which do not require as many assumptions about the probability distributions, or we must attempt to remove the drift. We start with a nonparametric approach.

## **4.2 Nonparametric Methods**

Nonparametric methods do not require that the underlying probability distributions be well characterized. They also do not require that properties of the probability distributions, such as a standard deviation, be uniform for different data locations (i.e., for different values of  $U_P$  for our case). The disadvantage of nonparametric methods is they are not as efficient as parametric methods (Miller and Freund, 1985). Parametric methods are more likely to accept a bad model as valid because they effectively give a larger benefit of doubt to a model before it can be rejected.

Here we will use the sign test (Brownlee, 1965; Miller and Freund, 1985) to test whether the median of the prediction differences for all of our data is zero. The sign test is useful since we have a natural pairing between the experimental and the prediction data (i.e., one predicted value for each experimental value) and since the test does not require that the standard deviation be uniform across the data. Note that this test says nothing about the ability of the model to predict shock wave speed as a function of particle speed. It only tests the median predictive capabilities of the model. However, if a model fails this test, then there is generally little chance that it will pass the more difficult tests of predicting shock wave speed as a function of particle speed.

We begin by assuming that a valid model is as likely to over predict shock wave speed as to under predict shock wave speed, and use the sign test to evaluate whether the data supports this assumption. We begin by taking the difference between the predicted shock speed and the measured shock speed for each prediction/measurement pair, and count the

number of positive and the number of negative results. Prediction/experimental pairs with zero differences are discarded. We then use the binomial distribution to evaluate the probability of these many positive differences relative to the total number of non-zero differences, given that our distribution is symmetric. The associated cumulative probabilities for the binomial distribution are tabulated in most statistical textbooks (for example, Miller and Freund, 1985). For a large number of data points ( $n > 20$ ), the binomial distribution is well approximated by the normal distribution with the appropriate transformation. Since we have 232 measurements, we will use this approximation here. The appropriate transformed normally distributed test statistic is (Miller and Freund, 1985)

$$Z = \frac{x - np_0}{\sqrt{np_0(1 - p_0)}} \quad (4.1)$$

where  $p_0=0.5$  for a symmetric distribution,  $x$  is the number of positive differences, and  $n$  is the total number of nonzero differences. The results of the sign test for our data are presented in Table 4.1.

**Table 4.1: Statistics for the Sign Test**

$U_{s\_pred} - U_{s\_exper}$		<i>N</i>
	Negative Differences	102
	Positive Differences	130
	Ties	0
	Total number of non-ties	232

Test Statistic  $Z = 1.773$   
Significance (two-tailed) = 0.076

The probability of obtaining a  $Z$  greater than 1.773 is 7.6%. Therefore, the probability that an experiment with 232 samples would produce 130 positive differences, assuming that we should have as many positive differences and negative differences, is 7.6%. If we desire to incorrectly reject a valid model only 5% of the time, then because 7.6% is greater than 5%, we do not have sufficient evidence to reject the hypothesis that the model over predicts as often as it under predicts. Therefore, this test does not provide sufficient evidence to reject the model as valid.

Inspection of Figure 4.1 clearly indicates that the model does tend to over predict at least as often as it under predicts. However, the results of Figure 4.1 also indicate that the model may not do an adequate job of predicting  $U_S$  as a function of  $U_P$ . We test this hypothesis in the next section.

### 4.3 Functional Dependence of $U_s$ on $U_p$

Inspection of Figure 4.1 indicates that the model predictions and the experimental observations of shock wave speed appear to be different linear functions of particle velocity. One possible method to test the model is to use linear regression to estimate the corresponding slope and intercept of both the experimental and the predicted data and compare the results. This method is applicable if the functional dependence of the measurements and predictions on the independent parameter ( $U_p$  in this case) are both linear. A more general approach is to plot the experimental shock wave speeds against the corresponding model predictions of the shock wave speeds as shown in Figure 4.2. This does not require separate regression on the model and experimental data.

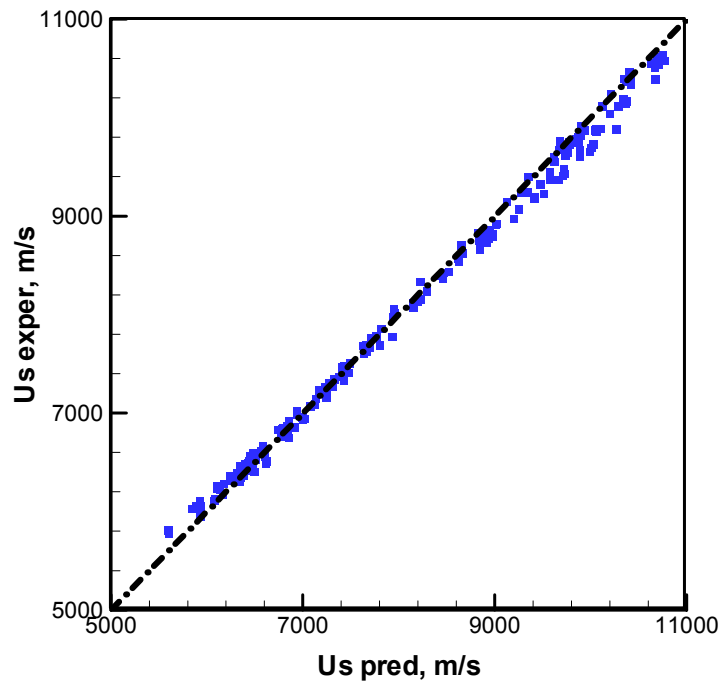


**Figure 4.2:** Scatter Plot of Experimental vs. Predicted Shock Wave Speed:  
Dashed line is  $U_{s\_exper} = U_{s\_pred}$ .

Data from a model that predicts the experimental data perfectly plotted this way will lie on a line with intercept of zero and slope of one. This will be true for both linear and nonlinear models. Reckhow et al. (1990) suggests that linear regression be used to fit a line to this data and statistical inference be used to evaluate whether this line has an intercept of zero and a slope of one. The results of performing such a regression on our data are shown in Figure 4.3. Note that the regression line (solid) does not line up with the perfect model (dashed) line and the intercept is not zero and the slope is not one. Are

these values significantly different from zero and one? To answer this question, we must first develop a probability model for the regression residuals.

The regression residuals ( $Us\_exper$  as measured –  $Us\_exper$  as predicted by the regression line) are shown in Figure 4.4. Note that the mean of these residuals appear to be distributed about zero for all  $Us\_pred$ . Also note that there does appear to be some variation in scatter of the residuals as a function of  $Us\_pred$ . However, this variation is small relative to the size of the  $Us\_exper$  (roughly less than 4% of given values of  $Us\_exper$ ) and we will assume that these residuals have a uniform standard deviation as a function of  $Us\_pred$ . A histogram of the regression residuals is shown in Figure 4.5. The equivalent normal distribution (using the mean and standard deviation as estimated from the residuals) is also shown in Figure 4.5 for comparisons. The results of the histogram suggest that the residuals are normally distributed. However, we can test this rigorously using a Kolmogorov-Smirnov test (Miller and Freund, 1985).

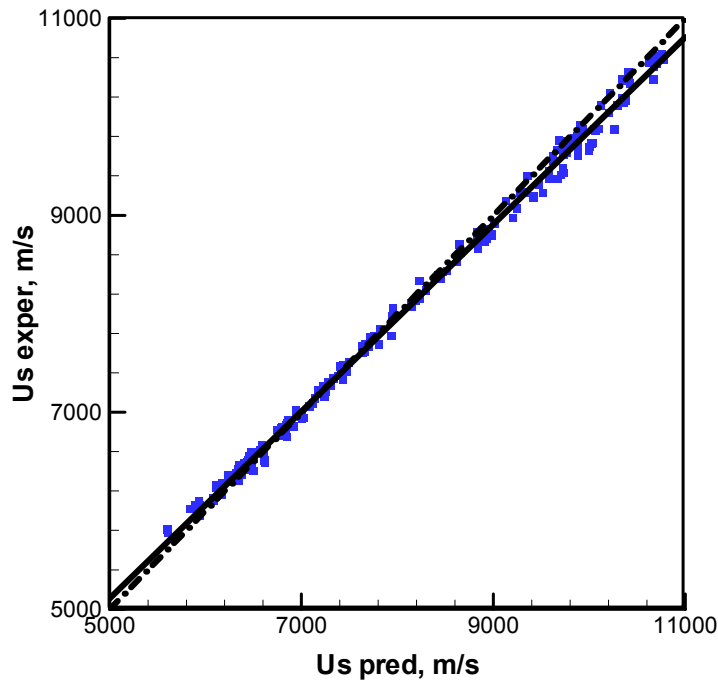


**Figure 4.3:** Scatter Plot of Experimental vs. Predictions Shock Wave Speed: Dashed line is given by  $Us\_exper = Us\_pred$ ; Solid line is the regression ( $Us\_exper = 0.950 Us\_pred + 360.2$ ).

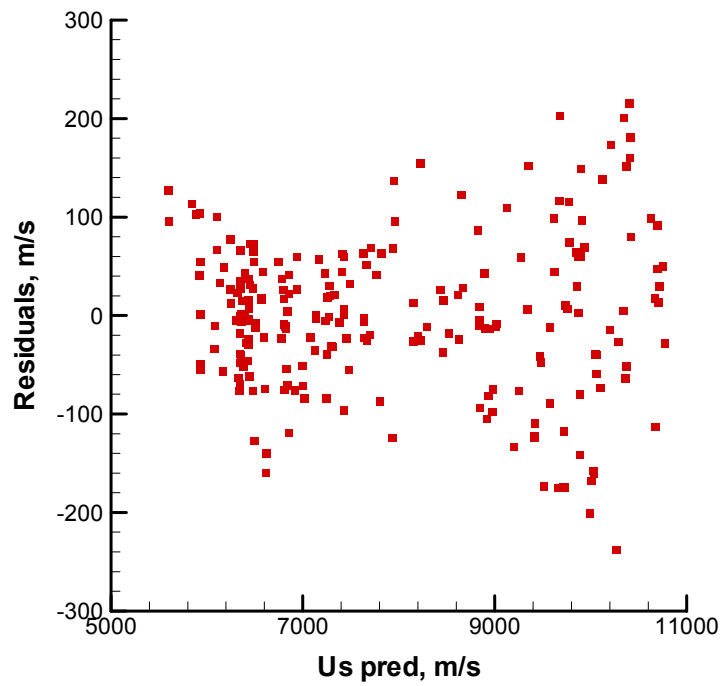


**Figure 4.4: Regression Residuals vs. Predictions Shock Wave Speed.**

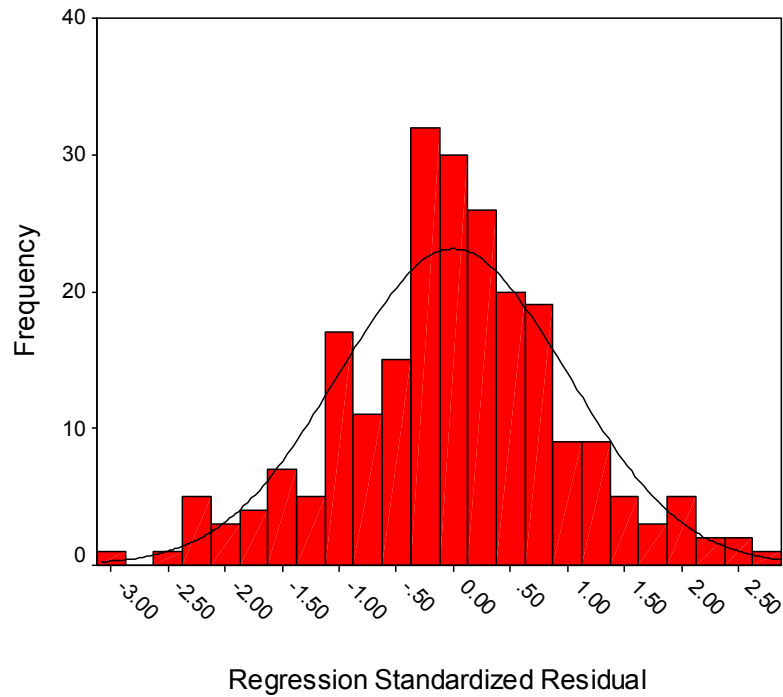


**Figure 4.5: Histogram of the Residuals**

The Komogorov-Smirnov one-sample test is a nonparametric test to evaluate whether the data has the same cumulative distribution as the test distribution (a normal distribution in our case). This test is based on the probability of observing the maximum absolute difference between the cumulative distribution of the sample and the test distribution. The results of this test are shown in Table 4.2.

**Table 4.2: Statistics for the Kolmogorov-Smirnov Test for a Normally Distributed Residuals.**

$n$		232
Normal Parameters	Mean	0.000
	Standard Deviation	77.56
Most Extreme Differences	Absolute	0.060
	Positive	0.043
	Negative	-0.060
Kolmogorov-Smirnov Z		0.908
Significance (two-tailed)		0.381

The probability of obtaining a Z greater than 0.908, given that the distribution is normal, is 38.1%. Since this is a very high level of probability (much higher than the usual 5% at which the hypothesis would typically be rejected), there is no significant statistical evidence that the residuals are not normally distributed. This observation allows us to assume a normal distribution of the residuals to evaluate error bounds – confidence intervals – on our regression coefficients (i.e., the intercept and slope) for the data in Figure 4.3.

The regression coefficients for  $U_s$ \_exper vs.  $U_s$ \_pred, and the associated 95% confidence intervals on these coefficients are listed in Table 4.3. The evaluation of these confidence intervals for normally distributed residuals are discussed in most text-books on parameter estimation or regression (for example, see Beck and Arnold, 1977) and provided by most computer statistical packages.

**Table 4.3: Regression of the Experimental Shock Wave Velocity as a Function of the Predicted Shock Wave Velocity.**

	Coefficient	95% Confidence Interval for Coefficients	
		Lower Bound	Upper Bound
Intercept	360.2	306.8	413.5
Slope	0.950	0.943	0.957

Note that a zero intercept and a slope of unity are not within the 95% confidence intervals for these quantities. We thus reject the hypothesis that the model is valid scientifically – has slope one and intercept zero – based on a non-zero intercept and a non-unity slope.

While this model does not appear to be valid scientifically in these terms, the model can still be very useful if we can evaluate confidence intervals on the predictions. To do this, we use the regression analysis performed above to generate confidence intervals on a prediction of the regression model. These, in turn, can be used to approximate the prediction differences in the shock wave speed as a function of particle velocity.

Figure 4.6 shows the 95% prediction bounds as a function of  $U_{s\_pred}$ , evaluated using standard techniques from regression (Beck and Arnold, 1977). These bounds reflect the uncertainty in estimating the intercept and slope, and the scatter of the data about the regression line. Recall that we assumed that the standard deviation (or variance) of the data was uniform for all values of particle speed. Since there does seem to be a bit more scatter at high shock speeds, a more accurate approach would be to divide the data into zones and evaluate a standard deviation for each. This would require that we use weighted residuals during the regression process such as presented in Beck and Arnold (1977). We could, of course apply such an approach if circumstances necessitated it.

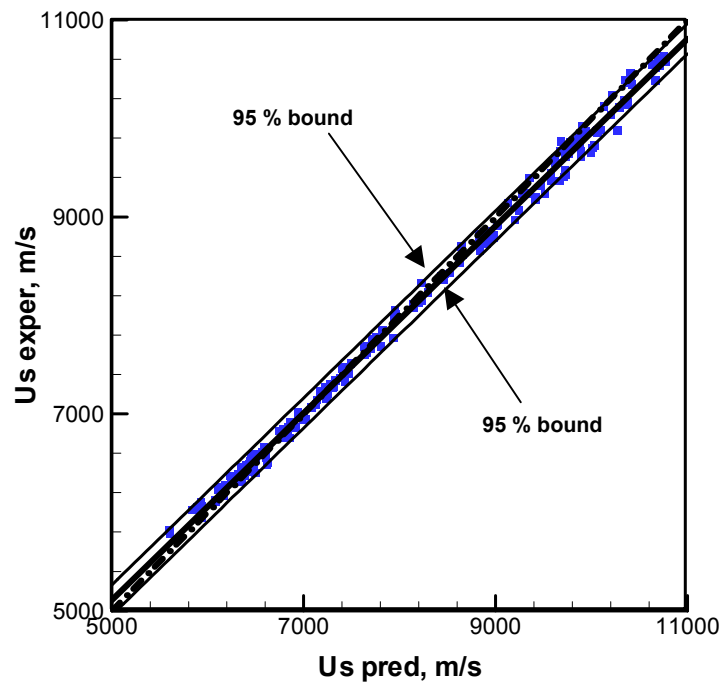


**Figure 4.6:** Prediction Bounds on the Regression of  $U_{s\_exper}$  vs.  $U_{s\_pred}$ . Solid thin lines are the 95% prediction bounds, solid thick line is the regression, dashed line is  $U_{s\_exper} = U_{s\_pred}$ .

Note that the perfect model, as represented by the dashed line, is within the confidence intervals for low values of  $U_s\_pred$  and outside the confidence intervals for high values of  $U_s\_pred$ . We can use these intervals to characterize the prediction error in our model. For example, the lower bound on the prediction at  $U_s\_pred = 11000$  m/s is approximately 10700 m/s. This represents a 3% error difference between experiment and observation. We can thus say that we have less than a 5% chance that a  $U_s\_exper$  will lie outside the confidence bounds for this range of data. Or we can say that we have less than a 5% chance that  $U_s\_exper$  will be different from  $U_s\_pred$  by more than 3% at  $U_s\_pred = 11000$  m/s.

#### **4.4 Summary**

We have found significant evidence that the CTH model for shock wave speed as a function of particle speed (or  $\frac{1}{2}$  impact speed) for the particular example studies does not provide predictions that are consistent with the experimental observations within the uncertainty associated with the validation exercise as we have defined it. Because of this, the specific data comparison that we have performed here does not provide supporting *evidence* that this model – CTH hydrodynamics plus SESAME 3700 EOS – is valid scientifically. This statement is clearly specific to this particular application and we intend no generalization beyond the work reported here. Since there is very little scatter in the data, the estimated uncertainty in the validation exercise is very small, and a model would have to provide very good predictions to not be rejected using this methodology.

However, the model is still very useful from an engineering point of view. Because of the form of the prediction differences, we were able to use linear regression to develop a model for these differences. The confidence intervals on this regression can then be used as confidence intervals on CTH prediction differences of shock wave speed. We found, for example, that the maximum prediction difference at  $U_s\_pred = 11,000$  m/s was less than 3% at the 95% confidence level. However, to develop such a model for prediction difference, we need sufficient experimental data over the range of data for which the model will be applied as the quality of the statistical test depends upon the number of samples. But an estimate could still be made using far fewer data. Less data would result in larger confidence intervals. In such a case, our statement may be that the maximum prediction difference at  $U_s\_pred = 11,000$  m/s was less than 6% at the 95% confidence level rather than less than 3%. While less data increases the uncertainty of our inferences, these increased uncertainties are characterized by statistical methods and the methods presented still apply.

The previous examples illustrate how we could use the population of prediction differences to develop models for the uncertainty in the prediction differences. Given these models, we can then test whether a model's predictions are statistically consistent with the experimental data. The example we discuss above is about as easy as it will ever get in testing complex engineering and scientific models! The experimental data were

plentiful and had very little scatter. The example test problem was univariate in the sense that we are modeling and measuring a single variable (shock wave speed) as a function of a single parameter (particle speed). Finally, because a linear relation existed between the predicted and measured shock wave speed, and because there was good evidence that the corresponding linear regression residuals were normally distributed with a uniform variance and mean, we could use standard statistical methods to estimate the error bounds on the regression coefficients. This allowed us to test whether the intercept was zero and whether the slope was unity, as would be the case for a valid model. In addition, this allowed us to establish a linear regression-based model for the prediction differences as a function of CTH's predictions of shock wave speed. In contrast, if a more complicated relation existed between the predicted and measured shock wave speed (i.e., nonlinear), then it would be more difficult to analyze and subtract this trend so that the assumption of uniform variance and mean of the resulting residuals would be justifiable.

In the next chapter, we look at the more complex case for which the model of uncertainty is not determined from the prediction differences directly, but from a propagation of uncertainty analysis.

## 5.0 Model Validation using Propagation of Uncertainty

### 5.1 Introduction

One method to estimate the overall uncertainty is to perform the experiment, independently, multiple times. For example, we could run the shock wave experiments discussed in Chapter 3 multiple times for each particle velocity  $U_p$ . If each performance of the experiment is independent, then the resulting scatter in the differences between model prediction and the experimental observation can be used to characterize the uncertainty in these prediction differences. We can then evaluate the level of confidence that we have that the mean of the prediction differences for each  $U_p$  is zero.

Alternatively, we can run the experiments once or a few times for each value of the independent parameter (each value of  $U_p$ , for example). If the statistics of the prediction differences are uniform for different values of the independent parameter, or if we can develop transformations such that the transformed variables have uniform statistics, then we can use the prediction differences directly to develop models for the uncertainty in the validation exercise.

Unfortunately, such multiple, independent runs of the model validation experiments are not practical for many of the models of interest, or the prediction differences are correlated in a fashion that does not lend itself to simple correlation models. We must estimate this uncertainty through analysis. In theory, this can be done if we have estimates of the probability density functions for those model parameters whose uncertainty significantly affects the model predictions. Given these estimates, a propagation of uncertainty analysis can be performed, as discussed in Hills and Trucano (1999), to characterize the uncertainty in the model predictions. The model can then be tested to evaluate whether the model predictions are statistically consistent with the experimental observations. This approach is appropriate if the cost of characterizing the uncertainty in the appropriate model parameters, and the cost of propagating this uncertainty through the model, is less than the cost of repeating the validation experiment a sufficient number of independent times.

There is an added benefit to using the propagation of uncertainty approach. The requirement that we characterize the uncertainty in the model predictions using the model forces us to better understand the sources of uncertainty in the model predictions.

## 5.2 Observations/Prediction Space

To help conceptualization of various issues associated with model validation, we use a geometric approach here. Consider a model validation exercise for which we take  $n$  experimental measurements and make the corresponding  $n$  model predictions. An  $n$ -dimensional space can be defined for which each of these  $n$  quantities is a component in the  $n$ -tuple of components defining the space (see Figure 5.1). Denote the measurement and predicted quantities by  $\theta_i$ ,  $i=1, n$  where  $n$  is the total number of measurements.

For the shock wave example presented in previous chapters, we take  $\theta_i$  to be the 232 shock wave speeds,  $U_s$ , as measured and predicted, for each of the 232 particle speeds  $U_P$ .

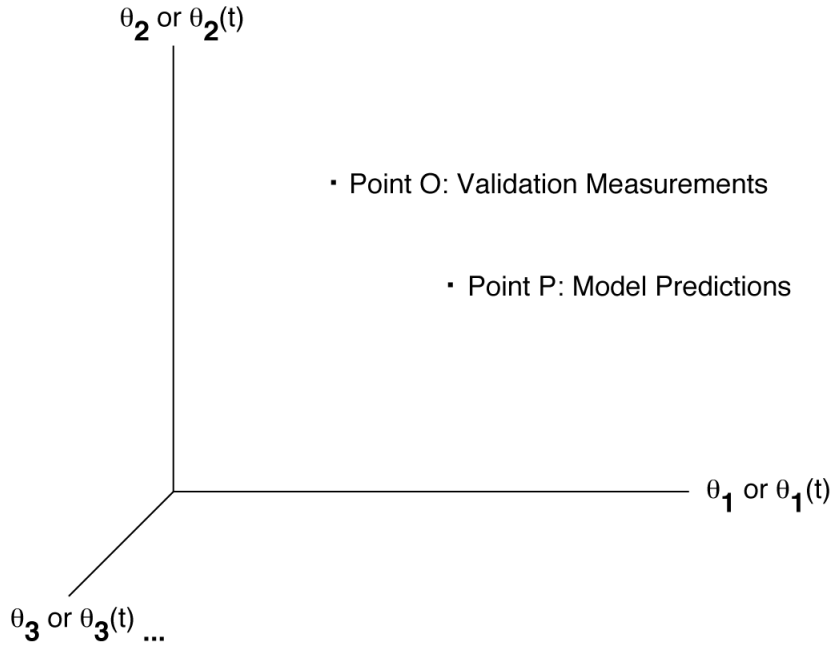


**Figure 5.1:  $n$ -Dimensional Validation Space**

Note that our  $n$  validation measurements and our  $n$  model predictions will each represent a single point in this  $n$ -dimensional space. We can now ask the question – *is the distance between the two points (see Figure 5.1) sufficiently large that we must consider this model invalid?* We cannot answer this question until we have some metric to measure this distance. The statistical approach proposed here is to measure this distance relative to the

uncertainty in the validation exercise (i.e., the uncertainty of the predicted differences). By using a propagation of uncertainty analysis to characterize the uncertainty in the predictions due to parameter uncertainty, and by using a model for the measurement uncertainty, we can develop a model for the uncertainty in the prediction differences (model predictions minus the experimental observations) for the validation exercise. Given this overall model for the validation uncertainty, we can now refine our question to ask – is the distance between the two points of Figure 5.1 sufficiently large relative to the validation exercise uncertainty that we must consider this model invalid?

To illustrate the concept of measuring distance relative to the uncertainty, consider Figure 5.2. The uncertainty in the model predictions (as estimated from the propagation of uncertainty) and in the experimental measurements (as characterized for that particular measurement technique) is represented by probability density function (PDF) clouds.

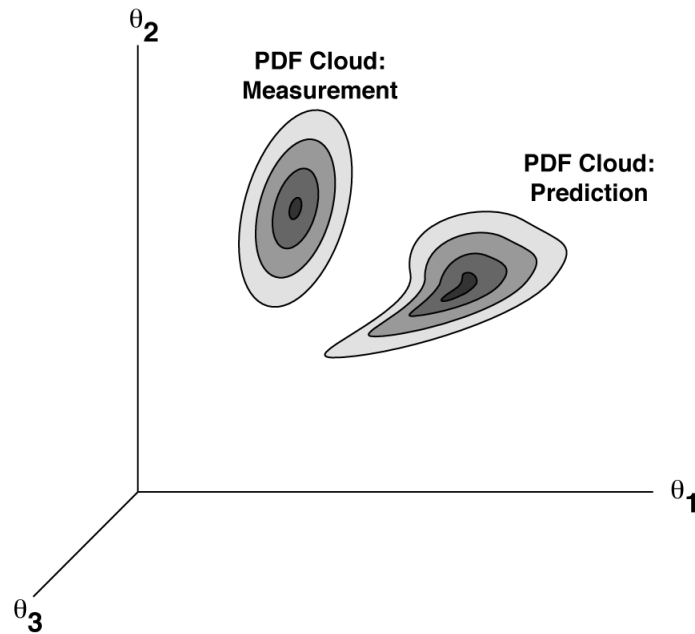


**Figure 5.2: Prediction and Measurement Uncertainty in the  $n$ -Dimensional Validation Space**

The dark regions are regions of high probability density and the lighter regions correspond to lower values for the probability density. The meaning and generation of these PDF clouds from uncertainty analysis is discussed in Hills and Trucano (1999). At this point, it is useful to combine the uncertainty of the experimental measurements and the model predictions into a single PDF cloud for uncertainty as shown in Figure 5.3 (also discussed in Hills and Trucano, 1999). Since our uncertainty in the measurements is, itself, just a model, we add this model of uncertainty to our model of prediction

uncertainty. The uncertainty of the differences between the predictions and the measurements can be developed from the uncertainties of the predictions and the uncertainties of the measurements. For measurements that are uncorrelated with the predictions, the covariance of the difference between the predictions and the measurements is equal to the sum of the covariances of the predictions and the measurements. Here we will consider the uncertainty in the difference between the measurements and the predictions as the combined or total modeled uncertainty of the validation exercise. We can represent this uncertainty as an uncertainty cloud (an  $n$ -dimensional pdf). Here we choose to center this cloud on the maximum likelihood prediction. The actual validation experiment measurements are now shown as a point since the experimental uncertainty is now included in the total uncertainty cloud. Note that the  $n$ -dimensional point corresponding to the experimental measurements is within the cloud for this particular example. Also note that we denote this cloud as the prediction + measurement uncertainty rather than prediction – measurement uncertainty. This is to reflect that the variances are additive, even though we are taking differences between the predictions and the measurements.

We are now in a position to better visualize what it is we are trying to accomplish in developing a metric to measure model validity from a correlated set of measurements. We wish to establish a region of acceptance that we expect the measurements to lie within. If the validation experiment results in measurements outside the acceptance region, then we reject the hypothesis that the model is valid.

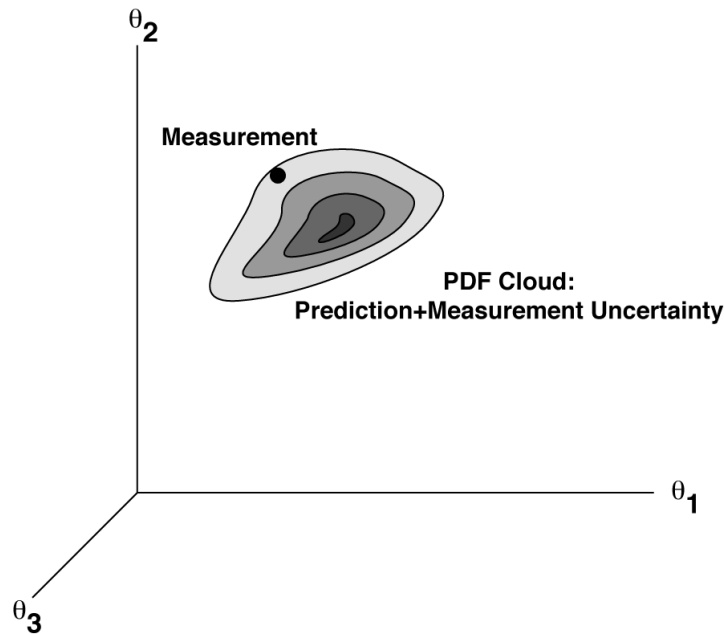


**Figure 5.3: Combined Prediction and Measurement Uncertainty.**

To establish such a region, we must first establish how we are going to measure distance from the center of the PDF cloud to the measurement. One possibility, as discussed in Hills and Trucano (1999), is to define our measurements in terms of constant PDF contours. We can consider all points on a constant PDF contour as equal-distance to the center (the point of maximum likelihood, i.e., the point of maximum PDF value). We can then define the region of acceptance of a model as that region within the constant PDF contour that contains 95% (or some other %) of the probability distribution. An example of such a 95% acceptance region is shown in Figure 5.4. Since the measurement point does not lie outside of the acceptance region, we accept the model as valid at the 95% confidence level. More concisely, if the model (and the model for uncertainty) is valid, we would have a 5% chance of observing measurements this far or farther from the prediction. We would thus have no statistically significant reason to reject this model at the 95% confidence level. In contrast, if the experimental point were just outside the acceptance region represented by the dashed line, our chances of observing these measurements, assuming a valid model, would be less than 5%. In this case we would reject the model at the 95% confidence level. Note that we are using the measurements to evaluate whether we have sufficient statistical evidence to reject the model as valid. In addition, we are testing at the 95% confidence level so that we have only a 5% chance of declaring the model invalid when it is, in-fact, valid. Declaring a model invalid when it is valid is known as a Type I error or an error of the first kind (Brownlee, 1965). We are not testing whether we have sufficient evidence to declare the model valid, only whether we have sufficient evidence to declare the model invalid.

While this approach is conceptually straight forward, it does have a practical issue. The evaluation of  $n$ -dimensional PDF clouds is very expensive, computationally, if one cannot assume simple parameterized forms for the clouds (such as a multi-normal distribution). Such can be the case for highly nonlinear problems. However, once the PDF clouds are adequately resolved, one can search along the clouds to define the appropriate constant PDF surface that contains 95% of the cumulative probability. The position of this measurement relative to this surface can then be used to establish whether there is sufficient statistical evidence to reject this model. An example of this approach was presented for a spring-damper-mass system in Hills and Trucano (1999).

A second issue is that there are other regions that include 95% of the cumulative probability, which are not bounded by constant PDF curves. For symmetric distributions such as a multi-normal distribution, the constant PDF approach leads to the acceptance region which is the most likely to reject a bad model as inferred from the measurements (Brownlee, 1965). This approach minimizes our probability of committing a Type II error - failing to reject a bad model. For non-symmetric distributions, the region that contains 95% cumulative probability and is most likely to reject a bad model will not necessarily be bounded by a constant PDF contour.

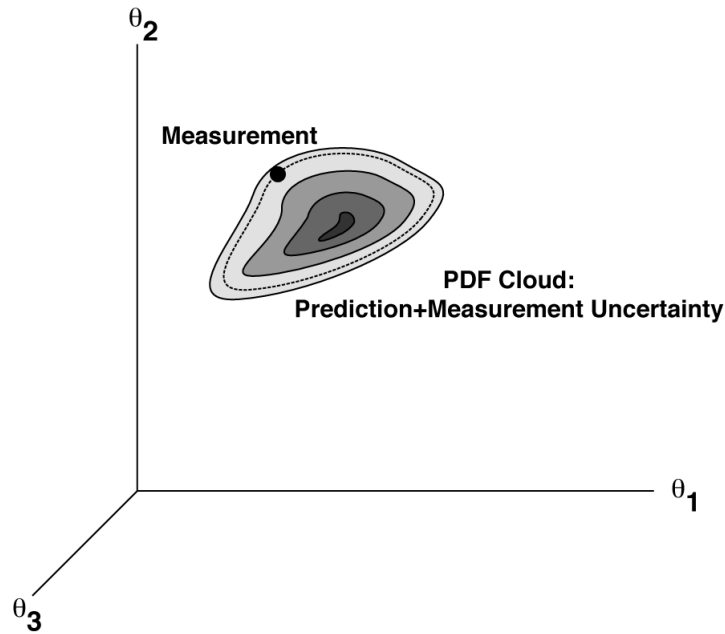


**Figure 5.4:** 95% Confidence Acceptance Region: Dashed line – outer boundary of the acceptance region.

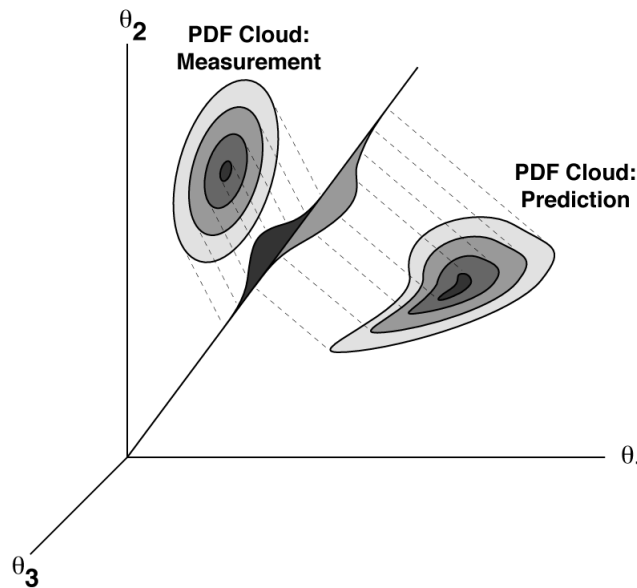
### 5.3 Integrated Measures

Another approach to model validation is to base validation metrics on integrated measures that are defined in terms of functionals of the predictions and measurements. For example, we would generally expect that the mean of the prediction differences (i.e., the differences between the prediction and the measurements) to be near zero for a scientifically valid model if we were to repeat the validation exercise a sufficient number of independent times. Since the mean is a sum of a set of quantities divided by the number in that set, we can consider the mean to be an integrated measure. Given a model for the distribution of the mean prediction differences, we can perform a test to evaluate whether there is significant statistical evidence that the mean of the prediction differences is not zero. Likewise, we could define and perform a test to evaluate whether this difference is within some acceptable value of zero where the acceptable value is defined by the user.

Other examples of integrated measures include the estimation of heat flux over a surface from measurements of heat flux at multiple points distributed across the surface; and the estimation of the net mass in the system from estimates of density from various points located across the system.

If these integrated measures can be written as a linear combination of the measurements, as they can for the 3 examples just given, then these measures can be looked at as linear mappings into subspaces of the validation space as illustrated in Figure 5.5. In this example, the measurements and predictions, and their uncertainty, are mapped onto a 1-dimensional subspace. Depending on the type of integrated measure, the width of the probability density functions may be larger, smaller, or the same as the width along the same direction of the PDF clouds in the full  $n$ -dimensional space. For example, the standard deviation (i.e., width) of the mean of a set of  $n$  normally distributed random variables, which each possess uniform means and standard deviations, is equal to the standard deviation of each variable, divided by the square root of  $n$ . The width of the mapped distribution will thus be narrower than the width of the full  $n$ -dimensional cloud for  $n > 1$ . This would be reflected as narrower PDFs, as mapped on the line, than those shown in Figure 5.5.

Once the integrated measure is defined, we can ask whether the distance between the clouds is large compared to the width of the clouds. If so, then there is little statistical evidence that the integrated measures of the model predictions and the experimental observations are the same and we can reject the hypothesis that the model is valid for this particular set of measurements. For the example presented in Figure 5.5, there is significant overlap of the two PDF's, as mapped onto our measure. We thus do not have significant evidence to reject the hypothesis that the model is valid.



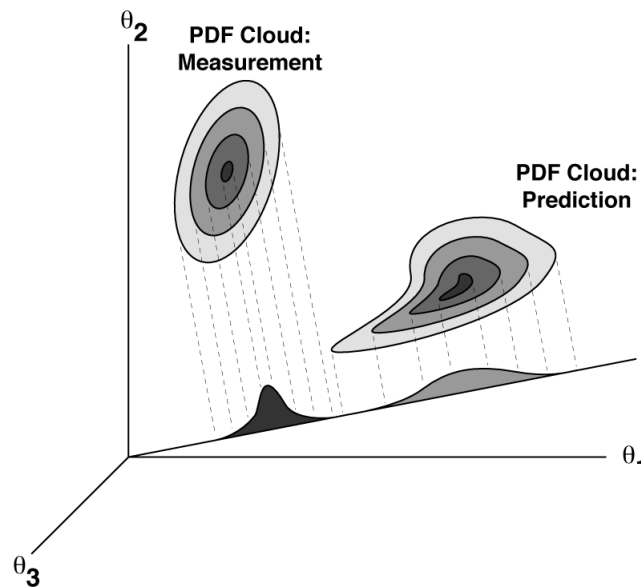
**Figure 5.5: Integrated Measure as Mapped onto a Subspace of the Validation Space.**

Figure 5.6 shows the mapping onto a different integrated measure. Note that for this case, the mapped measures do not overlap significantly. For this integrated measure, there is little evidence that the model predictions and the experimental observations are the same. This illustrates a characteristic of integrated measures. They only measure the behavior of the model along particular directions in the validation space. To test the model in all directions would require a sufficient number of linearly independent integrated measures equal to the dimension of the validation space.

An advantage of integrated measures is that it generally does not require as much computation to resolve lower dimensional PDF distributions that result from the mappings onto lower dimensional spaces.

#### 5.4 Application Specific Measures

As introduced in Section 3.4, a common feature of model validation is that the anticipated application of the model may be somewhat different than the model validation experiments. For example, we may plan to use a CTH model to predict the arrival time and strength of a shock wave. However, our model validation experiments may only measure shock wave speed as a function of particle velocity. Alternatively, we may have data to test our model over a large range of model parameters. But our application may only require that the model be valid over a small range of model parameters.



**Figure 5.6: Integrated Measure # 2 as Mapped onto a Subspace of the Validation Space.**

For example, we may be interested in the time of arrival of an impact generated shock through an axisymmetric object with fairly uniform cross-section for low impact velocities. In this case, we would be more interested in the performance of the model over a range of lower particle velocities. If we can develop a mapping between the important variables for the application and those measured for the validation experiments, we could use this mapping to weight the validation experiment measurements appropriately for this particular application.

A second feature of the actual applications is that the number of degrees of freedom of the application decision variables is generally lower than the number of model parameters for the application and for the validation experiments. Most applications have go/no-go decisions based on a small set of conditions. For example, we may desire to accurately predict the time of arrival of a shock wave on the back surface of an object and not the details of the propagation of the shock throughout the object. Or we may only care about the total energy delivered to a surface. In each of these cases, the number of quantities that we are interested in for the application is one. Thus the degrees-of-freedom for the decision variable is only one.

If the degrees-of-freedom of the decision variable is less than that of the number of model parameters, and if we can develop a mapping between the validation space and the application space, then we can use this mapping to develop integrated measures in the validation space. We will illustrate both point validation, and application based validation in the following sections.

## **5.5 Overview of Validation Examples**

The propagation of uncertainty approach to model validation is demonstrated in the following sections. We use a subset of the experimental  $U_P - U_S$  data to serve as validation test data and the remaining data to characterize the EOS model parameters and their uncertainty. The Mie-Grüneisen quadratic model is used as the EOS for this example since its parameters are easily related to the experimental  $U_P - U_S$  data. The uncertainty in the test data is characterized using standard statistical techniques. The EOS parameter uncertainty is propagated through CTH to develop a model for the uncertainty in the CTH predictions of shock wave speed as a function of particle speed. Several metrics are developed to compare these model predictions to the experimental observations. We begin with the characterization of the uncertainty in the validation test data and the EOS model parameters.

## **5.6 Calibration and Measurement Data**

Normally, model calibration data and model validation data are independent. In our case, we will use the  $U_P - U_S$  data from Table 3.1 to calibrate the model and to test it. To

provide some independence, we divide the data into two sets, one for calibration and one for model testing. The method used to divide the data depends on what one is trying to accomplish. For example, if we wish to test the ability of the model to extrapolate to higher values of  $U_P$ , we could use the  $U_P - U_S$  data in the low range to calibrate the model and use  $U_P - U_S$  data in the high range to test the model.

Here we sample calibration data from the entire range of  $U_P - U_S$  data. To define the subsets of data, we randomly assigned 0's and 1's (with equally probability) to each  $U_P - U_S$  pair. The data pairs assigned 0's are used for calibration and the data pairs assigned 1's are used for model testing. This random selection approach results in the calibration data that tends to span the entire range of particle velocities. This results in less uncertainty in the calibration constants, which in-turn, results in less uncertainty in the model predictions. The decreased model prediction uncertainty increases our ability to resolve whether the model is invalid, scientifically.

### **5.7 Model for Uncertainty in the Validation Measurement Data**

Application of the random sampling scheme to our data resulted in 112  $U_P - U_S$  pairs being selected for calibration and 120 pairs being selected for model testing. Figure 5.7 shows the subset of the experimental  $U_P - U_S$  data randomly selected from Table 3.1 for model testing.

We can either use prior knowledge of the uncertainty in the experimental technique to develop a probability model for the uncertainty in the measurements, or we can attempt to develop a probability model from the data directly. Here we use the second approach.

Because we do not have a sufficient number of multiple measurements of shock wave speed for each particle velocity, we need to use the data across the range (or sub-ranges) of  $U_P$  to estimate the statistics in a model for uncertainty. This requires that we develop a model for the trend in the measurements, and then look at the scatter of the data about this trend. Inspection of Figure 5.7 indicates that there appears to be a very strong linear relationship between  $U_S$  and  $U_P$ . Because of this, we can use linear regression to model the trend and look at the residuals (scatter) about this regression line to develop a model for measurement uncertainty.

The resulting regression line is shown in Figure 5.7. Close inspection of the figure indicates that there does not appear to be strong correlation in the scatter of the data about the line. Because of this, we can assume that the mean of the residuals is uniform over  $U_P$ . The scatter of the data about the regression line does appear to be somewhat non-uniform with more scatter at larger values of  $U_P$ . To account for this non-uniformity, we could divide the data into several regions along  $U_P$ , and estimate the standard deviation for each region. However, the differences in scatter are not large and we will assume that we can model this scatter with a uniform standard deviation across all  $U_P$ . This assumption should be revisited if we find that our model validation methodology results

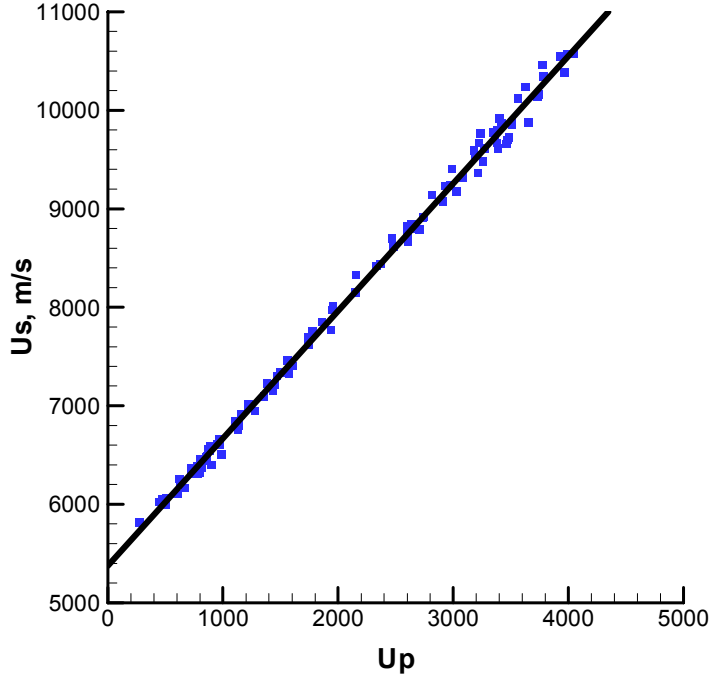


**Figure 5.7:** Validation Measurements: 120 measurements randomly sampled from the 232 experimental shock wave speed vs. particle speed measurements. Solid line – linear regression ( $U_s = 5377 + 1.294 U_p$ ). (The computational data is presented in Table D2.)

in the experimental data landing near the acceptance-rejection boundary of our validation tests. For example, this would certainly be the case if we had chosen to include some or all of the ultrahigh pressure data for aluminum mentioned in Section 3.

Because we are assuming that the standard deviation is uniform across  $U_p$ , we can use the residuals about the regression shown in Figure 5.7 to estimate the standard deviation at each  $U_p$ . This results in

$$\sigma_{meas} = 83.7 \text{ m/s} \quad (5.1)$$

We now apply the Kolmogorov-Smirnov test introduced in Chapter 4 to evaluate the normality of the residues. The results of this test are shown in Table 5.1. The probability of obtaining the test statistic  $|Z|$  greater than or equal to 0.759, given that the distribution is normally distributed about a mean of zero is 61%. This is very important, indicating

that there is little statistically significant evidence that the errors are not normally distributed with a zero mean and a standard deviation of 83.7 m/s. We therefore have no reason to reject this model for the uncertainty in the validation measurements.

**Table 5.1: Statistics for the Kolmogorov-Smirnov Test for Normally Distributed Residuals: Validation Data**

$n$		120
Normal Parameters	Mean	0
	Standard Deviation	83.7
Most Extreme Differences		
	Absolute	0.069
	Positive	0.057
	Negative	-0.069
Kolmogorov-Smirnov Z		0.759
Significance (two-tailed)		0.611

### 5.8 Model for Uncertainty in the Model Parameters

We use the quadratic  $U_P - U_S$  form of the Mie- Grüneisen Equation of State model (Hertel and Kerley, 1998):

$$U_S = C_S + S_1 U_P + (S_2 / C_S) U_P^2 \quad (5.2)$$

where  $C_S$ ,  $S_1$ , and  $S_2$  are calibration constants based on  $U_P - U_S$  data. Figure 5.8 shows the calibration data randomly selected for calibration from Table 3.1 using the selection procedure presented in Section 5.6. Note that in this case, we have 112 data pairs to be used for calibration. Inspection of Figure 5.8 indicates that the shock wave speed is linear in particle velocity. Because of this, we set the constant on the quadratic term to zero

$$S_2 = 0 \quad (5.3)$$

and use least squares to estimate the intercept,  $C_S$ , and the slope,  $S_1$ . The resulting regression line is shown in Figure 5.8 with the corresponding regression coefficients and their statistics listed in Table 5.2. Beck and Arnold (1977, p144) present the evaluation of the terms in the covariance matrix for linear regression. Note that the estimates of the two constants are correlated since the off-diagonal terms in the covariance matrix are nonzero. This is generally the case when we must estimate more than one model parameter simultaneously (i.e., using least squares). A Kolmogorov-Smirnov test for normality of the residuals is summarized in Table 5.3. Since the level of significance of the test statistic is larger than 0.05, we cannot reject the hypothesis that the residuals are normally distributed at the 5% confidence level. We therefore accept this model for the parameter uncertainty.

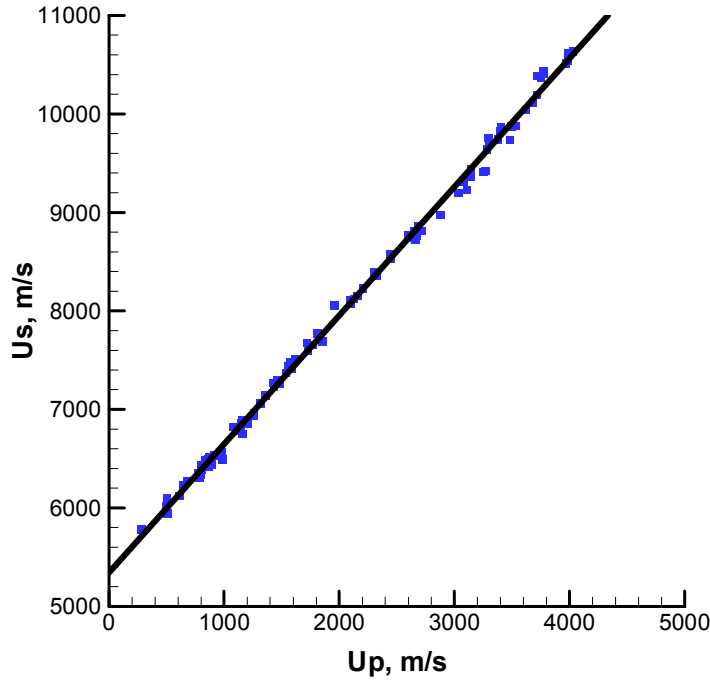


**Figure 5.8:** Calibration Measurements: 112 measurements randomly sampled from the 232 experimental shock wave speed vs. particle speed measurements. Solid line – linear regression ( $U_S = 5344 + 1.305 U_P$ ). (The computational data is presented in Table D3.)

### 5.9 Model for Prediction Uncertainty

Now that we possess a model for the uncertainty in the calibration constants (model parameters), we can use CTH to propagate this uncertainty through the model to evaluate the corresponding uncertainty in the predicted shock wave speed. A tutorial on the use of the Monte Carlo and sensitivity analysis methods to perform this propagation is presented in Hills and Trucano (1999).

The numerical evaluation of the PDF for the model predictions and the corresponding acceptance regions can be very computationally intensive for highly nonlinear problems. But the present case is unusual in that the calibration curve used for the EOS model gives shock wave speeds that vary linearly with changes in the calibration constants. This will significantly reduce the amount of computational work required to estimate the prediction uncertainty, but it is not a fundamental restriction on our analysis. Since CTH should maintain this relationship while applying the conservation of mass, momentum, and energy equations, we expect CTH predictions of shock wave speed to also be linear in the

calibration constants for our validation exercise. Because of this linear relation, propagation of the uncertainty for normally distributed model parameters (i.e., the calibration constants) will result in a multi-normal distribution for the uncertainty in the shock speed predictions. Likewise, the expected value of a model prediction will be equal to the model prediction using the expected values of the model parameters (see Hills and Trucano, 1999). The expected values of the model parameters are given by the least-squares estimates presented in Table 5.2. The resulting CTH predictions, using the model parameters given in Table 5.2, are shown with the experimental measurements in Figure 5.9. Note that the predictions and the measurements appear to agree within the scatter of the data. To evaluate whether this agreement is statistically significant, we must first characterize the PDF for the prediction errors.

**Table 5.2: Calibration Constants**

	Coefficient	Covariance Matrix	
		$C_S$	$S_1$
$C_S$	5344	166.4	-0.0663
$S_1$	1.305	-0.0663	3.50 E-5

**Table 5.3: Statistics for the Kolmogorov-Smirnov Test for Normally Distributed Residuals: Calibration Data**

$n$		112
Normal Parameters	Mean	0
	Standard Deviation	67.6
Most Extreme Differences		
	Absolute	0.104
	Positive	0.071
	Negative	-0.104
Kolmogorov-Smirnov Z		1.102
Significance (two-tailed)		0.176

Because the uncertainty in the model predictions is well modeled by a multi-normal distribution, we can completely characterize this distribution with the model predictions shown in Figure 5.9 and the prediction covariance matrix listed in Table 5.2. Because the shock speed should be linear in the model parameters, we can use a sensitivity analysis for the evaluation of the prediction covariance matrix (see Hills and Trucano, 1999) without any loss in generality.

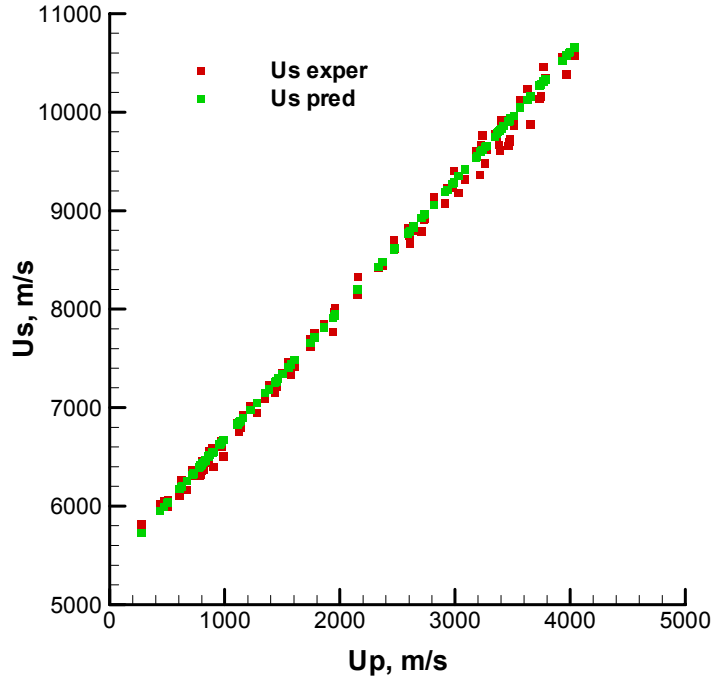


**Figure 5.9: Validation Predictions and Experimental Observations: 120 measurements**

We begin by deriving the sensitivity analysis method for two model parameters. Consider the general linear or nonlinear predictive model of the form

$$z = f(\alpha_1, \alpha_2, x) \quad (5.4)$$

where  $\alpha_1$  and  $\alpha_2$  are model parameters and  $x$  is an independent variable (or vector of independent variables). We can approximate the change in  $z$  from its mean due to changes in the model parameters from their means using a truncated Taylor's series expansion:

$$z - z_{mean} = \Delta z_i \cong \frac{\partial f}{\partial \alpha_1} \Delta \alpha_1 + \frac{\partial f}{\partial \alpha_2} \Delta \alpha_2 \quad (5.5)$$

For measurements at  $n$  values of  $x$ , we can write

$$\Delta \mathbf{z} = \mathbf{X} \Delta \mathbf{d} \quad (5.6)$$

where

$$\Delta \mathbf{z} = \begin{bmatrix} \Delta z_1 \\ \Delta z_2 \\ \vdots \\ \Delta z_n \end{bmatrix}, \quad \mathbf{X} = \begin{bmatrix} \frac{\partial f_1}{\partial \alpha_1} & \frac{\partial f_1}{\partial \alpha_2} \\ \frac{\partial f_2}{\partial \alpha_1} & \frac{\partial f_2}{\partial \alpha_2} \\ \vdots & \vdots \\ \frac{\partial f_n}{\partial \alpha_1} & \frac{\partial f_n}{\partial \alpha_2} \end{bmatrix} \quad (5.7, 5.8)$$

and

$$\Delta \mathbf{d} = \begin{bmatrix} \alpha_1 - \alpha_{1,mean} \\ \alpha_2 - \alpha_{2,mean} \end{bmatrix} = \begin{bmatrix} \Delta \alpha_1 \\ \Delta \alpha_2 \end{bmatrix} \quad (5.9)$$

The subscript  $i$  indicates that the function  $f$  is evaluated at the  $i^{\text{th}}$  value of  $x$  (see Eq. (5.4)). The derivatives that appear in Eq. (5.8) are known as sensitivity coefficients and  $\mathbf{X}$  is the sensitivity matrix. The sensitivity derivatives relate small changes in  $f$  to small changes in the parameters  $\alpha_1$  and  $\alpha_2$ .

We can now estimate the covariance of  $z$  using Eq. (5.9) by noting the following:

$$\Delta \mathbf{z} \Delta \mathbf{z}^T = \mathbf{X} \Delta \mathbf{d} \Delta \mathbf{d}^T \mathbf{X}^T \quad (5.10)$$

The expected value of Eq. (5.10) is (Beck and Arnold, 1977)

$$E(\Delta \mathbf{z} \Delta \mathbf{z}^T) = \text{cov}(\Delta \mathbf{z}) = E(\mathbf{X} \Delta \mathbf{d} \Delta \mathbf{d}^T \mathbf{X}^T) = \mathbf{X} \text{cov}(\Delta \mathbf{d}) \mathbf{X}^T \quad (5.11)$$

Equation (5.11) relates the covariance of the model parameters to the covariance of the model predictions, assuming that the model predictions are linearly related to the model parameters.

The sensitivity matrix, Eq. (5.8), can be approximated using finite differences. Since the shock wave speed appears to be linear in the parameters, we will use a simple first-order, finite difference to estimate the sensitivity coefficients

$$\frac{\partial f_i}{\partial \alpha_1} \approx \frac{f_i(\alpha_{1,mean} + \Delta \alpha_1, \alpha_{2,mean}, x_i) - f_i(\alpha_{1,mean}, \alpha_{2,mean}, x_i)}{\Delta \alpha_1}, \quad i = 1, n \quad (5.12)$$

$$\frac{\partial f_i}{\partial \alpha_2} \approx \frac{f_i(\alpha_{1,mean}, \alpha_{2,mean} + \Delta \alpha_2, x_i) - f_i(\alpha_{1,mean}, \alpha_{2,mean}, x_i)}{\Delta \alpha_2}, \quad i = 1, n \quad (5.13)$$

where  $n$  is the number of predicted measurements and  $\Delta\alpha_1$  and  $\Delta\alpha_2$  are small increments in the parameters. We use 10% increments from the calibrated values given in Table 5.2 for the present analysis. For our case,  $n = 120$ ,  $\alpha_1 = C_s$ , and  $\alpha_2 = S_1$  and the vector of predicted measures corresponds to  $\mathbf{z}$  (see Eqs. (5.2), (5.4)). We must run CTH 3 times for each of the 120 particle velocities to generate the components in the  $120 \times 2$  sensitivity matrix  $\mathbf{X}$  using Eqs. (5.12) and (5.13). The sensitivity matrix, along with the covariance matrix for the model parameters given in Table 5.2, are used in Eq. (5.11) to evaluate the  $120 \times 120$  covariance matrix for the 120 predictions.

The standard deviations of each of the 120 predictions are the square roots of the diagonal elements of the resulting prediction covariance matrix. These are shown graphically in Figure 5.10. Note that the general trend is quadratic. This is due to the correlation structure between the two model parameters that resulted from the use of least squares to estimate these parameters simultaneously. The slight scatter of the points shown in Figure 5.10 at larger  $Up$  is due to the numerical noise associated with modeling shock propagation which is further amplified by the evaluation of the sensitivity derivatives using finite differences. We would expect to see less scatter for more benign applications such as heat conduction in solids, or for smoother shock wave calculations.

### **5.10 Model of Uncertainty of Validation Exercise**

Now that we have a model for the measurement uncertainty and a model for the model prediction uncertainty due to the uncertainty in the model parameters, we can combine these to develop a model for the uncertainty of the prediction differences (predictions minus experimental measurements).

To begin with, we assume that the model calibration data are independent of the experimental data. This assumption is justified because we randomly sampled the experimental data from a set of 232 measurements of shock wave speed as a function of particle speed, and since we saw no evidence of correlation in the scatter of experimental shock wave speed as a function of particle speed.

Taking the difference between the model predictions and the validation measurements leads to the following (see Hills and Trucano, 1999)

$$E(Us\_pred - Us\_exper) = E(Us\_pred) - E(Us\_exper) \quad (5.14)$$

$$\text{cov}(Us\_pred - Us\_exper) = \text{cov}(Us\_pred) + \text{cov}(Us\_exper) \quad (5.15)$$

For our case, the  $120 \times 120$  covariance matrix for the model predictions is given by Eq. (5.11). The  $120 \times 120$  covariance matrix for the measurements is simply a diagonal matrix (all off-diagonal terms are zero if we assume the measurements are independent) with the

diagonal elements equal to the square of the standard deviation as given by Eq. (5.1). Using the results of Table 5.2 and Eqs. (5.1), (5.11) in Eq. (5.15) give

$$\text{cov}_{i,j}(Us\_pred - Us\_exper) = \begin{cases} \text{cov}_{i,j}(Us\_pred) + 83.7^2, & i = j \\ \text{cov}_{i,j}(Us\_pred), & i \neq j \end{cases} \quad (5.16)$$

where

$$\text{cov}(Us\_pred) = \mathbf{X} \begin{bmatrix} 166.4 & -0.0663 \\ -0.0663 & 3.50 \times 10^{-5} \end{bmatrix} \mathbf{X}^T \quad (5.17)$$

The standard deviations for each measurement location (i.e., each  $U_p$ ) are given by the square root of the diagonal elements of Eq. (5.16). These are plotted in Figure 5.11. Comparing Figures 5.10 and 5.11 and noting the value for the measurement standard deviation is 83.7, we see that the uncertainty due to the validation measurements dominates the uncertainty in the validation exercise. We also see that the scatter in the data caused by numerical noise is not as apparent due to the dominant effect of the measurement uncertainty.

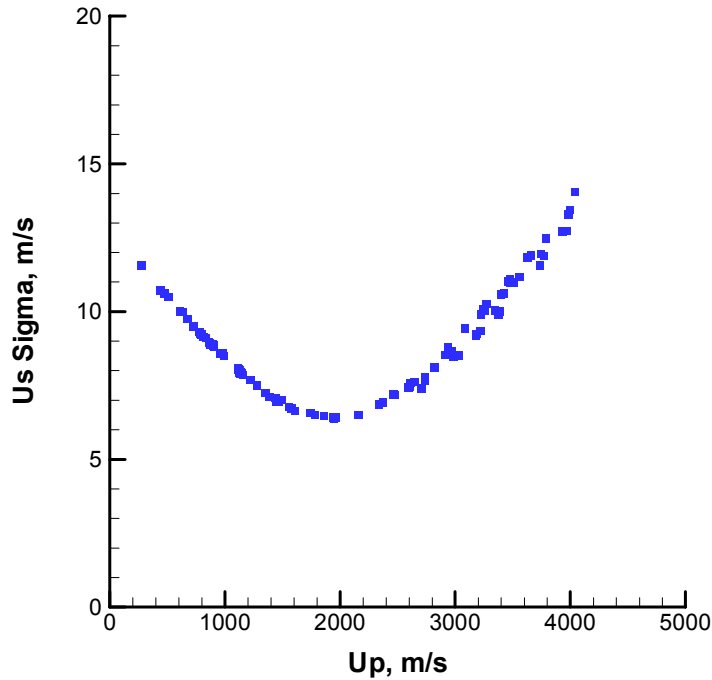


**Figure 5.10: Standard Deviation of Predicted Shock Wave Speeds**

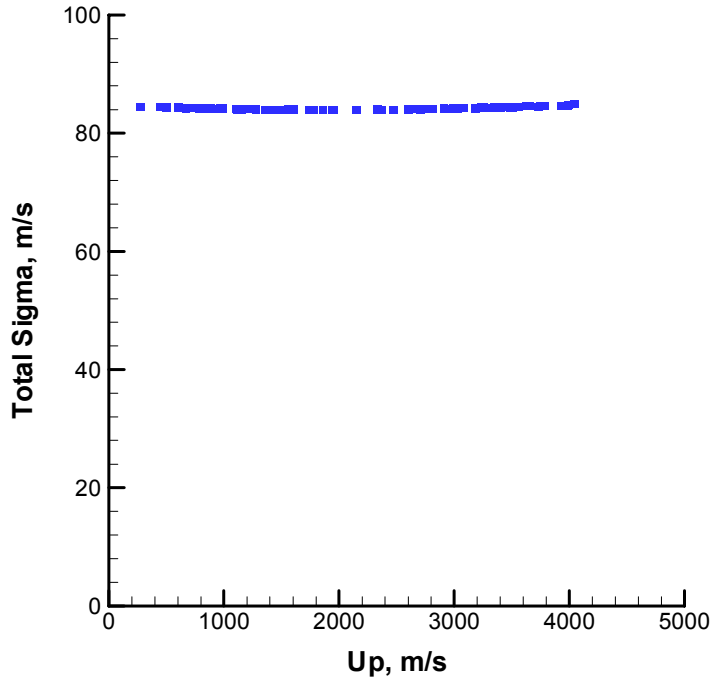


**Figure 5.11: Predicted Standard Deviation for the Prediction Differences**

Equations (5.14), (5.16), and (5.17), and knowledge that our error distributions are multi-normal completely defines the 120 dimensional PDF cloud for the validation exercise. Because the uncertainty is dominated by the measurement uncertainty, and because the correlation matrix for the measurement uncertainty is diagonal with a uniform variance, the resulting 120 dimensional PDF cloud will be nearly spherical in shape. If the model is valid, we would expect that the expected value of the prediction differences at each particle velocity to be zero.

### **5.11 The Point Validation Test**

We are now ready to define our validation metric for this application of point validation to test for zero prediction differences. Curves of iso-probability for a multi-normal PDF are given by constant  $r^2$  values for the following quadratic expression

$$r^2 = [p_1 - p_{mean1} \quad p_2 - p_{mean2} \quad \cdots \quad p_{120} - p_{mean120}] \text{cov}(\mathbf{p})^{-1} \begin{bmatrix} p_1 - p_{mean1} \\ p_2 - p_{mean2} \\ \vdots \\ p_{120} - p_{mean120} \end{bmatrix} \quad (5.18)$$

where

$$p = Us\_pred - Us\_exper \quad (5.19)$$

For our case, we wish to test the hypothesis that the mean prediction difference for each measurement location (i.e., each  $U_P$ ) is zero. In this case, Eq. (5.18) becomes

$$r^2 = [p_1 \quad p_2 \quad \cdots \quad p_{120}] \text{cov}(\mathbf{p})^{-1} \begin{bmatrix} p_1 \\ p_2 \\ \vdots \\ p_{120} \end{bmatrix} \quad (5.20)$$

Using our estimated covariance matrix for the validation exercise, Eqs. (5.16), and (5.17), and our prediction errors, we find

$$r^2 = 130.0 \quad (5.21)$$

This value represents a square of the distance, weighted by the inverse of the covariance matrix associated with the prediction differences.

We can now perform a statistical test for the probability of this value of our measure of prediction difference, given a multi-normal distribution with zero mean and our covariance of  $\mathbf{p}$ . The cumulative probability for some  $r^2$  in this PDF cloud is given by the  $\chi^2$  distribution for multi-normally distributed prediction errors (Beck and Arnold, p. 294). For 120 degrees of freedom

$$r^2 = \chi^2_{1-\alpha}(120) \quad (5.22)$$

where 120 represents the number of measurements and  $1-\alpha$  represents the cumulative probability. The value for  $r^2$  for which the cumulative probability inside the corresponding constant PDF surface is 95% is

$$r_{critical}^2 = \chi^2_{0.95}(120) = 146.6 \quad (5.23)$$

Since  $r^2=130.0$  is smaller than 146.6, we cannot reject the hypothesis that the mean prediction difference is zero. Therefore, we have no statistical evidence that the model is not valid at the 95% confidence level and therefore, accept the model as valid by this

measure. Using  $r^2=130.0$  in Eq. (5.22) and evaluating the corresponding  $\alpha$  gives  $\alpha=0.252$ . This level of significance of  $r^2=130.0$  is thus 25.2%. If we were to repeat this entire validation exercise many independent times, we would expect a valid model to produce prediction differences that are this far or farther from zero 25.2% of the time.

Note that these results contrast with the results presented in the previous chapter where we found that the model – CTH and the selected SESAME 3700 EOS table – provided predictions that were not consistent with the experimental results. Since the Mie-Grüneisen EOS model used in this section is calibrated using  $U_P - U_S$  data directly, we would expect the present agreement with the data to be improved. We would expect the opposite conclusion if we were investigating the ultrahigh pressure data. This is further evidence of how application sensitive validation really is, a key point we emphasize.

In the next section, we develop application specific metrics that have the effect of selectively weighting the measurements.

## **5.12 Application-Based Metric**

### **5.12.1 The Application**

Given an application for our model, we can modify the above approach to better reflect the directions or data in the validation space that are most important to the application. One approach is to simply use only the validation data that covers the range of data important for the application. A second approach is to use the application itself to evaluate how the validation data should be weighted in defining a validation metric. We look at both approaches in the following sections. The application we chose for illustration is the two-dimensional impact of a small aluminum cylindrical slug against a larger diameter aluminum plate at 6 km/s presented in Section 3.4.

### **5.12.2 Reduced Data Set**

How do we use information from the application to help define our metric in validation space? To begin with, we can simply use the subset of the test data that is appropriate for the application. For example, the geometry of our application is such that we expect the shock wave speed and corresponding particle speeds to decrease as the shock travels into the larger diameter aluminum plate (see Section 3.4 for the CTH predictions of particle velocity). This suggests that we need to use only the  $U_P - U_S$  test data that correspond to particle speeds equal or slower than what we expect at the time of impact. Conservation of momentum requires that, for our example application, the initial particle speed at the time of impact be one-half the initial impact speed. This corresponds to 3000 m/s. To provide a bit of a margin for the application at hand, we will use data with particle speeds

in the range 0 to 3100 m/s. This corresponds to 89 of our 120  $U_P - U_S$  pairs. We now simply repeat the previous procedure using this subset of data.

Our sensitivity matrix will contain only those rows of the original sensitivity matrix that correspond to the validation data in the 0 to 3100 km/s  $U_P$  range. Its dimension will thus be 89x2. Using this revised sensitivity matrix, we generate the prediction covariance using Eq. (5.17). The covariance matrix for the prediction differences is given by Eq. (5.16). Eq. (5.20) is then used to evaluate the corresponding metric for this subset of data. Evaluating this metric for our 89 measurements gives

$$r^2 = 58.6 \quad (5.24)$$

We can now perform a statistical test to evaluate whether this distance between the experimental measurements and the model predictions is large relative to the uncertainty. The cumulative probability for some  $r^2$  is given by the  $\chi^2$  distribution for multi-normally distributed prediction errors (Beck and Arnold, p294). For 89 validation measurements

$$r^2 = \chi^2_{1-\alpha}(89) \quad (5.25)$$

where  $1-\alpha$  represents the cumulative probability. The value for  $r^2$  that contains 95% of the cumulative probability is

$$r_{critical}^2 = \chi^2_{0.95}(89) = 112.0 \quad (5.26)$$

Since  $r^2=58.6$  is smaller than 112.0, the difference between the model predictions and the experimental observations lies within the critical region. Therefore, we have no significant statistical evidence to reject the model as valid at the 95% confidence level using the data in the particle velocity range 0 to 3100 km/s. The level of significance of  $r^2=58.6$  is 99%. This is a very high significance suggesting that the model is very good in this data range. Inspection of Figure 5.9 shows that the model predictions tend to go through the center of the experimental measurements over this particle range. This is not the case for larger particle velocities and explains why we obtained such a high level of significance for this range of data, but not for the metric that uses all of the data.

### 5.12.3 Application Defined Metric

The validation metric in the previous section utilized the subset of data that was relevant to a particular application. The metric weighted this data by the inverse of the covariance matrix (i.e., uncertain data was weighted less, Eq. (5.20)). While we expect that the behavior of the model at particle velocities of 3 km/s (half the impact speed) is important very near the impact region, the behavior at these particle speeds will be less important as the shock wave propagates through the large plate of our application. The results of Section 3.4 show that the particle velocities throughout most of the plate are considerably

less than 3 km/s. This suggests that we should weight the particle velocities differently than simply by the inverse of the covariance matrix. How do we do this?

We begin by looking at the relationship between the model parameters and the CTH model for the application decision variable as shown in Figure 5.12. We denote our application decision variable by  $m$ . For our example, we take the time at which some point on the top surface of the large diameter disk (see Section 3.4) first reaches a particle velocity of 0.25 km/s to be our decision variable  $m$ . Due to symmetry, this point will be along the axis of the disk. There will be uncertainty in the model prediction of this decision variable due to the uncertainty in the model parameters. The uncertainty in the model parameters ( $\alpha_i = C_S$ ,  $\alpha_2 = S_1$ ) is represented by the characterization part of Figure 5.12. The application prediction uncertainty due to the model parameter uncertainty is shown in the decision variable part of Figure 5.12. Note that the model maps the two-dimensional uncertainty to a one-dimensional decision variable uncertainty for our example.

As was the case for the validation measurement predictions, we use a sensitivity analysis to develop a mapping between the application decision variable  $m$  and the model parameters. For this case,  $f$  represents the time at which a point on the top surface (along the centerline) has a particle velocity of 0.25 km/s.

As in the previous case, we take  $\Delta\alpha_i$  and  $\Delta\alpha_2$  to be 10% of the corresponding base values of  $C_S$  and  $S_1$  as listed in Table 5.2. The evaluation of the sensitivity matrix by the finite difference approximation defined by Eqs. (5.12) and (5.13) will thus require 3 runs of CTH for the two-dimensional application. The resulting sensitivity matrix will possess only one row since our decision variable is one-dimensional (i.e., we are using only one decision variable). A sensitivity analysis of our application decision variable gives

$$\Delta\tau = \mathbf{a} \begin{bmatrix} \Delta C_S \\ \Delta S_1 \end{bmatrix} \quad (5.27)$$

where the time at which the top surface reaches 0.25 m/s is denoted by  $\tau$  and

$$\mathbf{a} = \begin{bmatrix} -1.1511E-9 \\ 4.7034E-7 \end{bmatrix} \quad (5.28)$$

With knowledge of the sensitivity matrix  $\mathbf{a}$ , we can evaluate which direction in the model parameter space has no effect on the decision variable. We denote this direction  $\mathbf{b}$  and evaluate it as follows:

$$\Delta\tau = 0 = \mathbf{a}^T \mathbf{b} \quad (5.29)$$

where  $\mathbf{b}$  is a column vector. Note that Eq. (5.29) defines a direction in the parameter space that results in no change in the value for the decision variable, but it does not define

a magnitude. This direction is illustrated conceptually in the upper right part of Figure 5.12. Since we normalize by the length of  $\mathbf{b}$  later, the choice of magnitude of  $\mathbf{b}$  is arbitrary. One choice of the magnitude gives

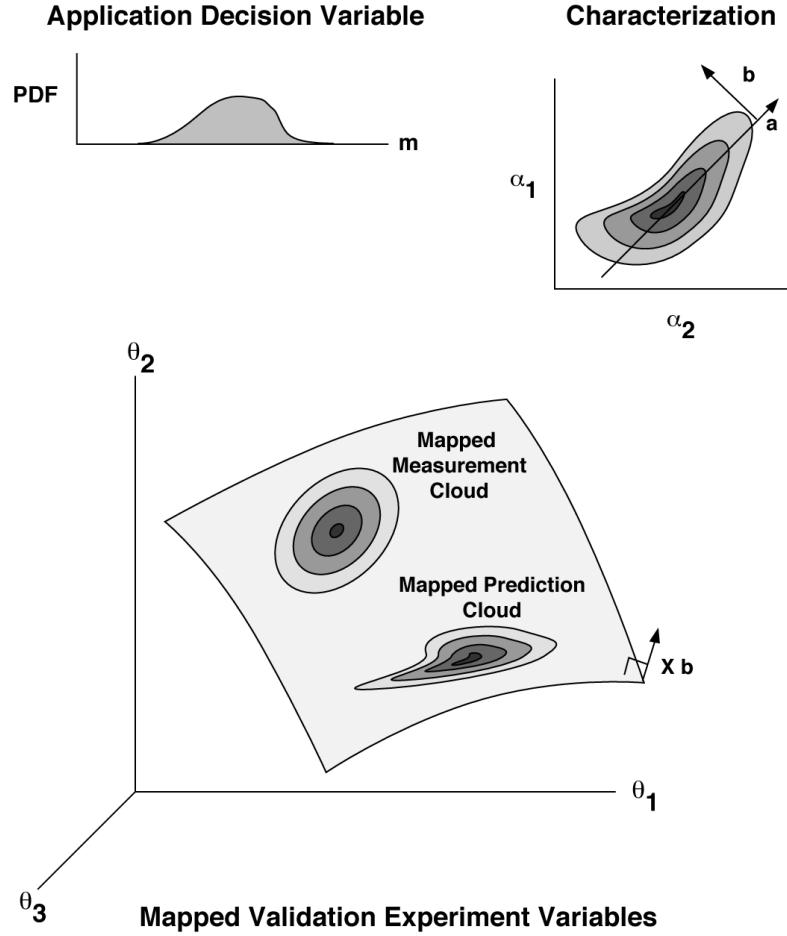


**Figure 5.12: Model Validation Sub-Space as Defined by an Application Decision Variable**

$$\mathbf{b} = \begin{bmatrix} 408.6 \\ 1.0 \end{bmatrix} \quad (5.30)$$

We can now map this direction into validation space using the sensitivity matrix found previously. Since we are developing an application specific metric, we will use the application specific subset of data (i.e., the 89 data pairs) and the corresponding sensitivity matrix defined in Section 5.12.2. The direction in 89 dimensional validation space that corresponds to the  $\mathbf{b}$  direction for the model parameters is given by

$$\boldsymbol{\beta} = \mathbf{X}\mathbf{b} \quad (5.31)$$

This direction is illustrated conceptually in the lower part of Figure 5.12. Since discrepancies between the model predictions and the experimental observations do not have an impact on the application decision variable along this direction (as defined by our CTH model for the application), we do not need to measure the prediction-measured differences along this direction. To remove the effect of this direction, we project the validation space into a hyperplane orthogonal to  $\boldsymbol{\beta}$  as follows:

The projection matrix that projects points in the  $n$ -dimensional ( $n = 89$ ) space into the  $n-1$  dimensional hyperplane is given by (Strang, 1976)

$$\mathbf{P} = \mathbf{I} - \boldsymbol{\beta}(\boldsymbol{\beta}^T\boldsymbol{\beta})^{-1}\boldsymbol{\beta}^T \quad (5.32)$$

where  $\mathbf{I}$  is the identity matrix. Note that application of the above projection to  $\boldsymbol{\beta}$  itself (or some multiple of  $\boldsymbol{\beta}$ ) should result in zero:

$$\begin{aligned} \mathbf{P}\boldsymbol{\beta} &= (\mathbf{I} - \boldsymbol{\beta}(\boldsymbol{\beta}^T\boldsymbol{\beta})^{-1}\boldsymbol{\beta}^T)\boldsymbol{\beta} \\ &= \boldsymbol{\beta} - \boldsymbol{\beta}(\boldsymbol{\beta}^T\boldsymbol{\beta})^{-1}(\boldsymbol{\beta}^T\boldsymbol{\beta}) \\ &= \boldsymbol{\beta} - \boldsymbol{\beta} = \mathbf{O} \end{aligned} \quad (5.33)$$

We see that this subspace ignores the direction in the  $n$ -dimensional validation space that corresponded to no change in the application decision variable. We can now use the projection  $\mathbf{P}$  to project quantities in our  $n$  dimensional validation space into the  $n-1$  subspace.

$$\mathbf{Us\_pred}^P = \mathbf{P} \mathbf{Us\_pred} \quad (5.34)$$

$$\mathbf{Us\_exper}^P = \mathbf{P} \mathbf{Us\_exper} \quad (5.35)$$

where the  $P$  superscript denotes a projection into the subspace and the bold  $\mathbf{Us}$  represents the vector of shock speed predictions and measurements. The expected value and covariance matrices for these quantities in the projected space are

$$E(\mathbf{Us\_pred}^P) = \mathbf{P} E(\mathbf{Us\_pred}) \quad (5.36)$$

$$\text{cov}(\mathbf{Us\_pred}^P) = \mathbf{P} \text{cov}(\mathbf{Us\_pred}) \mathbf{P}^T \quad (5.37)$$

$$E(\mathbf{Us\_exper}^P) = \mathbf{P} E(\mathbf{Us\_exper}) \quad (5.38)$$

$$\text{cov}(\mathbf{Us\_exper}^P) = \mathbf{P} \text{cov}(\mathbf{Us\_exper}) \mathbf{P}^T \quad (5.39)$$

We also have

$$E(\mathbf{Us\_pred}^P - \mathbf{Us\_exper}^P) = E(\mathbf{Us\_pred}^P) - E(\mathbf{Us\_exper}^P) \quad (5.40)$$

$$\text{cov}(\mathbf{Us\_pred}^P - \mathbf{Us\_exper}^P) = \text{cov}(\mathbf{Us\_pred}^P) + \text{cov}(\mathbf{Us\_exper}^P) \quad (5.41)$$

We can now define our measure in the projected space. Since our projections are linear, multivariate normal distributions project to multivariate normal distributions. The projected distributions are marginal distributions in the sense that the  $n$  dimensional PDF is integrated along the direction  $\beta$  to form the marginal distribution on the projection hyperplane.

For a multi-normal PDF, curves of constant probability are given by constant values of  $r^2$  where

$$r^2 = [p_1 - p_{mean1} \quad p_2 - p_{mean2} \quad \cdots \quad p_{89} - p_{mean89}] \text{cov}(\mathbf{p})^{-1} \begin{bmatrix} p_1 - p_{mean1} \\ p_2 - p_{mean2} \\ \vdots \\ p_{89} - p_{mean89} \end{bmatrix} \quad (5.42)$$

and

$$p = \mathbf{Us\_pred}^P - \mathbf{Us\_exper}^P \quad (5.43)$$

For our case, we wish to test the hypothesis that the mean prediction errors for each measurement location (i.e., each  $U_P$ ) is zero. In this case, Eq. (5.42) becomes

$$r^2 = [p_1 \quad p_2 \quad \cdots \quad p_{89}] \text{cov}(\mathbf{p})^{-1} \begin{bmatrix} p_1 \\ p_2 \\ \vdots \\ p_{89} \end{bmatrix} \quad (5.44)$$

The inverse of  $\text{cov}(\mathbf{p})$  does not exist in the  $n$  dimensional space because we have removed the uncertainty associated with the  $\beta$  direction. However, the inverse will exist in the projected subspace where we plan to use our metric. To evaluate the inverse in this subspace, we must remove the effect of the  $\beta$  direction from the  $n$ -dimensional covariance matrix. A procedure to do this is to use the singular value decomposition of  $\text{cov}(\mathbf{p})$  as follows (see Golub and Van Loan, 1989, p70)

$$\text{cov}(\mathbf{p}) = \mathbf{U} \mathbf{\Sigma} \mathbf{V}^T \quad (5.45)$$

where  $\mathbf{\Sigma}$  is a  $n \times n$  diagonal matrix of singular values:

$$\mathbf{\Sigma} = \text{diag}(\sigma_1, \sigma_2, \dots, \sigma_{n-1}, 0) \quad (5.46)$$

Since  $\text{cov}(\mathbf{p})$  is a projection into a  $n-1$  subspace, one of the singular values must be zero. The pseudo-inverse of our covariance matrix is given by (Golub and Van Loan, 1989, p243):

$$\text{cov}(\mathbf{p})^+ = \mathbf{V} \mathbf{\Sigma}^+ \mathbf{U}^T \quad (5.47)$$

where  $\mathbf{\Sigma}^+$  is a  $n \times n$  diagonal matrix with its components given by

$$\mathbf{\Sigma}^+ = \text{diag}\left(\frac{1}{\sigma_1}, \frac{1}{\sigma_2}, \dots, \frac{1}{\sigma_{n-1}}, 0\right) \quad (5.48)$$

Setting the last component to zero has the effect of ignoring the direction  $\mathbf{\beta}$  and our pseudo-inverse gives us the inverse for the  $n-1$  dimensional subspace. Note that the evaluation of pseudo-inverses is a common feature of most linear algebra packages. Here we used Mathematica (Wolfram Research, Champaign IL).

Writing our metric for the subspace in terms of the pseudo-inverse gives

$$r^2 = \begin{bmatrix} p_1 & p_2 & \cdots & p_{89} \end{bmatrix} \text{cov}(\mathbf{p})^+ \begin{bmatrix} p_1 \\ p_2 \\ \vdots \\ p_{89} \end{bmatrix} \quad (5.49)$$

We are now ready to perform our statistical inference in our application-defined subspace. Evaluating Eq. (5.49) for our 89 model predictions and experimental measurements gives

$$r^2 = 54.7 \quad (5.50)$$

We can now perform a statistical test for the probability of this measure of the prediction difference. As before, the cumulative probability for some  $r^2$  in this multi-normal PDF cloud is given by the  $\chi^2$  distribution (Beck and Arnold, p. 294). For 88 degrees of freedom of the subspace (i.e.,  $n-1$ )

$$r^2 = \chi^2_{1-\alpha}(88) \quad (5.51)$$

where  $1-\alpha$  represents the cumulative probability. The value for  $r^2$  which contains 95% of the cumulative probability is

$$r_{critical}^2 = \chi_{0.95}^2(88) = 110.9 \quad (5.52)$$

Since  $r^2=54.7$  is smaller than 110.9, we cannot reject the hypothesis that the mean prediction error is zero. Therefore, there is no statistical evidence to reject the model as valid at the 95% confidence level. The level of significance of  $r^2=54.7$  is greater than 99.8%. For this particular 2-dimensional application, with this set of boundary conditions and mean parameter values, the model appears valid based on this application dependent metric.

### 5.13 Summary

In this chapter, we illustrated the use of a propagation of uncertainty analysis (specifically, sensitivity analysis) with a description for the uncertainty in the experimental observations, to perform several statistical tests for model validity for a shock wave physics application. Because the model predictions were sufficiently linear in the model parameters, and because the uncertainty in the model parameters were well represented by a correlated, multi-normal probability distribution, the resulting uncertainty in the model predictions were also well represented by a correlated, multi-normal distribution. This eases the analytical effort in performing the statistical inference, but is not fundamental to our approach.

Several validation metrics (measures of distance between the model prediction and experimental observations) were considered. First, we utilized the uncertainty in the model predictions due to model parameter uncertainty and the uncertainty in the experimental observations to develop a metric that is based on equal PDF curves using all of the experimental data. This approach corresponds to that presented in Hills and Trucano (1999) and weights those prediction errors based on their uncertainty. No consideration of the ultimate application of the metric is made.

We then specialized the metric to be application specific. Initially, we defined a metric utilizing a subset of validation data that corresponds to the range of particle velocities important for the application considered.

Finally, we used the same subset of data, but developed a procedure to weight the data according to how an application weights the data based on a sensitivity analysis. This measure is a form of an integrated measure metric in that the metric is defined in a subspace of the validation space.

For the example presented, the model passed all of the validation tests. This suggests that CTH, when using the Mie-Grüneisen EOS model calibrated using the selected aluminum  $U_P - U_S$  data, provides scientifically valid predictions of shock wave speed versus particle

speed, over the range of the validation data. Such was not the case for CTH when the SESAME 3700 EOS model was used. The reverse conclusion would be expected to be true for data corresponding to much higher shock velocities given the greater theoretical completeness of the EOS represented by the SESAME model.

We will comment in our conclusions about the likely source of the particular problem of consistency with the data for this choice of model. However, we stress here that the purpose of our work in this report is focused on means of measuring such discrepancies and their interpretation in terms of statistical inference. The particular source of the validity problem for CTH plus the SESAME table for computing shocks in aluminum is not of great concern in this context.

The probability level for the resulting measures was 99% or higher for the tests using a subset of data and the weighted subset of data, but 25% for the tests using all of the data. This suggests that better agreement between model predictions and the experimental results were obtained in the  $U_p < 3100$  m/s range. Close inspection of Figure 5.9 shows that there appears to be a little more bias in the predictions from the data in the  $U_p > 3100$  m/s range.

(Page Left Blank)

## 6.0 Discussion and Recommendations

### 6.1 Overview of Work Accomplished

Our increasing reliance on computer models and our decreasing use of experimental testing has elevated our need for rigorous model validation methodology. Comparisons of model predictions to experimental observations through traditional “view graph metrics” are no longer acceptable for critical applications. More rigorous techniques must be used to establish whether observed differences between model predictions and experimental observations are due to the model itself, or due to uncertainty in the model parameters and experimental observations.

Statistical concepts can be used to develop rigorous methodology to compare model predictions to experimental observations. This methodology is well established for simple models and can be, in concept, extended to the more complex models associated with engineering and scientific applications. One of the requirements in the application of statistical methodology is the development of the probability models for the uncertainty in the prediction differences (predicted measurements minus experimental measurements). These probability models allow statistically meaningful tests to be performed to evaluate the probability of an observed set of differences between predictions and observations.

The traditional approach to develop this model for uncertainty is to use the set of differences directly. One typically assumes a distribution for the differences, evaluates the statistical parameters for this distribution, and then tests the hypothesized distribution against the data to evaluate where there is evidence that the distribution is not valid. If there is no evidence, then statistical inference can be used to evaluate whether the model predictions are consistent with the experimental observations. A characteristic of this approach is that the statistical properties (mean, variance) are generally assumed to be uniform over the data and the data is generally assumed to be independent. These assumptions will rarely be appropriate for the complex models considered here. However, one may be able to remove the trend in the differences so that the resulting residuals are well approximated by a standard distribution with uniform statistics. We provided an example of such an approach in Chapter 4 for a shock wave physics model.

The alternative approach is to develop the statistical model for differences using the experimental data and using the model itself. It is generally easier to characterize the uncertainty in experimental data than to characterize the uncertainty in the differences since the experiment can generally be designed so that there is little correlation, or easily identifiable correlation between measurements. In contrast, the very act of subtracting experimental observations from model predictions can introduce a complex correlation structure in the resulting differences since the model predictions typically possess a complex correlation structure due to the nonlinear dependence of the model on uncertain model parameters. If the uncertainty in the model parameters can be characterized, then

this uncertainty can be propagated through the model to develop an uncertainty model, including correlation, for the model predictions. This prediction uncertainty can then be added to the measurement uncertainty to establish an overall uncertainty for the validation experiment. The overall uncertainty can then be used to test the predictive model for validity, as inferred from a particular set of experimental data. A detailed example of this approach was provided in Chapter 5 for the shock wave physics model using a sensitivity analysis.

We can further refine the above approach if we have a particular application in mind. For example, our application may require that the model be valid over a limited range of data. In this case, only the model validation data that represents application can be used to test the model. This approach can be further focused if we use a model for the application to estimate how the validation data should be weighted during the validation test. Even though the application may require that the model be valid over a range of data, the performance of the model for the application may depend very heavily on the performance in a subrange of the data. We developed and demonstrated an approach to define a weighted validation metric at the end of Chapter 5. This development was also based on a sensitivity analysis.

## **6.2 Application to Nonlinear Problems**

The use of sensitivity analysis to evaluate the prediction probability distributions assumes that the predictions are locally linear in the model parameters. While this limitation may seem very restrictive at first glance, it is not as restrictive as one might think for model validation involving engineering applications. Many such model validation experiments are carefully controlled so that there is little uncertainty in the model parameters (such as those characterizing geometry, material properties, and in the boundary conditions). As a result, there will be little uncertainty in the model predictions for the validation experiment. The locally linear approximation for this application of sensitivity analysis must be valid only over the scale associated with the prediction uncertainty (say out to the 95% confidence intervals) for the model validation experiments. If the scale of the corresponding prediction uncertainty is small compared to the scale of the non-linearity, then the use of sensitivity analysis will be appropriate.

Even though the validation experiments are carefully controlled so that the sensitivity analysis approach is appropriate, such careful control may not be the possible for the final application of the model. For example, the material properties may be well defined for a validation experiment since they can be measured using samples from that manufacturing batch. In contrast, the uncertainty in the material properties for the application may not be as well defined since they may come from different batches and from different manufacturers. Boundary conditions are generally well controlled for validation experiments whereas they are not for the actual application. In these cases, the uncertainty in the model parameters for the application can be much larger than for the validation experiments. So while a sensitivity analysis may be appropriate for the development of a

validation metric, a nonlinear approach may be required for predicting uncertainty during the actual application of the model.

There are also cases for which the sensitivity analysis approach may not be appropriate for validation experiments. For example, validation experiments in the geosciences can have very large uncertainties in model predictions due to the large uncertainties in the characterization of the geological media. In such cases, nonlinear approaches, such as Monte Carlo analysis, rather than sensitivity analysis, may be required to characterize the uncertainty of the model validation experiments. Engineering applications for which there is large uncertainty in model parameters for the validation experiments (such as joint to joint friction in a structure) may also require nonlinear approaches for model validation.

### **6.3 Recommendations**

We feel that this report represents good progress toward developing rigorous methodology to compare model predictions to experimental observations. As such, we suggest that this methodology is ready to be applied to a broader class of applications than the one presented here. However, there are outstanding issues that should be addressed to increase the range of application.

The application-defined metric developed in Chapter 5 uses a sensitivity analysis of the application to define the directions in the model parameter space that are not important for the application. This approach is appropriate for cases where the corresponding directions do not change significantly across the scales of uncertainty of these parameters for the validation experiments. However, there are applications for which a strong nonlinearity is exhibited for small changes in the model parameters, or for which the uncertainty in the model parameters for the validation experiments are large. Field scale validation experiments in the geotechnical fields, such as penetrator experiments, or experiments involving transport through geological media, are examples of applications with large uncertainties in the model parameters. The use of sensitivity analysis to define the validation metric is suspect for these cases. Computationally efficient, nonlinear methods should be developed which don't require the evaluation of the full  $n$ -dimensional probability density function for validation.

A second area that should be addressed is to expand the present work to include non-standard probability distributions. For the shock wave problems presented, there was good statistical evidence that the uncertainties associated with the model parameters, the model predictions, and the experimental observations were all well represented by multi-normal probability distributions. This greatly simplified the definition of the validation metrics as they are related to the well known  $\chi^2$  distribution. For problems for which the model predictions are not distributed in a fashion that is well modeled by standard probability distributions, the computational effort required to resolve these probability distributions and to define metrics can be large, and in many cases, prohibitive. Techniques are needed to handle such distributions, preferably in application defined

subspaces, so as to reduce the computational requirements to resolve the validation metrics.

A third area that should be addressed in the future is to further develop the relationship between the validation experiments and the anticipated application of the model. Just as the application can be used to help define a metric for the validation experiments, we should be able to extend this idea to multiple sets of validation experiments, each designed to test a subset of the physics. This relationship should tell us how to weight the results from the different sets of data and whether the different sets of data adequately test the model over the anticipated range of model parameters.

#### **6.4 Comment on the Discrepancy**

It has been our experience that this report is frustrating to a certain audience because of our rather glib approach to dealing with the discrepancy reported between the model, with the specification of the 3700 SESAME table, and the 2024 aluminum shock experimental data. Our stated focus in this report is on how to compare models and data and how to assess validity of the model from the resulting information. For this report we are, in fact, fairly uninterested in the specific cause of the lack of validity we observed for the model which used the 3700 SESAME table. We will now briefly comment on the likely cause.

The fact that we have consistently distinguished the use of the specific SESAME table in the inconsistent data comparisons we report strongly suggests that we believe that the source of the problem is the particular material EOS chosen. It is well understood in computational shock wave physics that calculation accuracy is limited by the accuracy of the underlying material models, and the current work is no exception. A simple illustration supports this understanding in the present case. Figure 6.1 shows a comparison of a prediction of the Hugoniot for the 3700 table with the experimental data. The Hugoniot is constructed from the SESAME table using a tool that analyzes the table data directly.

On the face of it the differences between prediction and experimental data in Figure 6.1 are very close to those observed in Figure 3.8, which compared CTH results and the experimental data. In particular, the bias towards larger errors at higher impact velocities is clearly present in Figure 6.1. Thus, the use of the 3700 SESAME table almost certainly is the main source of the invalidity of the model reported earlier in this report.

However, in the spirit of the underlying goals and principles of this paper it is important to quantitatively confirm this hypothesis. In particular, a statistical analysis of the comparison of the SESAME table and the data similar to that of Section 4 should be undertaken. The results of such an analysis should remain invariant with respect to the results reported in Section 4 to make a scientifically precise statement that the chosen EOS model is indeed the main source of the invalidity. For example, if some results of the statistical analysis of Section 4 changed significantly when analyzing the differences

seen in Figure 6.1 then this is evidence that the model is introducing additional factors into the error structure that are not fully accounted for by the equation of state alone. Such an analysis is beyond the scope of the present paper.

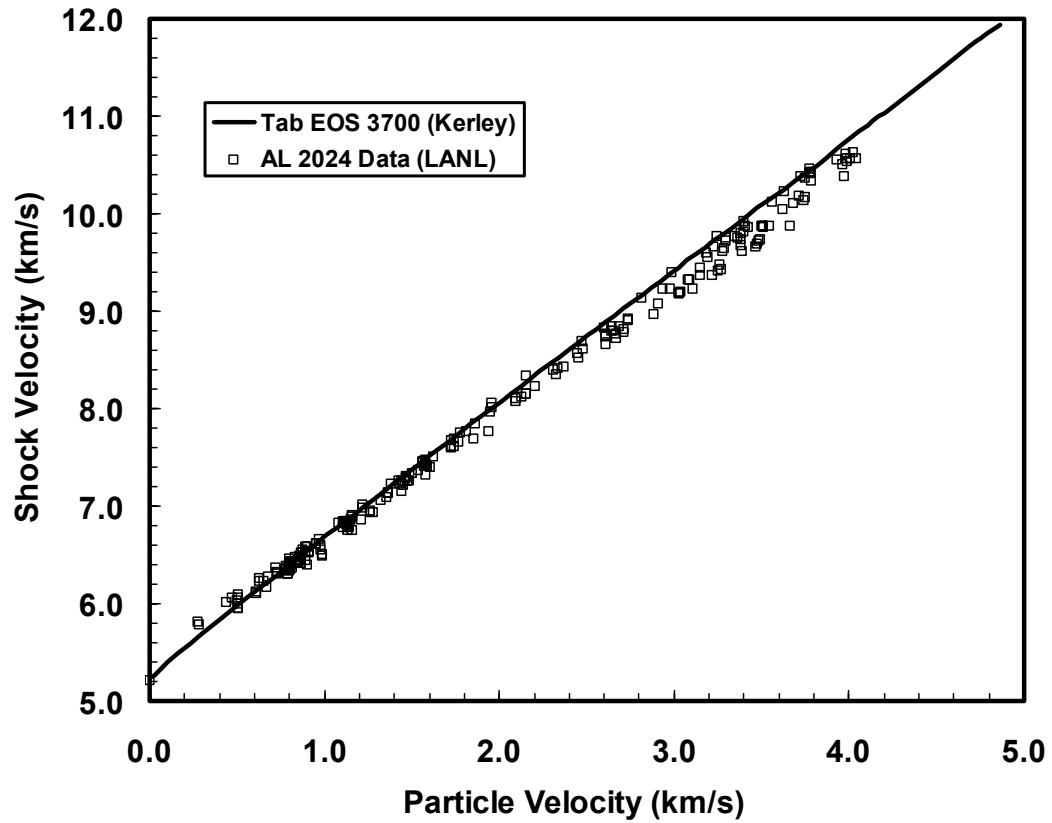


**Figure 6.1** Comparison of 2024 aluminum shock data with predicted Hugoniot data from the 3700 SESAME table.

(Page Left Blank)

## References

- Al'tshuler, L. V., R. F. Trunin, K. K. Krupnikov, N. V. Panov, 1996, *Explosive Laboratory Devices for Shock Wave Compression Studies*, **Physics – Uspekhi**, Volume 39, No. 5, pp. 539-544.
- Ang, J. A., T. G. Trucano, and D. R. Luginbuhl, 1999, *Confidence in ASCI Scientific Simulations*, Sandia National Laboratories, unpublished manuscript.
- Asay, J. R., 1981, **The Sandia National Laboratories Shock Thermodynamics Applied Research (STAR) Facility**, SAND81-1901, Sandia National Laboratories.
- Asay, J. R., L. C. Chabildas, and L. M. Barker, 1985, **Projectile and Impactor Designs for Plate-Impact Experiments**, SAND85-2009, Sandia National Laboratories, Albuquerque, New Mexico.
- Avrorin, E. N., B. K. Vodolaya, V. A. Simonenko, and V. E. Fortov, 1993, *Intense Shock Waves and Extreme States of Matter*, **Physics – Uspekhi**, Volume 36, No. 5, pp. 337-364.
- Beck, J. V. and K. J. Arnold, 1977, **Parameter Estimation in Engineering and Science**, John Wiley & Sons, Inc., New York.
- Bell, R. L., M. R. Baer, R. M. Brannon, M. G. Elrick, E. S. Hertel, Jr., S. A. Silling, and P. A. Taylor, 1998, **CTH User's Manual and Input Instructions, Version 4.0**, Sandia National Laboratories, Albuquerque.
- Bland, D. R. (1965), "On Shock Structure in a Solid," *J. Inst. Math. Applies.*, Vol. 1, pp. 56-75.
- Brownlee, K. A., 1965, **Statistical Theory and Methodology in Science and Engineering**, John Wiley & Sons, Inc., New York.
- Cable, A. J., 1970, *Hypervelocity Accelerators*, in **High-Velocity Impact Phenomena**, ed. R. Kinslow, Academic Press, New York, pp. 1-21.
- Chhabildas, L. C., 1987, *Survey of Diagnostics Tools Used in Hypervelocity Impact Studies*, *Int. J. Impact Engng.*, Vol. 5, No. 5, 205-220.
- Davison, L. and R. A. Graham, 1979, *Shock Compression of Solids*, **Physics Reports**, Vol. 55, No. 4, pp. 255-379.
- Duvall, G. E. and R. A. Graham, 1977, *Phase Transitions Under Shock-Wave Loading*, **Reviews of Modern Physics**, Vol. 49, No. 3, pp. 523-579.

Golub, G. H., and Van Loan, C. F., 1989, **Matrix Computations**, The Johns Hopkins University Press, Baltimore.

Graham, R. A. and J. R. Asay, 1978, *Measurement of Wave Profiles in Shock-Loaded Solids*, **High Temperatures – High Pressures**, Vol. 10, pp. 355-390.

Graham, R. A., 1993, **Solids Under High-Pressure Shock Compression**, Springer-Verlag, New York.

Hertel, E. S. Jr., and G. I. Kerley, 1998, **CTH EOS Package: Introductory Tutorial**, SAND98-0945, Sandia National Laboratories, Albuquerque.

Hills, R. G., and T. G. Trucano, 1999, **Statistical Validation of Engineering and Scientific Models: Background**, SAND99-1256, Sandia National Laboratories, Albuquerque.

Holian, K. S., 1986, *A New Equation of State for Aluminum*, **Journal of Applied Physics**, Vol. 59, No. 1, pp. 149-157.

Johnson, J. D., 1996, **General Features of Hugoniot**, LA-13137-MS, Los Alamos National Laboratory.

Johnson, J. D., 1996, **General Features of Hugoniot – II**, LA-13217-MS, Los Alamos National Laboratory.

Kerley, G. I., Theoretical Equation of State for Aluminum, *Int. J. Impact Engng.*, Vol. 5, No. 5, 441-449.

Kerley, G. I., 1991, **User's Manual for PANDA II: A Computer Code for Calculating Equations of State**, SAND88-2291, Sandia National Laboratories, Albuquerque.

Lee, J. R., 1998, **Certainty in Stockpile Computing: Recommending a Verification and Validation Program for Scientific Software**, SAND98-2420, Sandia National Laboratories, Albuquerque, New Mexico.

Marsh, S. P., editor, 1980, **LASL Shock Hugoniot Data**, University of California Press, Berkley, pp. 166-172.

McQueen, R. G., S. P. Marsh, J. W. Taylor, J. N. Fritz, and W. J. Carter, 1970, *The Equation of State of Solids From Shock Wave Studies*, in **High-Velocity Impact Phenomena**, ed. R. Kinslow, Academic Press, New York, pp. 293-416.

- McGlaun, J. M., S. L. Thompson, and M. G. Elrick, 1990, *CTH: A Three-Dimensional Shock Wave Physics Code*, **International Journal of Impact Engineering**, Vol. 10, No. 1-4, pp. 351-360.
- Miller, I. and J. E. Freund, 1985, **Probability and Statistics for Engineers**, Prentice-Hall, Inc., Englewood Cliffs, New Jersey.
- Mitchell, A. C., W. J. Nellis, J. A. Moriarty, R. A. Heinle, N. C. Holmes, R. E. Tipton, G. W. Repp, 1991, *Equation of State of Al, Cu, No, and Pb at Shock Pressure Up to 2.4 Tpa (24 Mbar)*, **Journal of Applied Physics**, Vol. 69, No. 5, pp. 2981-2986.
- Nicholas, T. and A. M. Rajendran, 1990, *Material Characterization at High Strain Rates*, in **High Velocity Impact Dynamics**, ed. J. A. Zukas, John Wiley & Sons, New York.
- Reckhow, K. H., J. T. Clements, and R.C. Dodd, 1990, *Statistical Evaluation of Mechanistic Water Quality Models*, **Journal of Environmental Engineering**, Vol. 116, No. 2, pp. 250-268.
- Rice, M. H., R. G. McQueen, and J.M. Walsh, 1958, *Compression of Solids by Strong Shock Waves*, **Solid State Physics**, Academic Press, New York, Vol. 6, pp. 1-63.
- Roache, P. J., 1998, **Verification and Validation in Computational Science and Engineering**, Hermosa Publishers, Albuquerque, New Mexico.
- Strang, G., 1976, **Linear Algebra and Its Applications**, Academic Press, New York.
- Trainor, R. J., J. W. Shaner, J. M. Auerbach, and N. C. Holmes, 1979, *Ultrahigh-Pressure Laser-Driven Shock-Wave Experiments in Aluminum*, **Physical Review Letters**, Vol. 42, No. 17, pp. 1154-1157.
- Trunin, R. F., 1994, *Shock Compressibility of Condensed Materials in Strong Shock Waves Generated by Underground Nuclear Explosions*, **Physics – Uspekhi**, Vol. 37, No. 11, pp. 1123-1146.
- Vladimirov, A. S., N. P. Voloshin, V. N. Nogin, A. V. Petrovtsev, V. A. Simonenko, 1984, *Shock Compressibility of Aluminum at Pressure approximately equal to or greater than 1 Gbar*, **JETP Letters**, Vol. 39, No. 2, pp. 81-85.
- Zel'Dovich, Ya. B. and Yu. P. Raizer, 1967, **Physics of Shock Waves and High-Temperature Hydrodynamic Phenomena**, Academic Press, New York.

(Page Left Blank)

## Appendix A: Multiple Runs of CTH and Post Processing

The example problems presented required CTH to be run multiple times to generate shock speeds for multiple impact velocities. To facilitate this, we developed a simple scheme to automate this process:

1. A file of the experimental  $U_P - U_S$  pairs was first generated (cut and pasted) from the data. Two versions were generated, one containing all 232 data pairs for the analysis performed in Chapter 4, and one containing the randomly selected subset of 120 validation data pairs for the analysis performed in Chapter 5.
2. A simple program was written (called RANDOM) to read the data pair file from item 1, and write out another file containing 232 (or 120) records corresponding to the initial material velocities (i.e.,  $2 U_P$ ) in the format required by CTH.
3. A CTH preprocessor was written (called INPUT) to read a record from the initial material velocity file of item 2, and use this record to replace the corresponding record in the CTH input file.
4. A CTH history postprocessor was written (HISTORY) to read a CTH history file, and write selected data (particle velocity as a function of time at the 4 cm tracer point as defined in the CTH input file) to the end of a results file.
5. A simple script was written to loop through calls of INPUT, CTHGEN, CTH, and HISTORY multiple times (i.e., 232 or 120). Upon execution of the script, the results file defined in item 4 contains time traces of particle speed at the tracer point for each of the 232 (or 120) CTH runs.
6. A postprocessor was written (POSTPROC) to read the results file containing the 232 (or 120) time traces of particle speed, and the corresponding experimental  $U_P - U_S$  pairs from the file defined in item 1. The traces were analyzed to evaluate the arrival time of the shock, and the corresponding predicted shock wave speed as discussed below. The particle speed, experimental shock speed, and the resulting predicted shock speed were then written to a file for each of the 232 (or 120) impact speeds. This file was used as the basis for all statistical processing.

The evaluation of the shock speed using the tracer point particle speed history was fairly straight forward. We first evaluated the time of arrival of the shock at the tracer point initially located 4 cm from the impact surface in the initially stationary plate. The arrival time is taken to be that time at which the tracer particle speed reaches  $0.5 U_P$ . To evaluate this time, the postprocessor simply searches along a history trace of time vs. tracer speed until a tracer speed greater than  $0.5 U_P$  is found. This defines a time interval (i.e., bounded by this time and the previous time in the history trace) containing the time at which the tracer speed reaches  $0.5 U_P$ . Linear interpolation was then used to estimate the time in this interval at which the tracer speed reaches  $0.5 U_P$ . The corresponding

shock speed was then estimated by dividing the distance traveled (4 cm) by the interpolated shock arrival time.

The same linear interpolation process was used to determine the time at which the particle speed on the back surface of the large cylinder of the 2-dimensional example (as described in Section 3.4) reached 0.25 km/s.

The derivatives for the sensitivity analysis for the 120 validation data pairs (Chapter 5) were estimated by running the above script three times; once for the base model parameters, and once each for the perturbations of the two EOS parameters. This resulted in three data files (see item 6), each giving the corresponding predicted shock wave speeds for each of the 120 particle speeds. Another program was used to read these three data files and estimate the corresponding sensitivity derivatives using finite differences.

We comment that our method of determining shock velocity suffers from one weakness associated with steadiness of the wave. At the impact position the shock wave is not yet steady, and this will introduce a small error into this analysis. A simple discussion of this problem is given in (Bland, 1965). A method that would correct this error is to use two downstream points where the shock would be steady at both locations. We thank Marlin Kipp for reminding us of this difficulty.

Following is a listing of the base CTH input deck for the SESAME AL2024 EOS model.

95



```

*
control
  tstop=9.0e-6
*  ncycle = 50
  rdumpf = 3600.
  cpshift = 30.
endc
*
*****
*
*  time step records
*
mindt
  time = 0.  dt = 1.e-9
endn
*
maxdt
  time = 0.  dt = .01
endx
*
*****
*
*  tracer records
*
tracer
  add 0.
  add 4.
endt
*
*****
*
*  edit records
*
edit
  exact
  shortt
    time = 0.  dt = 1.0e-7
  ends
  longt
    time = 0.  dt = 10.
  endl
  plott
    time = 0.  dt = 10.
  endp
  histt
    time = 0.  dt = 1.0e-7
    htracer1
    htracer2
  endh
ende
*
*****
*
*  boundary condition records
*
boundary
  bhydro
    block 1
    bxb = 0  bxt = 0
  endb
endh
endb
*
*  end of cth input

```



## Appendix C: CTH Input File Listing for a Two Dimensional Application

Following is a listing of the base CTH input deck for the two-dimensional application model discussed in Section 3.4.

```
*****  
*  
*eor* cgenin  
*  
*****  
*  
*   cthgen input for aluminum impact  
*  
*   >>>>>>>>>>>>>>>>>>>>>>>>>>>>>>>*****  
*   aluminum at various km/s      stationary aluminum  
*  
*****  
*  
*   Title record  
*  
Two-Dimensional Benchmark Problem - Aluminum impact at 6 km/s  
*  
*****  
*  
*   control records  
*  
control  
endc  
*  
*****  
*  
*   edit records  
*  
*edit  
*   block 1  
*     expanded  
*   endb  
*ende  
*  
*****  
*  
*   mesh records  
*  
mesh  
  block 1 geom=2dc type=e  
    x0 0.0  
      x1 n=240 dxf=.025 w=6.0  
    endx  
  
  y0 -2.0  
    y1 n=400 dyf=.025 w=10.0
```



```

*
*****
*
*   Title record
*
Two-Dimensional Benchmark Problem - Aluminum impact with mean of various
km/s
*
*****
*
*   control records
*
restart
  nu = 1
endr
*
control
  tstop=8.0e-6
*   nscycle = 50
  rdumpf = 3600.
  cpshift = 30.
endc
*
*****
*
*   time step records
*
mindt
  time = 0.  dt = 1.e-9
endn
*
maxdt
  time = 0.  dt = .01
endx
*
*****
*
*   tracer records
*
tracer
  add 0. 0.
  add 0. 5.
endt
*
*****

*
*   edit records
*
edit
  exact
  shortt
    time = 0.  dt = 1.0e-6
  ends
  longt
    time = 0.  dt = 10.
  endl
  plott
    time = 0.  dt = 1.0e-6
  endp
  histt
    time = 0.  dt = 1.0e-7

```





## Appendix D: Data

The following tables provide the model predictions and the sampled data used for the CTH analysis presented in Chapters 4 and 5.

**Table D1: Predicted Shock Speed vs. Experimental Measurements (m/s): 232 data sets, see Figure 3.8.**

Up	Us_exp	Us_pred	Up	Us_exp	Us_pred	Up	Us_exp	Us_pred
278	5811	5604.6	818	6366	6376.8	1134	6826	6819.7
279	5782	5606.1	831	6436	6396.9	1136	6831	6823.7
440	6021	5839.4	833	6483	6399.8	1141	6795	6831.0
472	6054	5885.4	839	6419	6407.4	1144	6783	6835.4
497	6025	5920.4	850	6415	6422.1	1146	6861	6838.3
502	6098	5930.2	854	6443	6428.1	1157	6893	6853.7
503	5996	5931.7	858	6488	6434.0	1157	6752	6853.7
507	6055	5937.4	859	6445	6435.5	1159	6915	6856.7
509	5947	5938.6	859	6470	6435.5	1206	6857	6919.4
509	5953	5938.6	860	6446	6436.9	1220	6981	6941.8
608	6125	6079.5	862	6472	6439.1	1220	7014	6941.8
609	6103	6080.9	863	6486	6440.5	1260	6955	6995.3
626	6262	6106.8	864	6418	6441.9	1263	6938	6999.3
627	6228	6107.0	865	6518	6443.3	1277	6943	7018.5
650	6226	6139.7	871	6561	6450.2	1318	7062	7077.6
671	6164	6169.1	873	6522	6453.0	1352	7092	7123.3
677	6277	6176.4	888	6541	6476.9	1362	7143	7138.8
722	6367	6241.4	891	6589	6481.0	1362	7139	7138.8
727	6323	6248.8	892	6442	6482.3	1383	7225	7166.5
728	6310	6250.2	896	6589	6487.7	1426	7268	7226.6
768	6348	6308.0	897	6579	6489.0	1432	7228	7235.2
778	6388	6320.9	901	6402	6494.2	1437	7156	7242.3
786	6312	6332.2	910	6530	6507.0	1445	7268	7252.0
790	6304	6337.5	910	6534	6507.0	1446	7211	7253.4
792	6365	6340.3	953	6616	6567.9	1461	7269	7273.9
792	6314	6340.3	953	6617	6567.9	1465	7295	7279.4
793	6308	6341.7	966	6659	6584.2	1467	7305	7278.2
798	6342	6347.4	975	6607	6599.1	1479	7266	7301.8
798	6418	6347.4	979	6560	6604.8	1481	7268	7304.6
799	6353	6348.9	988	6507	6617.6	1498	7342	7327.9
800	6393	6350.3	990	6490	6620.4	1539	7366	7382.0
800	6459	6350.3	1081	6824	6747.2	1557	7462	7409.3
802	6397	6353.3	1107	6779	6781.5	1558	7444	7410.5
802	6355	6353.3	1110	6844	6785.9	1568	7413	7423.1
802	6393	6353.3	1116	6843	6796.3	1574	7479	7430.9
803	6432	6354.8	1119	6846	6800.3	1574	7426	7430.9
803	6432	6354.8	1121	6840	6802.9	1578	7326	7433.5
805	6394	6357.8	1124	6818	6806.8	1588	7416	7451.8
809	6422	6365.6	1128	6756	6811.9	1605	7407	7475.8
809	6422	6365.6	1130	6823	6814.5	1617	7508	7489.9

**Table D1: Continued**

Up	Us_exp	Us_pred	Up	Us_exp	Us_pred	Up	Us_exp	Us_pred
1722	7678	7636.2	2664	8724	8914.8	3387	9609	9884.5
1728	7596	7640.2	2671	8764	8931.7	3395	9821	9895.6
1728	7612	7640.2	2687	8853	8953.9	3400	9916	9902.5
1728	7615	7640.2	2709	8792	8978.6	3406	9872	9910.8
1742	7690	7662.0	2710	8816	8980.0	3419	9866	9933.8
1744	7616	7664.7	2735	8909	9011.1	3463	9654	9994.2
1770	7659	7703.5	2738	8916	9015.1	3472	9697	10005.0
1779	7758	7715.0	2817	9144	9130.9	3481	9727	10026.1
1812	7775	7761.7	2878	8971	9204.2	3487	9732	10034.4
1851	7690	7807.8	2911	9070	9248.7	3500	9870	10052.3
1858	7850	7817.6	2935	9231	9275.4	3508	9861	10062.8
1939	7773	7934.2	2974	9236	9336.0	3508	9880	10062.8
1948	7973	7941.5	2987	9401	9356.7	3538	9880	10098.2
1957	8054	7954.4	3030	9177	9411.3	3563	10117	10124.9
1959	8015	7957.3	3031	9180	9412.7	3618	10040	10204.9
2095	8114	8148.3	3035	9198	9418.4	3629	10238	10215.7
2096	8076	8149.6	3081	9317	9471.9	3658	9876	10266.7
2130	8127	8197.8	3086	9317	9478.6	3680	10113	10294.2
2154	8149	8226.2	3108	9228	9517.1	3717	10190	10342.9
2154	8150	8226.2	3148	9446	9577.3	3718	10388	10344.3
2156	8332	8229.1	3148	9369	9577.3	3736	10138	10360.0
2206	8231	8297.7	3181	9596	9617.8	3745	10162	10372.7
2306	8396	8431.8	3187	9549	9626.3	3748	10370	10376.9
2327	8358	8458.0	3217	9365	9662.8	3772	10458	10402.8
2335	8421	8468.9	3225	9666	9673.6	3777	10409	10409.5
2371	8436	8520.6	3238	9762	9683.7	3778	10431	10410.8
2446	8570	8619.9	3251	9409	9708.8	3786	10341	10421.7
2449	8529	8624.0	3260	9477	9720.3	3930	10552	10624.8
2467	8699	8649.2	3269	9426	9726.9	3966	10513	10669.3
2477	8618	8663.5	3274	9617	9733.3	3967	10384	10670.8
2595	8829	8823.9	3287	9642	9763.6	3983	10611	10694.5
2604	8762	8834.9	3293	9758	9770.8	3988	10572	10699.7
2604	8748	8834.9	3297	9721	9775.7	3991	10542	10703.9
2605	8744	8836.2	3347	9775	9842.5	4001	10572	10718.0
2608	8664	8840.1	3361	9751	9854.6	4026	10631	10759.0
2641	8848	8889.7	3376	9803	9876.8	4041	10572	10778.9
2645	8797	8894.5	3376	9746	9876.8			
2650	8803	8900.6	3381	9670	9883.8			

**Table D2: Predicted Shock Speed vs. Experiment (m/s) - Validation Data: 120 data sets, see Figure 5.7.**

Up	Us_exp	Us_pred	Up	Us_exp	Us_pred	Up	Us_exp	Us_pred
278	5811	5604.6	1121	6840	6802.9	2738	8916	9015.1
440	6021	5839.4	1128	6756	6811.9	2817	9144	9130.9
472	6054	5885.4	1130	6823	6814.5	2911	9070	9248.7
503	5996	5931.7	1134	6826	6819.7	2935	9231	9275.4
507	6055	5937.4	1136	6831	6823.7	2974	9236	9336.0
609	6103	6080.9	1141	6795	6831.0	2987	9401	9356.7
626	6262	6106.8	1159	6915	6856.7	3030	9177	9411.3
627	6228	6107.0	1220	6981	6941.8	3031	9180	9412.7
671	6164	6169.1	1220	7014	6941.8	3086	9317	9478.6
722	6367	6241.4	1277	6943	7018.5	3181	9596	9617.8
727	6323	6248.8	1352	7092	7123.3	3187	9549	9626.3
728	6310	6250.2	1383	7225	7166.5	3217	9365	9662.8
778	6388	6320.9	1437	7156	7242.3	3225	9666	9673.6
786	6312	6332.2	1446	7211	7253.4	3238	9762	9683.7
792	6314	6340.3	1467	7305	7278.2	3260	9477	9720.3
792	6365	6340.3	1498	7342	7327.9	3274	9617	9733.3
799	6353	6348.9	1557	7462	7409.3	3347	9775	9842.5
800	6393	6350.3	1574	7426	7430.9	3361	9751	9854.6
800	6459	6350.3	1578	7326	7433.5	3376	9803	9876.8
802	6397	6353.3	1605	7407	7475.8	3381	9670	9883.8
802	6355	6353.3	1742	7690	7662.0	3387	9609	9884.5
809	6422	6365.6	1744	7616	7664.7	3400	9916	9902.5
818	6366	6376.8	1779	7758	7715.0	3419	9866	9933.8
831	6436	6396.9	1858	7850	7817.6	3463	9654	9994.2
859	6470	6435.5	1939	7773	7934.2	3472	9697	10005.0
863	6486	6440.5	1948	7973	7941.5	3481	9727	10026.1
871	6561	6450.2	1959	8015	7957.3	3508	9861	10062.8
888	6541	6476.9	2154	8150	8226.2	3508	9880	10062.8
891	6589	6481.0	2156	8332	8229.1	3563	10117	10124.9
896	6589	6487.7	2335	8421	8468.9	3629	10238	10215.7
897	6579	6489.0	2371	8436	8520.6	3658	9876	10266.7
901	6402	6494.2	2467	8699	8649.2	3736	10138	10360.0
953	6616	6567.9	2477	8618	8663.5	3745	10162	10372.7
953	6617	6567.9	2595	8829	8823.9	3772	10458	10402.8
966	6659	6584.2	2605	8744	8836.2	3786	10341	10421.7
975	6607	6599.1	2608	8664	8840.1	3930	10552	10624.8
988	6507	6617.6	2641	8848	8889.7	3967	10384	10670.8
1110	6844	6785.9	2645	8797	8894.5	3988	10572	10699.7
1116	6843	6796.3	2709	8792	8978.6	4001	10572	10718.0
1119	6846	6800.3	2735	8909	9011.1	4041	10572	10778.9

**Table D3: Experimental Shock vs. Particle Speed (m/s) – Calibration Data: 112 data pairs, see Figure 5.8.**

Up	Us_exp	Up	Us_exp	Up	Us_exp
279	5782	1146	6861	2449	8529
497	6025	1157	6893	2604	8762
502	6098	1157	6752	2604	8748
509	5947	1206	6857	2650	8803
509	5953	1260	6955	2664	8724
608	6125	1263	6938	2671	8764
650	6226	1318	7062	2687	8853
677	6277	1362	7143	2710	8816
768	6348	1362	7139	2878	8971
790	6304	1426	7268	3035	9198
793	6308	1432	7228	3081	9317
798	6418	1445	7268	3108	9228
798	6342	1461	7269	3148	9446
802	6393	1465	7295	3148	9369
803	6432	1479	7266	3251	9409
803	6432	1481	7268	3269	9426
805	6394	1539	7366	3287	9642
809	6422	1558	7444	3293	9758
833	6483	1568	7413	3297	9721
839	6419	1574	7479	3376	9746
850	6415	1588	7416	3395	9821
854	6443	1617	7508	3406	9872
858	6488	1722	7678	3487	9732
859	6445	1728	7596	3500	9870
860	6446	1728	7612	3538	9880
862	6472	1728	7615	3618	10040
864	6418	1770	7659	3680	10113
865	6518	1812	7775	3717	10190
873	6522	1851	7690	3718	10388
892	6442	1957	8054	3748	10370
910	6530	2095	8114	3777	10409
910	6534	2096	8076	3778	10431
979	6560	2130	8127	3966	10513
990	6490	2154	8149	3983	10611
1081	6824	2206	8231	3991	10542
1107	6779	2306	8396	4026	10631
1124	6818	2327	8358		
1144	6783	2446	8570		

(Page Left Blank)

## **Distribution**

### EXTERNAL DISTRIBUTION

M. A. Adams  
Jet Propulsion Laboratory  
4800 Oak Grove Drive, MS 97  
Pasadena, CA 91109

M. Aivazis  
Center for Advanced Computing  
Research  
California Institute of Technology  
1200 E. California Blvd./MS 158-79  
Pasadena, CA 91125

Charles E. Anderson  
Southwest Research Institute  
P. O. Drawer 28510  
San Antonio, TX 78284

Bilal Ayyub (2)  
Department of Civil Engineering  
University of Maryland  
College Park, MD 20742

Osman Balci  
Department of Computer Science  
Virginia Tech  
Blacksburg, VA 24061

Steven Batill (2)  
Dept. of Aerospace & Mechanical Engr.  
University of Notre Dame  
Notre Dame, IN 46556

S. Beissel  
Alliant Techsystems, Inc.  
600 Second St., NE  
Hopkins, MN 55343

David Belk  
WL/MNAA  
101 W. Eglin Blvd., Suite 219  
Eglin AFB, FL 32542-6810

Ted Belytschko (2)  
Department of Mechanical Engineering  
Northwestern University  
2145 Sheridan Road  
Evanston, IL 60208

James Berger  
Institute of Statistics and Decision Science  
Duke University  
Box 90251  
Durham, NC 27708-0251

Pavel A. Bouzinov  
ADINA R&D, Inc.  
71 Elton Avenue  
Watertown, MA 02472

John A. Cafeo  
General Motors R&D Center  
Mail Code 480-106-256  
30500 Mound Road  
Box 9055  
Warren, MI 48090-9055

James C. Cavendish  
General Motors R&D Center  
Mail Code 480-106-359  
30500 Mound Road  
Box 9055  
Warren, MI 48090-9055

Chun-Hung Chen (2)  
Associate Professor  
Department of Systems Engineering &  
Operations Research  
George Mason University  
4400 University Drive, MS 4A6  
Fairfax, VA 22030

Wei Chen  
Dept. of Mechanical Engr. (M/C 251)  
842 W. Taylor St.  
University of Illinois at Chicago  
Chicago, IL 60607-7022

Kyeongjae Cho (2)  
Dept. of Mechanical Engineering  
MC 4040  
Stanford University  
Stanford, CA 94305-4040

Thomas Chwastyk  
U.S. Navel Research Lab.  
Code 6304  
4555 Overlook Ave., SW  
Washington, DC 20375-5343

Hugh Coleman (2)  
Department of Mechanical &  
Aero. Engineering  
University of Alabama/Huntsville  
Huntsville, AL 35899

Raymond Cosner (2)  
Boeing-Phantom Works  
MC S106-7126  
P. O. Box 516  
St. Louis, MO 63166-0516

Thomas A. Cruse  
398 Shadow Place  
Pagosa Springs, CO 81147-7610

P. Cuniff  
U.S. Army Soldier Systems Center  
Kansas Street  
Natick, MA 01750-5019

Frank Dean (2)  
Strategic Systems Programs  
Nebraska Avenue Complex  
287 Somers Court NW, Suite 10041  
Washington, DC 20393-5446

Department of Energy (4)  
Attn: Kevin Greenaugh, DP-153  
Paul Messina, DP-51  
Juan Meza, DP-51  
William Reed, DP-51

Department of Energy  
1000 Independence Ave., SW  
Washington, DC 20585

U. M. Diwekar (2)  
Center for Energy and  
Environmental Studies  
Carnegie Mellon University  
Pittsburgh, PA 15213-3890

David Dolling  
Department of Aerospace Engineering  
& Engineering Mechanics  
University of Texas at Austin  
Austin, TX 78712-1085

Isaac Elishakoff (2)  
Dept. of Mechanical Engineering  
Florida Atlantic University  
777 Glades Road  
Boca Raton, FL 33431-0991

Joseph E. Flaherty (2)  
Dept. of Computer Science  
Rensselaer Polytechnic Institute  
Troy, NY 12181

John Fortna  
ANSYS, Inc.  
275 Technology Drive  
Canonsburg, PA 15317

Roger Ghanem  
Dept. of Civil Engineering  
Johns Hopkins University  
Baltimore, MD 21218

Mike Giltrud  
Defense Threat Reduction Agency  
DTRA/CPWS  
6801 Telegraph Road  
Alexandria, VA 22310-3398

James Glimm (2)  
Dept. of Applied Math & Statistics  
P138A  
State University of New York  
Stony Brook, NY 11794-3600

James Gran  
SRI International  
Poulter Laboratory AH253  
333 Ravenswood Avenue  
Menlo Park, CA 94025

Bernard Grossman (2)  
Dept. of Aerospace &  
Ocean Engineering  
Mail Stop 0203  
215 Randolph Hall  
Blacksburg, VA 24061

Sami Habchi  
CFD Research Corp.  
Cummings Research Park  
215 Wynn Drive  
Huntsville, AL 35805

Raphael Haftka (2)  
Dept. of Aerospace and Mechanical  
Engineering and Engineering Science  
P. O. Box 116250  
University of Florida  
Gainesville, FL 32611-6250

Achintya Haldar (2)  
Dept. of Civil Engineering  
& Engineering Mechanics  
University of Arizona  
Tucson, AZ 85721

Tim Hasselman  
ACTA  
2790 Skypark Dr., Suite 310  
Torrance, CA 90505-5345

George Hazelrigg  
Division of Design, Manufacturing  
& Innovation  
Room 508N  
4201 Wilson Blvd.  
Arlington, VA 22230

David Higdon  
Institute of Statistics and Decision Science  
Duke University  
Box 90251  
Durham, NC 27708-0251

Richard Hills (20)  
College of Engineering, MSC 3449  
New Mexico State University  
P. O. Box 30001  
Las Cruces, NM 88003

F. Owen Hoffman (2)  
SENES  
102 Donner Drive  
Oak Ridge, TN 37830

G. Ivy  
Logicon R&D Associates  
P.O. Box 92500  
Los Angeles, CA 90009

Ralph Jones (2)  
Sverdrup Tech. Inc./AEDC Group  
1099 Avenue C  
Arnold AFB, TN 37389-9013

Leo Kadanoff  
Research Institutes Building  
University of Chicago  
5640 South Ellis Ave.  
Chicago, IL 60637

George Karniadakis (2)  
Division of Applied Mathematics  
Brown University  
192 George St., Box F  
Providence, RI 02912

Alan Karr  
Institute of Statistics and Decision Science  
Duke University  
Box 90251  
Durham, NC 27708-0251

J. Keremes  
The Boeing Company  
Rocketdyne Propulsion & Power  
P. O. Box 7922  
6633 Canoga Avenue  
Canoga Park, CA 91309-7922

Hyoung-Man Kim  
Boeing Company  
M/S: ZC-01  
502 Gemini Ave.  
Houston, TX 77058

K. D. Kimsey  
U.S. Army Research Laboratory  
Weapons & Materials Research  
Directorate  
AMSRL-WM-TC 309 120A  
Aberdeen Proving Gd, MD 21005-5066

B. A. Kovac  
The Boeing Company  
Rocketdyne Propulsion & Power  
P. O. Box 7922  
6633 Canoga Avenue  
Canoga Park, CA 91309-7922

P. Krysl  
Department of Computer Science  
California Institute of Technology  
1200 E. California Blvd./MS 256-80  
Pasadena, CA 91125

W. K. Liu (2)  
Northwestern University  
Dept. of Mechanical Engineering  
2145 Sheridan Road  
Evanston, IL 60108-3111

Robert Lust  
General Motors, R&D and Planning  
MC 480-106-256  
30500 Mound Road  
Warren, MI 48090-9055

Sankaran Mahadevan (2)  
Dept. of Civil &  
Environmental Engineering  
Vanderbilt University  
Box 6077, Station B  
Nashville, TN 37235

Hans Mair  
Institute for Defense Analysis  
Operational Evaluation Division  
1801 North Beauregard Street  
Alexandria, VA 22311-1772

W. McDonald  
Naval Surface Warfare Center  
Code 420  
101 Strauss Avenue  
Indian Head, MD 20640-5035

Gregory McRae (2)  
Dept. of Chemical Engineering  
Massachusetts Institute of Technology  
Cambridge, MA 02139

Michael Mendenhall (2)  
Nielsen Engineering & Research, Inc.  
510 Clyde Ave.  
Mountain View, CA 94043

Sue Minkoff (2)  
Dept. of Mathematics and Statistics  
University of Maryland, Baltimore Co.  
1000 Hilltop Circle  
Baltimore, MD 21250

Max Morris (2)  
Department of Statistics  
Iowa State University  
304A Snedecor-Hall  
Ames, IW 50011-1210

Paul Muessig  
Naval Air Warfare Center  
Joint Accreditation Support Activity  
Weapons Division, Code 418000D  
1 Administration Circle  
China Lake, CA 93555-6100

R. Namburu  
U.S. Army Research Laboratory  
AMSRL-CI-H  
Aberdeen Proving Gd, MD 21005-5067

NASA/Ames Research Center  
Attn: U. B. Mehta  
MS: T27 B-1  
Moffett Field, CA 94035-1000

NASA/Glen Research Center  
Attn: Chris Steffen, MS 5-11  
Cleveland, OH 44135

NASA/Langley Research Center (5)  
Attn: Michael Hemsch, MS 280  
Jim Luckring, MS 280  
Ahmed Noor, MS 369  
Sharon Padula, MS 159  
Jim Weilmuenster, MS 408A  
Hampton, VA 23681-0001

C. Needham  
Applied Research Associates, Inc.  
4300 San Mateo Blvd., Suite A-220  
Albuquerque, NM 87110

A. Needleman  
Division of Engineering, Box D  
Brown University  
Providence, RI 02912

Robert Nelson (2)  
Dept. of Aerospace &  
Mechanical Engineering  
University of Notre Dame  
Notre Dame, IN 46556

Efstratios Nikolaidis (2)  
MIME Dept.  
4035 Nitschke Hall  
University of Toledo  
Toledo, OH 43606-3390

Tinsley Oden (2)  
Texas Institute of Comp. Mechanics  
University of Texas at Austin  
Austin, TX 78712

Michael Ortiz (2)  
Graduate Aeronautical Laboratories  
California Institute of Technology  
1200 E. California Blvd./MS 105-50  
Pasadena, CA 91125

Dale Pace  
Applied Physics Laboratory  
Johns Hopkins University  
111000 Johns Hopkins Road  
Laurel, MD 20723-6099

Alex Pang  
Computer Science Department  
University of California  
Santa Cruz, CA 95064

Allan Pifko  
2 George Court  
Melville, NY 11747

Cary Presser (2)  
Process Measurements Div.  
National Institute of Standards  
and Technology  
Bldg. 221, Room B312  
Gaithersburg, MD 20899

P. Radovitzky  
Graduate Aeronautical Laboratories  
California Institute of Technology  
1200 E. California Blvd./MS 105-50  
Pasadena, CA 91125

W. Rafaniello  
DOW Chemical Company  
1776 Building  
Midland, MI 48674

Chris Rahaim (2)  
SAIC  
14 East Washington St., Suite 401  
Orlando, FL 32801-2320

Pradeep Raj (2)  
Computational Fluid Dynamics  
Lockheed Martin Aeronautical Sys.  
86 South Cobb Drive  
Marietta, GA 30063-0685

J. N. Reddy  
Dept. of Mechanical Engineering  
Texas A&M University  
ENPH Building, Room 210  
College Station, TX 77843-3123

John Renaud (2)  
Dept. of Aerospace & Mechanical Engr.  
University of Notre Dame  
Notre Dame, IN 46556

E. Repetto  
Graduate Aeronautical Laboratories  
California Institute of Technology  
1200 E. California Blvd./MS 105-50  
Pasadena, CA 91125

Patrick J. Roache  
1108 Mesa Loop NW  
Los Lunas, NM 87031

A. J. Rosakis  
Graduate Aeronautical Laboratories  
California Institute of Technology  
1200 E. California Blvd./MS 105-50  
Pasadena, CA 91125

Tim Ross (2)  
Dept. of Civil Engineering  
University of New Mexico  
Albuquerque, NM 87131

J. Sacks  
Institute of Statistics and Decision Science  
Duke University  
Box 90251  
Durham, NC 27708-0251

Sunil Saigal (2)  
Carnegie Mellon University  
Department of Civil and  
Environmental Engineering  
Pittsburgh, PA 15213

Len Schwer  
Schwer Engineering & Consulting  
6122 Aaron Court  
Windsor, CA 95492

Paul Senseny  
Factory Mutual Research Corporation  
1151 Boston-Providence Turnpike  
P.O. Box 9102  
Norwood, MA 02062

E. Sevin  
Logicon RDA, Inc.  
1782 Kenton Circle  
Lyndhurst, OH 44124

Mark Shephard (2)  
Rensselaer Polytechnic Institute  
Scientific Computation Research Center  
Troy, NY 12180-3950

T. P. Shivananda  
Bldg. SB2/Rm. 1011  
TRW/Ballistic Missiles Division  
P. O. Box 1310  
San Bernardino, CA 92402-1310

Y.-C. Shu  
Graduate Aeronautical Laboratories  
California Institute of Technology  
1200 E. California Blvd./MS 105-50  
Pasadena, CA 91125

Don Simons  
Logicon  
222 W. Sixth St.  
P.O. Box 471  
San Pedro, CA 90733-0471

Munir Sindir  
Boeing Company, MC IB39  
Rocketdyne Propulsion & Power  
P. O. Box 7922  
6633 Canoga Avenue  
Canoga Park, CA 91309-7922

Ashok Singhal (2)  
CFD Research Corp.  
Cummings Research Park  
215 Wynn Drive  
Huntsville, AL 35805

R. Singleton  
Engineering Sciences Directorate  
Army Research Office  
4300 S. Miami Blvd.  
P.O. Box 1221  
Research Triangle Park, NC 27709-2211

W. E. Snowden  
DARPA  
7120 Laketree Drive  
Fairfax Station, VA 22039

Bill Spencer (2)  
Dept. of Civil Engineering  
and Geological Sciences  
University of Notre Dame  
Notre Dame, IN 46556-0767

D. E. Stevenson (2)  
Computer Science Department  
Clemson University  
442 Edwards Hall, Box 341906  
Clemson, SC 29631-1906

Tim Swafford  
Sverdrup Tech. Inc./AEDC Group  
1099 Avenue C  
Arnold AFB, TN 37389-9013

Kenneth Tatum  
Sverdrup Tech. Inc./AEDC Group  
740 Fourth Ave.  
Arnold AFB, TN 37389-6001

Ben Thacker  
Southwest Research Institute  
6220 Culebra Road  
Postal Drawer 28510  
San Antonio, TX 78228-0510

Robert W. Walters  
Aerospace and Ocean Engineering  
Virginia Tech  
215 Randolph Hall, MS 203  
Blacksburg, VA 24061-0203

Ren-Jye Yang  
Ford Research Laboratory  
MD2115-SRL  
P.O.Box 2053  
Dearborn, MI 4812

Simone Youngblood  
DOD/DMSO  
Technical Director for VV&A  
1901 N. Beauregard St., Suite 504  
Alexandria, VA 22311

M. A. Zikry  
North Carolina State University  
Mechanical & Aerospace Engineering  
2412 Broughton Hall, Box 7910  
Raleigh, NC 27695

J. G. Zwissler  
Jet Propulsion Laboratory  
4800 Oak Grove Drive, MS 97-8  
Pasadena, CA 91109-8099

#### FOREIGN DISTRIBUTION:

Yakov Ben-Haim (2)  
Department of Mechanical Engineering  
Technion-Israel Institute of Technology  
Haifa 32000  
ISRAEL

Gert de Cooman (2)  
Universiteit Gent  
Onderzoeksgroep, SYSTeMS  
Technologiepark - Zwijnaarde 9  
9052 Zwijnaarde  
BELGIUM

Graham de Vahl Davis (2)  
CFD Research Laboratory  
University of NSW  
Sydney, NSW 2052  
AUSTRALIA

Luis Eca (2)  
Instituto Superior Tecnico  
Department of Mechanical Engineering  
Av. Rovisco Pais  
1096 Lisboa CODEX  
PORTUGAL

Charles Hirsch (2)  
Department of Fluid Mechanics  
Vrije Universiteit Brussel  
Pleinlaan, 2  
B-1050 Brussels  
BELGIUM

Igor Kozin  
Systems Analysis Department  
Riso National Laboratory  
P. O. Box 49  
DK-4000 Roskilde  
DENMARK

K. Papoulia  
Inst. Eng. Seismology & Earthquake  
Engineering  
P.O. Box 53, Finikas GR-55105  
Thessaloniki  
GREECE

Malcolm Wallace  
National Engineering Laboratory  
East Kilbride  
Glasgow  
G75 0QU  
UNITED KINGDOM

Peter Walley  
36 Bloomfield Terrace  
Lower Hutt  
NEW ZEALAND

Dr. Max Ruppert  
UniBw Munich - BauV 2.2  
Inst. Engng.Mech. & Struct.Mech.  
D - 85577 Neuibiberg  
GERMANY

Los Alamos National Laboratory (40)  
Mail Station 5000  
P.O. Box 1663  
Los Alamos, NM 87545

Attn: Peter Adams, MS B220  
Attn: Mark C. Anderson, MS D411  
Attn: Thomas Bement, MS F600  
Attn: Terrence Bott, MS K557  
Attn: D. Cagliostro, MS F645  
Attn: David Crane, MS P946  
Attn: John F. Davis, MS B295  
Attn: Helen S. Deaven, MS B295  
Attn: Scott Doebling, MS P946  
Attn: S. Eisenhower, MS K557  
Attn: Dawn Flicker, MS F664  
Attn: George T. Gray, MS G755  
Attn: Ken Hanson, MS P940  
Attn: R. Henninger, MS D413  
Attn: Brad Holian, MS B268  
Attn: Kathleen Holian, MS B295  
Attn: Darryl Holm, MS B284  
Attn: James Hyman, MS B284  
Attn: Michael E. Jones, MS B259  
Attn: Cliff Joslyn, MS B265  
Attn: James Kamm, MS D413  
Attn: Jeanette Lagrange, MS D445  
Attn: S. Keller-McNulty, MS F600  
Attn: Elizabeth Kelly, MS F600  
Attn: Ken Koch, MS F652  
Attn: Len Margolin, MS D413  
Attn: Harry Martz, MS F600  
Attn: Mike McKay, MS F600  
Attn: Mark P. Miller, MS P946  
Attn: John D. Morrison, MS F602  
Attn: Karen I. Pao, MS B256  
Attn: M. Peterson-Schnell,  
MS B295  
Attn: William Rider, MS D413  
Attn: Tom Seed, MS F663  
Attn: David Sharp, MS B213  
Attn: Richard N. Silver, MS D429  
Attn: Ronald E. Smith, MS J576  
Attn: Christine Treml, MS H851  
Attn: Daniel Weeks, MS B295  
Attn: Morgan White, MS F663  
Attn: Alyson G. Wilson, MS F600

University of California (20)  
Lawrence Livermore National Laboratory  
7000 East Ave.  
P.O. Box 808  
Livermore, CA 94550

Attn: T. F. Adams, MS L-095  
Attn: Steven Ashby, MS L-561  
Attn: John Bolstad, MS L-023  
Attn: Peter N. Brown, MS L-561  
Attn: T. Scott Carman, MS L-031  
Attn: R. Christensen, MS L-160  
Attn: Evi Dube, MS L-095  
Attn: Richard Klein, MS L-023  
Attn: Byung S. Lee, MS L-550  
Attn: Roger Logan, MS L-125  
Attn: C. F. McMillan, MS L-098  
Attn: C. Mailhiot, MS L-055  
Attn: J. F. McEnerney, MS L-023  
Attn: M. J. Murphy, MS L-282  
Attn: Daniel Nikkel, MS L-342  
Attn: Cynthia Nitta, MS L-096  
Attn: Douglas Post, MS L-038  
Attn: Peter Raboin, MS L-125  
Attn: Peter Terrill, MS L-125  
Attn: Charles Tong, MS L-560

Argonne National Laboratory  
Attn: Paul Hovland  
MCS Division  
Bldg. 221, Rm. C-236  
9700 S. Cass Ave.  
Argonne, IL 60439

#### SANDIA INTERNAL

1 MS 1152 1642 M. L. Kiefer  
1 MS 1186 1674 R. J. Lawrence  
1 MS 0525 1734 P. V. Plunkett  
1 MS 0525 1734 R. B. Heath  
1 MS 0525 1734 S. D. Wix  
1 MS 1393 1902 J. R. Garcia  
1 MS 0457 2001 W. J. Tedeschi  
1 MS 0429 2100 J. S. Rottler  
1 MS 0453 2104 D. L. McCoy  
1 MS 0475 2105 R. C. Hartwig  
1 MS 1393 2106 F. F. Dean  
1 MS 0447 2111 J. O. Harrison  
1 MS 0447 2111 P. D. Hoover  
1 MS 0479 2151 P. A. Sena  
1 MS 0479 2151 M. H. Abt  
1 MS 0482 2161 V. J. Johnson  
1 MS 0482 2161 R. S. Baty  
1 MS 0481 2167 M. A. Rosenthal

1 MS 0481 2167 W. C. Moffatt  
1 MS 0481 2168 K. D. Meeks  
1 MS 0481 2168 K. Ortiz  
1 MS 0509 2300 M. W. Callahan  
1 MS 0769 5800 D. S. Miyoshi  
1 MS 0759 5845 I. V. Waddoups  
1 MS 0759 5845 M. S. Tierney  
1 MS 0782 5861 R. V. Matalucci  
1 MS 0737 6114 P. A. Davis  
1 MS 0751 6117 L. S. Costin  
1 MS 0718 6141 C. D. Massey  
1 MS 0708 6214 P. S. Veers  
1 MS 0747 6410 R. L. Camp  
1 MS 0747 6410 G. D. Wyss  
1 MS 0746 6411 R. M. Cranwell  
1 MS 0746 6411 D. J. Anderson  
1 MS 0746 6411 J. E. Campbell  
1 MS 0746 6411 D. G. Robinson  
1 MS 0746 6411 L. P. Swiler  
1 MS 1140 6500 J. K. Rice  
1 MS 0974 6522 G. D. Valcez  
1 MS 0977 6524 W. R. Cook  
3 MS 0977 6524 S. M. DeLand  
1 MS 1138 6533 E. Shepherd  
1 MS 1138 6534 L. M. Claussen  
1 MS 1137 6534 A. L. Hodges  
1 MS 1138 6534 M. T. McCornack  
1 MS 1137 6534 S. V. Romero  
1 MS 1137 6535 G. K. Froehlich  
1 MS 0771 6805 P. G. Kaplan  
1 MS 1395 6821 J. W. Garner  
1 MS 1395 6821 P. Vaughn  
1 MS 0779 6849 J. C. Helton  
1 MS 0779 6849 R. P. Rechard  
1 MS 0779 6849 M. J. Shortencarier  
1 MS 0778 6851 G. E. Barr  
1 MS 0778 6851 R. J. MacKinnon  
1 MS 9051 8351 C. A. Kennedy  
1 MS 9202 8418 W. P. Ballard  
1 MS 9202 8418 R. M. Zurn  
1 MS 9405 8700 T. M. Dyer  
1 MS 9042 8725 W. A. Kawahara  
1 MS 9405 8726 R. E. Jones  
1 MS 9161 8726 P. A. Klein  
1 MS 9161 8726 E. P. Chen  
1 MS 9042 8728 C. D. Moen  
1 MS 9405 8743 R. A. Regueiro  
1 MS 9003 8900 K. E. Washington  
1 MS 9012 8920 P. E. Nielan  
1 MS 9217 8950 P. T. Boggs  
1 MS 9217 8950 P. D. Hough  
1 MS 9217 8950 M. L. Koszykowski  
1 MS 1110 8950 L. J. Lehoucq  
1 MS 9217 8950 K. R. Long

1	MS 0841 9100	T. C. Bickel	1	MS 0828 9133	W. R. Witkowski
1	MS 0836 9100	M. R. Baer	1	MS 1135 9134	S. Heffelfinger
1	MS 0828 9100	T. Y. Chu	1	MS 0555 9134	J. T. Nakos
1	MS 0828 9100	C. W. Peterson	1	MS 0835 9140	J. M. McGlaun
1	MS 0835 9100	D. K. Gartling	1	MS 0835 9140	J. A. Fernandez
1	MS 0834 9112	A. C. Ratzel	1	MS 0835 9140	A. Gurule
1	MS 0826 9113	W. Hermina	1	MS 0835 9140	R. Garber
1	MS 0826 9113	T. J. Bartel	1	MS 0835 9141	S. N. Kempka
1	MS 0827 9114	J. E. Johannes	1	MS 0835 9141	S. P. Burns
1	MS 0827 9114	K. S. Chen	1	MS 0835 9141	R. J. Cochran
1	MS 0827 9114	L. A. Mondy	1	MS 0835 9141	B. Hassan
1	MS 0827 9114	R. R. Rao	1	MS 0835 9141	C. Roy
1	MS 0827 9114	P. R. Schunk	1	MS 0835 9142	J. S. Peery
3	MS 0825 9115	W. H. Rutledge	1	MS 0847 9142	S. W. Attaway
3	MS 0825 9115	S. J. Beresh	1	MS 0847 9142	M. L. Blanford
3	MS 0825 9115	F. G. Blottner	1	MS 0847 9142	M. W. Heinstein
1	MS 0828 9115	K. V. Chavez	1	MS 0847 9142	S. W. Key
3	MS 0825 9115	D. W. Kuntz	1	MS 0847 9142	G. M. Reese
1	MS 0825 9115	M. A. McWherter-Payne	1	MS 0835 9142	J. R. Weatherby
3	MS 0825 9115	J. L. Payne	1	MS 0826 9143	J. D. Zepper
3	MS 0825 9115	D. L. Potter	1	MS 0827 9143	K. M. Aragon
1	MS 0825 9115	K. Salari	1	MS 0827 9143	H. C. Edwards
1	MS 0825 9115	L. W. Young	1	MS 0847 9143	G. D. Sjaardema
1	MS 0825 9115	W. P. Wolfe	1	MS 0826 9143	J. R. Stewart
1	MS 0836 9116	E. S. Hertel	1	MS 0321 9200	W. J. Camp
1	MS 0836 9116	S. R. Tieszen	1	MS 0310 9209	G. S. Heffelfinger
1	MS 0827 9117	R. O. Griffith	1	MS 1111 9209	S. J. Plimpton
1	MS 0367 9117	R. J. Buss	1	MS 1110 9211	D. E. Womble
1	MS 0827 9117	R. B. Campbell	1	MS 1110 9211	R. Carr
1	MS 0827 9117	D. Dobranich	1	MS 1110 9211	S. Y. Chakerian
1	MS 0836 9117	R. E. Hogan	1	MS 0847 9211	M. S. Eldred
1	MS 0827 9117	T. E. Voth	1	MS 0847 9211	A. A. Giunta
1	MS 0847 9120	H. S. Morgan	1	MS 1110 9211	W. E. Hart
1	MS 0555 9122	M. S. Garrett	1	MS 1110 9211	A. Johnson
1	MS 0847 9123	A. F. Fossum	1	MS 1110 9211	V. J. Leung
1	MS 0847 9124	D. R. Martinez	1	MS 1110 9211	C. A. Phillips
3	MS 0847 9124	K. F. Alvin	1	MS 1110 9211	J. R. Red-Horse
1	MS 0847 9124	T. B. Carne	20	MS 0819 9211	T. G. Trucano
1	MS 0847 9124	J. L. Dohner	1	MS 0847 9211	B. A. vanBloemen
1	MS 0847 9124	R. V. Field			Waanders
1	MS 0847 9124	D. O. Smallwood	1	MS 0318 9212	G. S. Davidson
1	MS 0557 9125	T. J. Baca	1	MS 1109 9212	R. J. Pryor
1	MS 0553 9126	R. A. May	1	MS 1110 9214	J. DeLaurentis
1	MS 0828 9132	J. L. Moya	1	MS 1110 9214	R. B. Lehoucq
1	MS 0828 9132	S. N. Burchett	1	MS 0321 9220	A. L. Hale
3	MS 0828 9133	M. Pilch	1	MS 1110 9223	N. D. Pundit
1	MS 0828 9133	B. F. Blackwell	1	MS 0321 9224	J. A. Ang
1	MS 0828 9133	K. J. Dowding	1	MS 0321 9224	R. E. Benner
1	MS 0828 9133	A. R. Lopez	1	MS 0321 9224	J. L. Tompkins
1	MS 0828 9133	K. E. Metzinger	1	MS 0847 9226	R. W. Leland
1	MS 0828 9133	W. L. Oberkampf	1	MS 0847 9226	B. A. Hendrickson
1	MS 0828 9133	T. L. Paez	1	MS 0847 9226	P. Knupp
1	MS 0828 9133	C. Romero	1	MS 0318 9227	P. D. Heermann
1	MS 0828 9133	V. J. Romero	1	MS 0318 9227	C. F. Diegert
1	MS 0828 9133	A. Urbina			

1	MS 0310	9230	P. Yarrington
1	MS 0819	9231	E. A. Boucheron
1	MS 0819	9231	K H. Brown
1	MS 0819	9231	K. G. Budge
1	MS 0819	9231	D. E. Carroll
1	MS 0819	9231	M. Christon
1	MS 0819	9231	R. R. Drake
1	MS 0819	9231	A. C. Robinson
1	MS 0819	9231	R. M. Summers
1	MS 0819	9231	M. K. Wong
1	MS 0820	9232	P. F. Chavez
1	MS 0820	9232	R. M. Brannon
1	MS 0820	9232	M. E. Kipp
1	MS 0820	9232	S. A. Silling
1	MS 0820	9232	P. A. Taylor
1	MS 0316	9233	S. S. Dosanjh
1	MS 1111	9233	D. Gardner
1	MS 1111	9233	A. G. Salinger
1	MS 1111	9233	J. N. Shadid
1	MS 0316	9235	J. B. Aidun
1	MS 1111	9235	H. P. Hjalmarson
1	MS 0660 9519		D. S. Eaton
1	MS 0660 9519		M. A. Ellis
1	MS 0419 9800		R. G. Easterling
1	MS 0421 9814		J. M. Sjulín
1	MS 0423 9817		R. A. Paulsen
1	MS 0423 9817		S. E. Dingman
1	MS 9003 9900		D. L. Crawford
1	MS 9003 9904		J. E. Kelly
1	MS 0139 9905		R. K. Thomas
1	MS 0428 12300		D. D. Carlson
1	MS 0490 12331		J. A. Cooper
1	MS 0829 12323		F. W. Spencer
1	MS 0829 12323		M. L. Abate
3	MS 0829 12323		B. M. Rutherford
1	MS 0638 12326		M. A. Blackledge
1	MS 0638 12326		D. E. Percy
1	MS 0638 12326		D. L. Knirk
1	MS 0490 12331		P. E. D'Antonio
1	MS 0492 12332		D. R. Olson
1	MS 0405 12333		T. R. Jones
1	MS 0434 12334		R. J. Breeding
3	MS 0829 12335		K. V. Diegert
1	MS 1221 15002		R. D. Skocypec
1	MS 1179 15340		J. R. Lee
1	MS 1179 15341		L. J. Lorence
1	MS 0301 15400		J. L. McDowell
1	MS 9018 8945-1		Central Technical Files
2	MS 0899 9616		Technical Library
1	MS 0612 9612		Review & Approval Desk For DOE/OSTI